

**MINIMALLY INVASIVE BIOMATERIALS FOR CENTRAL NERVOUS SYSTEM
THERAPIES**

by

Britta Mary Rauck

Bachelor of Science, The Johns Hopkins University, 2009

Submitted to the Graduate Faculty of
Swanson School of Engineering in partial fulfillment
of the requirements for the degree of
Doctor of Philosophy

University of Pittsburgh

2014

UNIVERSITY OF PITTSBURGH
SWANSON SCHOOL OF ENGINEERING

This dissertation was presented

by

Britta Mary Rauck

It was defended on

March 26, 2014

and approved by

Thomas R. Friberg, M.D., Professor, Department of Ophthalmology

Steven Little, Ph.D., Chair, Department of Chemical and Petroleum Engineering

Martin Oudega, Ph.D., Assistant Professor, Department of Physical Medicine and
Rehabilitation

Dissertation Director: Yadong Wang, Ph.D., Professor, Department of Bioengineering

Copyright © by Britta Mary Rauck

2014

MINIMALLY INVASIVE BIOMATERIALS FOR CENTRAL NERVOUS SYSTEM THERAPIES

Britta Mary Rauck, Ph.D.

University of Pittsburgh, 2014

The inability of the adult central nervous system (CNS) to regenerate combined with the progressive nature of many CNS pathologies poses a significant challenge in developing effective treatments. Biomaterials-based systems designed to deliver drugs and/or cells hold immense potential for moderating disease progression and promoting repair. Ideally, such systems should (1) allow minimally invasive administration, (2) provide localized and controlled delivery, and (3) protect the activity of their cargo for maximal therapeutic effect. Additionally, the ability to incorporate multiple treatment modalities is desirable as many CNS disorders are multi-faceted and complex in nature. Designing delivery systems that incorporate these features while simultaneously improving therapeutic outcomes, however, poses a significant challenge. This dissertation covers the formulation and application of polymer-based delivery systems for CNS repair, with specific focus given to the spinal cord and visual systems.

We first demonstrated the biocompatibility and feasibility of a reverse thermal gel, poly(ethylene glycol)–poly(serinol hexamethylene urethane) (ESHU) for intraocular drug delivery. This injectable formulation is capable of sustaining the bevacizumab release *in vivo*, and ultimately may be used to reduce the injection frequency in patients with ocular diseases such as age-related macular degeneration. To emphasize the versatility of ESHU, it was combined with bone marrow stromal cells (BMSCs) for treatment of traumatic spinal cord injury in rats. ESHU improved BMSC survival 3.5-fold one week post-injury compared to BMSCs

injected in PBS, which was accompanied by increased nervous tissue sparing and functional recovery. Finally, we demonstrated the feasibility of a coacervate-based growth factor delivery system for treatment of traumatic spinal cord injury. Ultimately, we hope the coacervate may be used in combination to augment cell therapy and drive the development of innovative solutions to treat injuries for where there are no cures.

TABLE OF CONTENTS

TABLE OF CONTENTS	VI
LIST OF TABLES	XI
LIST OF FIGURES	XII
PREFACE	XVI
1.0 INTRODUCTION	1
1.1 OCULAR DRUG DELIVERY: INSIGHTS AND CHALLENGES	2
1.1.1 Significance	2
1.1.2 Barriers to Efficient Posterior Segment Delivery	3
1.1.3 Bioengineering Strategies to Improve Ophthalmic Drug Delivery	5
1.2 BIOMATERIALS FOR SPINAL CORD REPAIR	8
1.2.1 Nervous System Biology	10
1.2.2 Materials Used in Nerve Regeneration	17
1.2.3 Materials-Based Delivery of Bioactive Agents	22
1.3 OBJECTIVES	29
1.3.1 Objective 1: Deliver bevacizumab intravitreally using a biocompatible reverse thermal gel	30
1.3.2 Objective 2: Improve the survival of transplanted bone marrow stromal cells in a rat model of spinal cord injury	31
1.3.3 Objective 3: Study the effect of controlled growth factor release to the injured spinal cord using a coacervate-based protein delivery system.	31

2.0	FORMULATION AND CHARACTERIZATION OF REVERSE THERMAL GEL FOR OCULAR DRUG DELIVERY	33
2.1	INTRODUCTION.....	33
2.2	MATERIALS AND METHODS	35
	2.2.1 Materials.....	35
	2.2.2 Equipment	35
	2.2.3 Synthesis of ESHU	36
	2.2.4 Cell Culture.....	37
	2.2.5 Live-Dead Cytocompatibility Experiment	38
	2.2.6 Immunoassay of Bevacizumab	38
	2.2.7 Release Profile of Bevacizumab	39
2.3	RESULTS AND DISCUSSION	40
	2.3.1 Cytocompatibility of ESHU with Ocular Cell Types	40
	2.3.2 Thermal Behavior of Bevacizumab-Loaded ESHU	43
	2.3.3 In Vitro Bevacizumab Release	44
2.4	CONCLUSIONS	47
3.0	INJECTABLE THERMORESPONSIVE HYDROGEL SUSTAINS THE RELEASE OF INTRAVITREAL BEVACIZUMAB IN VIVO	48
3.1	INTRODUCTION.....	48
3.2	MATERIALS AND METHODS	50
	3.2.1 Materials.....	50
	3.2.2 Preparation of Bevacizumab-Loaded ESHU	51
	3.2.3 Injection Force Measurements	51
	3.2.4 In Vitro Cytotoxicity	51
	3.2.5 Intravitreal Injection.....	52
	3.2.6 Clinical Examination.....	53

3.2.7	In Vivo Bevacizumab Release.....	54
3.2.8	Histological Analysis	54
3.2.9	Statistical Analysis.....	55
3.3	RESULTS	55
3.3.1	Feasibility of ESHU Injection.....	55
3.3.2	In Vitro Cytotoxicity of ESHU	57
3.3.3	Effect of ESHU on Intraocular Pressure.....	58
3.3.4	Effect of ESHU on Inflammatory Response	58
3.3.5	In Vivo Bevacizumab Release.....	60
3.4	DISCUSSION	62
3.5	CONCLUSIONS	65
4.0	INJECTABLE THERMORESPONSIVE HYDROGELS ENHANCE CELLULAR TRANSPLANT SURVIVAL AND IMPROVE OUTCOMES FOLLOWING TRAUMATIC SPINAL CORD INJURY	66
4.1	INTRODUCTION.....	66
4.2	MATERIALS AND METHODS	68
4.2.1	Ethics and Surgical Approval.....	68
4.2.2	Transplant Preparation	68
4.2.3	ESHU	69
4.2.4	Surgical Procedures.....	70
4.2.5	Post-Surgery Procedures	71
4.2.6	Motor Function Assessment	71
4.2.7	Histological Procedures.....	72
4.2.8	Immunocytochemistry	72
4.2.9	Cell Quantification	73
4.2.10	Measurement of Nervous Tissue Sparing.....	74

4.2.11	In Vitro Assessment of the Protective Effect of ESHU	74
4.2.12	Quantification of ESHU’s Antioxidant Ability	75
4.2.13	Statistical Analysis	75
4.3	RESULTS	76
4.3.1	BMSC Transplant Survival	76
4.3.2	Effect of BMSC Transplant Survival on Neuroprotection	78
4.3.3	Effect of BMSC Transplant Survival on Motor Recovery	79
4.3.4	Inflammatory Response	81
4.3.5	Oxidative Stress-Mediated Cell Death In Vitro	83
4.4	DISCUSSION	84
4.5	CONCLUSIONS	86
5.0	INJECTABLE COACERVATE FOR GROWTH FACTOR DELIVERY TO THE CONTUSED SPINAL CORD	88
5.1	INTRODUCTION	88
5.2	MATERIALS AND METHODS	90
5.2.1	Coacervate Preparation	90
5.2.2	Spinal Cord Contusion Model	91
5.2.3	Post-Surgical Care	92
5.2.4	Motor Function Assessment	92
5.2.5	Histological Analysis	93
5.2.6	Quantitative Immunofluorescence Analysis	94
5.2.7	Statistical Analysis	94
5.3	RESULTS AND DISCUSSION	95
5.3.1	Biocompatibility of PEAD in the Injured Spinal Cord	95
5.3.2	Effect of Controlled Shh Delivery on Nervous Tissue Sparing	98
5.3.3	Neuronal Fiber Density	99

5.3.4 Motor Function Outcomes.....	100
5.4 CONCLUSIONS	104
6.0 FINAL SUMMARY	105
6.1 OCULAR DRUG DELIVERY USING REVERSE THERMAL GELS – MAJOR FINDINGS, LIMITATIONS AND FUTURE WORK	105
6.2 IMPROVED TRANSPLANT SURVIVAL USING REVERSE THERMAL GELS FOR TREATMENT OF SPINAL CORD INJURY – MAJOR FINDINGS, LIMITATIONS AND FUTURE WORK.....	108
6.3 COACERVATE-BASED PROTEIN DELIVERY TO THE INJURED SPINAL CORD – MAJOR FINDINGS, LIMITATIONS AND FUTURE WORK	109
6.4 OVERALL CONCLUSIONS.....	110
DETAILED ANALYSIS OF BEVACIZUMAB CONCENTRATIONS	111
BIBLIOGRAPHY	114

LIST OF TABLES

Table 1. Pros and cons of the different ocular drug delivery routes	5
Table 2. Commonly used base materials may be combined with one or more bioactive cues to create bioactive materials to facilitate nerve regeneration.....	10

LIST OF FIGURES

- Figure 1. Anatomy of the eye and representation of ophthalmic drug delivery routes. Topical delivery via eye drops must diffuse across the anterior structures of the eye before reaching posterior targets (a). 3
- Figure 2. Structure of the CNS. The spinal cord has four segments (C: cervical; T: thoracic; L: lumbar; S: sacral) which connect to discrete body regions. These segments connect to the brain via ascending (red) and descending (blue) pathways which transmit neural impulses to and from the brain, respectively (B). 13
- Figure 3. Following trauma, an influx of inflammatory cells and reactive astrocytes causes the lesion cavity to expand (A). Reactive astrocytes secrete inhibitory molecules, resulting in secondary damage to axons spared by the initial insult. This causes demyelination and increased concentrations of myelin-associated inhibitors. Combined, these factors inhibit regeneration [122]. (B) Biomaterials-based therapies can promote neural repair. They can be designed as conduits or lesion-filling scaffolds and can incorporate various bioactive factors which interact with surrounding cells and tissues to elicit a pro-regenerative response..... 16
- Figure 4. A heparin-based delivery system generated from modified fibrin gels (A) used to deliver NT-3 causes infiltration of neurons (red) and astrocytes (green) into spinal cord lesions (B, 2) NT-3 delivery caused more neuronal growth than TBS-injected controls (B,1). I: intact cord; L: lesion..... 26
- Figure 5. Representative fluorescence micrograph images of bovine CE cells exposed to control (A,B) and ESHU (C,D) at 24h. Both groups show comparable intense nuclei staining (A,C) with scarce red-stained dead cells (B,D) indicating little cell death..... 41
- Figure 6. In vitro cytotoxicity of ESHU against bovine CE cells after 1, 12, and 24 hour incubation. The number of dead CE cells was determined by counting the number of PI+ cells, and was expressed as a function of the total number of cells labeled by Hoechst staining. Values are expressed as the means \pm SD (n=3). 41
- Figure 7. Representative fluorescence micrograph images of human ARPE-19 cells exposed to control (A,B) and ESHU (C,D) at 72h. There was no difference between experimental groups in the total number of viable cells (A,C) and dead cells (B,D)..... 42
- Figure 8. In vitro cytotoxicity of ESHU against human ARPE-19 cells after 24, 48, and 72 hour incubation. The percentage of dead ARPE-19 cells was determined by expressing the number PI+ cells over the total number of cells labeled by Hoechst staining. Values are the means \pm SD (n=3). 43

- Figure 9. Thermal behavior of bevacizumab-loaded ESHU formulated with 20 wt% ESHU and 1.25 mg bevacizumab. The steep increase in G' from 33 to 39 °C indicated a sol-gel phase transition. The phase transition behavior is similar to pure ESHU [193]. 44
- Figure 10. The release profile of bevacizumab from (A) 15 and (B) 20 wt% ESHU systems. The release was sustained over the 17-week period with initial burst releases. The 20 wt% ESHU systems resulted in slower release rates, and smaller burst releases due to its higher concentration..... 46
- Figure 11. The force required to inject a 15% w/v solution of ESHU (A) through a 31G needle is less than for a 1% solution of HA, a commonly-injected ophthalmic material (B). Upon injection to a solution of hyaluronic acid at 37°C, ESHU forms a spherical hydrogel (C). 56
- Figure 12. Bovine CE cells survive well over a 24-hour period following exposure to ESHU gels, with no significant difference when compared to TCPS controls. In contrast, silicone oil caused significant cell death compared to all other experimental groups ($p < 0.05$)..... 57
- Figure 13. IOP measurements return to baseline values 15 minutes following intravitreal injection. Throughout the study, IOP was not significantly different between ESHU and control groups ($p > 0.05$). 58
- Figure 14. ESHU is biocompatible in the eye. (A) Indirect images of the hydrogel in the vitreous space. The surface of the gel (traced in black) is free of inflammatory cells and the vitreous humor is clear. (B) Hematoxylin and eosin stains comparing the retinal structure of ESHU and control groups. The two groups are morphologically indistinguishable, suggesting that the presence of ESHU did not adversely affect retinal health. Scale bar: 100 μm 60
- Figure 15. ESHU sustains bevacizumab release for over 9 weeks. The concentration of bevacizumab in AC samples over time is plotted on a semi-log scale (A). On average, animals receiving the delivery system had 4.7-fold more bevacizumab present (B). 62
- Figure 16. Schematic representations of transplant preparation and ESHU. (a) Isolation and transduction of bone marrow stromal cells. Plastic-adherent cells from femurs of adult Sprague-Dawley rats were collected, lentivirally transduced with green fluorescent protein, and passaged four times before used for transplantation. (a') Green fluorescent protein-expressing BMSCs in culture. Smaller panels show examples of cultured BMSC morphologies. (b) Structural formula of ESHU with the urethane bond in gray box. Bar = 50 μm in a' and 25 μm in panels below..... 69
- Figure 17. ESHU improves survival of BMSC transplants in a spinal cord contusion. 15 minutes after injection, transplanted cells (green) occupy most of the contusion regardless of whether they were suspended in ESHU (a) or PBS (b). Staining for GFAP (red) was used to outline the contusion. Transplanted cells (green) were mostly rounded in ESHU (inset a) and PBS (inset b). 1 week after injection, the transplant occupies only part of the contusion site but more so when suspended in ESHU (c) than PBS (d). Transplanted cells at this time point were mostly elongated with bipolar morphologies. 4 weeks after

injection, hardly any cells were detected in the contusion in either group. Similar results were observed after 6 weeks (not shown). (g) More transplanted cells survive in the contusion site 1 week after injection when suspended in ESHU than PBS. Survival rate was measured against total number of injected cells. Error bars in graph display standard error of the mean (SEM). Asterisk = $p < 0.05$. Bar in a = 350 μm in a-d and 30 μm in insets. 77

Figure 18. ESHU augments neuroprotection by BMSC transplants in the contused spinal cord. Damage and loss of nervous tissue were observed 4 weeks after a BMSC transplant in ESHU (a) or PBS (b), or ESHU (c) or PBS (d) alone into the contused spinal cord. (e) Spared tissue volume was larger with the transplant in ESHU compared with all other groups. Error bars represent SEM, and asterisks = $p < 0.05$. Bar in = 600 μm in a-d. 78

Figure 19. ESHU leads to enhancement of motor function recovery by a BMSC transplant in the contused spinal cord. (a) Overground walking ability was significantly improved in rats with a BMSC transplant in ESHU compared with BMSCs in PBS 4-6 weeks post-injury. Rats with BMSC in ESHU performed better than rats with ESHU or PBS alone at 1-6 weeks post-injury. Rats with BMSCs in PBS walked better overground than rats with ESHU or PBS alone only at 1-3 weeks post-injury. (b) Improvement in overground walking ability during the 4th-6th week post-injury was significantly improved in rats with a transplant in ESHU compared with all over groups. (c) Improved higher motor function in rats with BMSCs in ESHU compared with PBS at 6 weeks post-injury. (d) Improved sensorimotor recovery in rats with the transplant in ESHU over all other groups and in rats with BMSCs in PBS over the control groups without BMSCs at 6 weeks post-injury. Error bars in bar graph display SEM. Asterisks signify $p < 0.05$. Pound sign signifies $p < 0.05$ 80

Figure 20. ESHU does not affect the injury-induced macrophage response. Macrophages (ED-1+, red) were found in the contusion with transplanted BMSC (green) in ESHU (a-c) or PBS (d-f). (g) ESHU as a transplant matrix or alone did not affect the presence of macrophages in the contusion at one and four weeks after transplantation. Error bars display SEM. Bar in a = 15 μm in a-f. 82

Figure 21. ESHU protects BMSCs in suspension and scavenges hydrogen peroxide in vitro. (a) Schematic representation of in vitro assay of ESHU's ability to protect BMSCs from H_2O_2 -induced death. (b) Cell survival from H_2O_2 -induced oxidative stress is better in ESHU than PBS. (c) Fewer BMSCs positive for caspase 3 and 8-oxo-dG with ESHU (red) than with PBS (green). (d) ESHU scavenges H_2O_2 in PBS. Error bars in bar graphs display SEM. Asterisks represent $p < 0.05$ 83

Figure 22. Effect of PEAD injection on the inflammatory response. PEAD does not increase the macrophage density at the lesion epicenter (A, D). Glial scarring, as measured by the intensity of GFAP staining, was also not different in groups receiving the coacervate compared to PBS controls. The intensity of the entire glial scar was quantified (B) as well as at the lesion epicenter, where presumably scarring would be the most prominent (C). In both cases, animals receiving the Shh coacervate had a significant ($p < 0.05$) reduction

in GFAP intensity compared to PBS and empty coacervate groups, indicating a possible effect of Shh delivery on scar formation. (Scale bar = 500 μ m)	97
Figure 23. Effect of Shh administration on nervous tissue sparing. Nervous tissue sparing was not statistically significant between experimental groups; however Shh-coacervate treatment did result in the largest percentage of tissue sparing.	98
Figure 24. Density of axons and serotonergic fibers rostral and caudal to the lesion. The amount of positive neurofilament (A) and serotonergic fiber (B) staining was determined by calculating the area of positive staining as a fraction of total tissue area.	100
Figure 25. BBB results. Free Shh groups performed well early, whereas Shh-coacervate groups had steadily increasing BBB scores throughout the study.....	101
Figure 26. Improvement in hindlimb stepping over time. Shh-coacervate groups had the largest decrease in the number of slips made over the time course of the study period. This indicates that improvements in sensorimotor function were the largest in the controlled delivery groups.....	102
Figure 27. Gait analysis reveals slight improvements in overground walking ability of Shh-coacervate animals. In control groups, three animals were unable to walk at the recording speed of 20 cm/s. All animals in free Shh and Shh-coacervate groups were capable of walking (A). The stride length of Shh-coacervate animals was not significantly different than healthy animals, suggesting an improvement in stepping (B). The paw angle of free Shh and Shh-coacervate animals was significantly less than in controls, suggesting an improved stability when stepping, though the paw angles were still significantly different than in uninjured controls (C).	103

PREFACE

Those familiar with bioengineering know that the classic proverb “it takes a village” is especially pertinent when considering the keys to success in the field. My accomplishments over the past five years are, without a doubt, the culmination of the tireless, dedicated efforts of a village of individuals spanning across multiple specialties and disciplines. It is these people to whom I am forever indebted, and it is with great pleasure and humility that I have the opportunity to thank them for their contributions to my development, both personally and professionally.

First and foremost, I owe my mentor, Dr. Yadong Wang, my sincerest gratitude for taking me under his wing and fostering my growth into a capable and competent researcher. He taught me how to ask the right questions and the skills required to answer them, which oftentimes exceeded beyond the realm of scientific aptitude. I will be able to utilize his lessons throughout my professional career. I would also like to thank my committee members, Dr. Thomas Friberg, Dr. Steven Little, and Dr. Martin Oudega, for their guidance and support throughout my doctoral candidacy. Their insights, as both mentors and collaborators, have contributed immensely to my growth and development.

I would also like to thank the members of the Wang Lab and our collaborators for their input and experimental expertise. I am truly grateful for everything you have done for me. A special thank-you to Dr. Daewon Park, Dr. Carlos Medina, and Tabitha Novosat, whose hard work was critical to the design and implementation of the experiments described henceforth. Thank you to Dr. Jin Gao, Dr. Keewon Lee, Dr. Mantosh Sinha, Dr. Kyobum Kim, Dr.

Zhengwei You, Dr. Hunghao Chu, Noah Johnson, Eric Jeffries, Robert Allen, Hassan Awada, Chelsea Stowell and Mirrah Almira for your encouragement and comraderie, to Deanna Rhoads for histological processing, and Callen Wallace for your imaging expertise. Additionally, I would like to acknowledge my undergraduate mentors, whose continued support has been critical to my pursuit of a doctorate: Dr. Angelo Lepore and Dr. Nicholas Maragakis.

Finally, I wish to acknowledge my friends and family, who have encouraged me through difficult times and provided me with love when I needed it most. My deepest gratitude goes to my fiancé and best friend, Dr. Srikanth Divi, whose love and devotion has kept me going; I owe everything to him. To my parents, Sara and Frank, whose unconditional faith in me is humbling; I am a better person because of them. To my future in-laws, Dr. Mahesh Divi and Kathy Divi, for welcoming me into their family with open arms. To my cousin Jon Soderberg and his wife Elizabeth, for being the siblings I always wished I had. Thank you to Peter and Elsa Soderberg, Norm and Jennifer Burstein, Frank and Betty Rauck and the rest of my family for their undying support. Without the guidance, mentorship, love and faith of this village, I would be nothing. I dedicate my thesis to them.

1.0 INTRODUCTION

Current clinical strategies fall short in treating central nervous system (CNS) injury and disease in a manner that minimizes patient stress while improving outcomes. Major organs of the CNS such as the visual system, spinal cord and brain are isolated from the systemic circulation due to the impermeable blood brain barrier systems, which severely limit the bioavailability of conventional, intravenously administered drugs; oftentimes high doses must be given to achieve efficacy, introducing considerable risk for adverse side effects. As such, materials-based approaches are actively being pursued as they offer a way to deliver therapies locally, reducing toxicity and increasing efficacy. However, successful clinical translation of drug and cell delivery technologies has yet to be achieved in part due to the immense complexity of the CNS, and inhibitory environments in and around the affected region [1]. The visual system and spinal cord each have a set of unique challenges that must be considered when formulating biomaterials for regenerative therapies, and a complete understanding of these obstacles will help drive the development of effective interventions.

1.1 OCULAR DRUG DELIVERY: INSIGHTS AND CHALLENGES

1.1.1 Significance

Efficient and effective ocular drug delivery is limited by the many barriers protecting the eye. While topical formulations such as eye drops and drug-eluting contact lenses have improved delivery to anterior targets (the cornea, iris, lens, anterior chamber, Figure 1), reaching the posterior segment of the eye (the retina, choroid, vitreous and optic nerve, Figure 1) poses a significant challenge. Posterior segment diseases such as age-related macular degeneration (AMD), retinitis pigmentosa, and diabetic retinopathy are among the leading causes of irreversible vision loss worldwide, affecting over 10 million people in the United States alone [2, 3]. Current treatments involve repeated long-term administration of therapeutics at high doses, imposing significant burdens on both patients and hospitals, and increasing the risk of adverse side effects. In recent years, the rapid evolution of biomaterials technology for drug delivery applications and an increased understanding of the physiology and pharmacokinetic properties of the eye have enabled researchers to design and implement new strategies for targeting the posterior segment. These new approaches hold great promise in combating vision loss and have the potential to reduce healthcare costs and increase quality of life for patients worldwide.

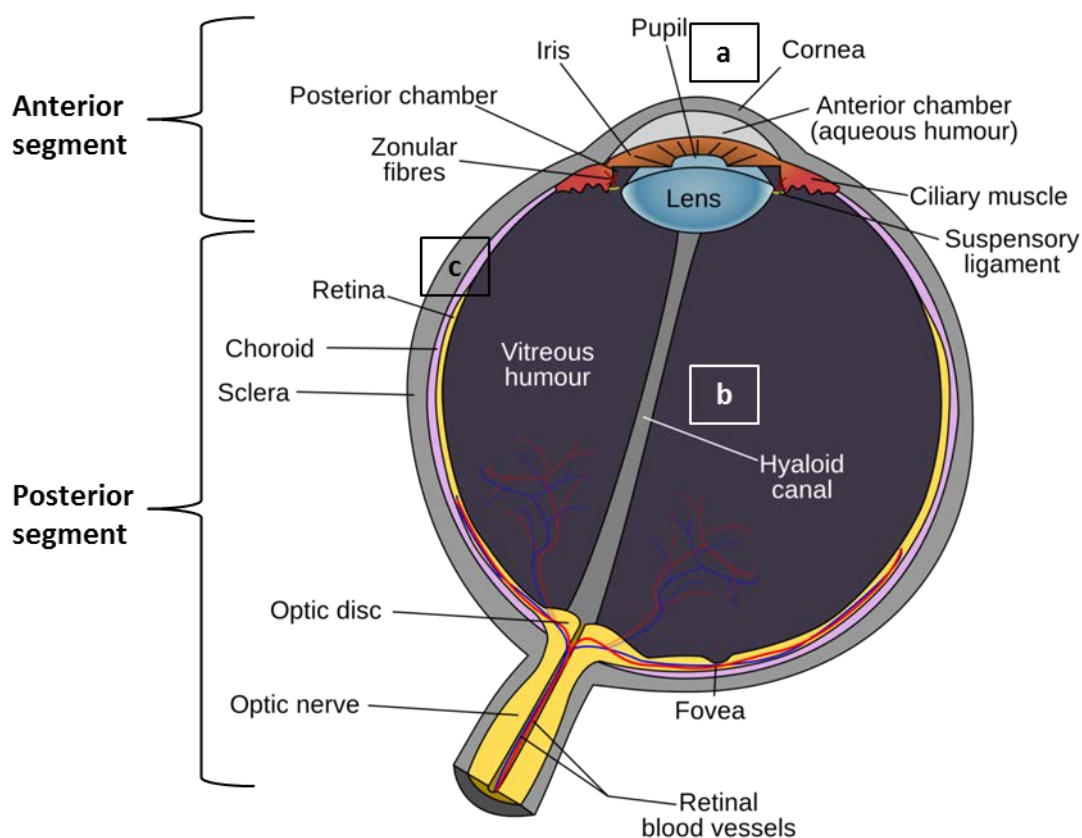


Figure 1. Anatomy of the eye and representation of ophthalmic drug delivery routes. Topical delivery via eye drops must diffuse across the anterior structures of the eye before reaching posterior targets (a).

1.1.2 Barriers to Efficient Posterior Segment Delivery

There are four principal routes employed to target drugs to the eye: topical, systemic, intraocular and periocular (e.g. subconjunctival and sub-Tenon injections) [4]. Each mode possesses strengths and weaknesses as summarized in Table 1, and the choice of delivery route is dependent on the target tissue and the drug being delivered. Topical administration (Figure 1, a) involves the use of eye drops, ophthalmic ointments, or gels; due to their ease of use and established safety, topical medications are the most commonly utilized formulation in ocular

treatment, especially for conditions affecting the anterior of the eye. However, much of the drug will be eliminated via the nasolacrimal duct, dilution by tears, and systemic absorption [5]. Additionally, the cornea presents an efficient barrier, composed of an epithelium with tight junctions which protect the eye from foreign materials [6]. Combined, these factors allow only about 5% of drug in an eye drop to permeate the cornea [4] and reach the aqueous humor, which necessitates frequent administration and results in poor patient compliance. With such limited permeation into the aqueous humor, the probability of therapeutic levels of topically administered drugs reaching the posterior of the eye is extremely low.

Systemically administered therapies also have limited effect in the eye. The blood-ocular barriers limit diffusion of drugs to the posterior segment and separate the eye from the surrounding tissue. The blood-retinal barrier, which separates the neural retinal tissue from the blood supply, consists of two separating levels: the endothelium of the vasculature within the retina, and the retinal pigment epithelium (RPE), which separates the entire retina from the more highly vascularized and leaky choroidal layer (Figure 1) [7]. Together, these barriers regulate the diffusion of molecules into the posterior segment. Even when drugs are capable of penetrating the blood-ocular barriers, low blood flow to the region means that large doses must be administered, increasing the risk for adverse effects.

Intravitreal injection offers the most direct access to the posterior segment (Figure 1b). However, this approach comes with inherent risks of endophthalmitis, retinal detachment, cataract, and uveitis [8, 9]. Intravitreally administered drugs often have rapid clearance and require frequent injections, imposing a significant burden on patients. Despite the risk of complications and inconvenience to the patient, intravitreal administration of anti-angiogenic

drugs for treatment of AMD remains the most common treatment modality, as it represents the best compromise among the administration routes.

Periocular injection (such as subconjunctival or sub-Tenon injection, Figure 1c) provides an alternative to intravitreal injection that involves administration of therapeutic agents into layers of tissue surrounding the eye. This route is advantageous because drugs must cross the sclera, which is more permeable than the cornea [10] and therefore most therapies easily reach the choroid. However, efficient delivery to the retina remains a challenge as drugs must pass through the choroid where systemic absorption is a concern [11], then cross the RPE which is highly impermeable and can be considered the rate-limiting step in getting drugs to the retina [12].

Table 1. Pros and cons of the different ocular drug delivery routes

Administration Route	Pros	Cons
Systemic (oral, intravenous)	<ul style="list-style-type: none"> • Ease of administration 	<ul style="list-style-type: none"> • Poor posterior segment delivery • High doses required • Adverse side effects
Topical (eye drops, ointments)	<ul style="list-style-type: none"> • Ease of administration • Good anterior segment delivery 	<ul style="list-style-type: none"> • Poor posterior segment delivery • Rapid drug clearance
Intravitreal	<ul style="list-style-type: none"> • Good posterior segment delivery 	<ul style="list-style-type: none"> • Invasive • Short half-life → repeated injections • ↑ risk of side effects (retinal detachment, endophthalmitis)
Periocular	<ul style="list-style-type: none"> • Delivery to anterior and posterior segments • Less invasive than intravitreal 	<ul style="list-style-type: none"> • Poor penetration to retina • Risk of subconjunctival hemorrhage

1.1.3 Bioengineering Strategies to Improve Ophthalmic Drug Delivery

In order to circumvent the challenges surrounding drug delivery to the posterior segment, a number of biomaterials-based solutions have been investigated. While non-biodegradable implants have demonstrated superior drug delivery and therapeutic effect, the necessity of a second procedure to remove the device once all drug has been expended introduces the risk for

unnecessary complications. Therefore, most of the focus of current ophthalmic drug delivery research has been on biodegradable delivery systems. There are several systems in the clinical trial stage and a number more that show promise in preclinical studies.

There are currently a handful of devices that are undergoing clinical trials in the United States. Ozurdex® (Allergan, Irvine, CA) is an injectable, rod-shaped implant composed of poly(lactic-co-glycolic acid) (PLGA) containing dexamethasone for treatment of macular edema and uveitis. This device releases dexamethasone for up to six months. In clinical investigations such as the HURON and GENEVA studies, Ozurdex ® implants significantly improved visual acuity in patients with posterior uveitis and macular edema for extended periods of time [13-15]. Verisome ® (Icon Biosciences, Sunnyvale, CA) is an injectable drug delivery system that forms a spherule upon intravitreal injection. It is a versatile system that can deliver a broad range of therapeutic agents for up to one year, and is currently in clinical trials for delivery of triamcinolone acetonide to treat uveitis [16].

A number of investigational implants also demonstrate promise for intravitreal delivery. Particulate formulations, for example, are a hot topic in ophthalmic drug delivery. Typically composed of PLGA, these formulations are capable of sustaining drug release for extended periods and demonstrate good biocompatibility [17-22]. Other materials studied include polyethylene glycol-coated cyanoacrylate nanoparticles to deliver tamoxifen, which significantly inhibited autoimmune uveoretinitis. When tamoxifen alone was delivered, the disease course was unaffected [23]. Chitosan nanoparticles have been studied as well and because they are naturally-derived, possess inherent biocompatibility. However, rapid drug release (on the order of hours) will likely limit their use to short-term applications [24, 25]. Micro- and nano-particles are versatile and effective; however harsh preparation conditions may make them unsuitable for

unstable drugs, and intravitreal injection of particle suspensions may cause vitreous turbidity, affecting visual acuity.

Liposomes, which are colloidal carriers composed of phospholipid layers ranging in size from 100-400 nm, are attractive due to their inherent biocompatibility and the ability to encapsulate both hydrophobic and hydrophilic drugs [26]. One study in rats found that when liposomes were used to deliver vasoactive intestinal peptide intravitreally, drug levels were 15 times higher at 24h in eyes injected with liposome-delivered drugs, compared to drug alone [27]. Liposome-mediated delivery, while promising, is limited by a relatively short residence time, instability, and little control over drug release kinetics [28]. Encapsulation within polymer scaffolds or gels could further sustain release from liposomes; liposomal technology itself however would be likely most appropriate for treatment of conditions where the therapeutic window is a period of days to weeks.

In situ-forming biodegradable gels are promising for intravitreal drug delivery as they can incorporate a multitude of drugs at varying doses. In some cases, microparticles and /or liposomes have been embedded within intraocular hydrogels to further prolong drug release [29, 30]. Thermoresponsive hydrogels for intravitreal applications have been explored using non-degradable poly(*N*-isopropylacrylamide) (PNIPAAm)-based hydrogels, as well as biodegradable poly(2-ethyl-2-oxazoline)-*b*-poly(ϵ -caprolactone)-*b*-poly(2-ethyl-2-oxazoline) gels, PEG gels, and chitosan/alginate polysaccharide gels [31-36]. These studies demonstrated that intravitreal injection of synthetic hydrogels caused no long-term (up to 2 months) changes to retinal function, intraocular pressure or histomorphology in rabbits. However, non-degradable PNIPAAm gels would require surgical removal. Biodegradable injectable hydrogel

formulations, while not extensively studied yet, are garnering more interest in the ophthalmology field as effective and practical drug delivery vehicles.

In summary, the anatomy and physiology of the ocular system presents a unique set of challenges which limit effective treatment of ocular disease. An increased understanding of these barriers and rapidly evolving biomaterials technology are continuing to drive innovation in the field of ocular drug delivery such that a new standard of care can be achieved.

1.2 BIOMATERIALS FOR SPINAL CORD REPAIR

(Note: Portions of this chapter were published previously as: Gumera C & Rauck B, Wang Y. Materials for central nervous system regeneration: bioactive cues. *Journal of Materials Chemistry* 2011;21:7033-51 and is reproduced here with permission from the publisher.)

Complete restoration of function in damaged nerves will significantly improve the lives of affected individuals and reduce the associated socioeconomic costs. In the U.S., it is estimated that 12,000 individuals sustain SCI each year, while more than 250,000 are already affected [37]. Patient care is estimated to cost more than \$4 billion annually, a figure that does not include an additional \$2.6 billion due to loss of productivity [38].

Injuries to the CNS are extremely difficult to reverse, with no current treatment capable of completely restoring function after traumatic injury. Depending on the severity of the injury, patients can experience respiratory complications, arrhythmias, blood clots, bladder and bowel problems, loss of sensation and paralysis [39, 40]. Currently the most commonly-used treatment for acute SCI is methylprednisolone, a synthetic glucocorticoid which is capable of reducing

inflammation and mitigating the progression of secondary injury [41]. However, to be effective high doses must be delivered systemically over prolonged time periods, introducing the risk of deleterious side effects. Intensive physical therapy can also help patients regain motor control, but is not always successful, especially in cases of severe trauma. As such, numerous alternative strategies are actively being researched including cell therapy, delivery of biomolecules, and implantation of biomaterial conduits [42-45]. Many of these bring hope that significant improvement in clinical outcome can be achieved in the near future for people suffering from serious nerve damages.

Materials science and engineering is an integral part of many treatment methods under investigation. Such strategies are attractive because the complexity of CNS injury likely will necessitate a multi-faceted approach to regeneration. Materials of both synthetic and natural origin have been investigated for use as nerve guides, scaffolds, and drug and cell delivery vehicles [42-44, 46], with specific attention given to biodegradable materials. Non-degradable materials are impractical for use the CNS because they remain in the body indefinitely and can cause nerve compression as well as chronic inflammation, and require a second surgery for removal [47]. “Bioactive materials” – materials that improve the interaction with cells and tissues to enhance regeneration—will enable such combinatorial strategies [48-53]. Drug delivery, immobilization of ECM molecules, neurotransmitter-based materials, topographical cues and electrically-conducting materials are just a few examples of ways bioactivity can be imparted into materials (**Table 1**), and when utilized in combination may maximize the regenerative capacity of the CNS.

Table 2. Commonly used base materials may be combined with one or more bioactive cues to create bioactive materials to facilitate nerve regeneration.

Base Material		Bioactive Cues
Naturally-derived	Alginate Cellulose Chitosan Collagen Gelatin Fibrin Fibronectin Hyaluronan Keratin Silk	<u>Neurotrophic factors</u> BDNF [54-56] EGF [57-59] FGF-1 [60]+ FGF-2 [57, 61] GDNF [62] NGF [63, 64] NT-3 [54, 65-71]
Synthetic	PCL PEG PGA, PLA, PLGA PGS PHB Self-assembling peptides	<u>ECM</u> IKVAV [53, 56, 72-75] Laminin [50, 76, 77] RGD [51, 78, 79] RNIAEIIKDI [49] Tenascin-C [80, 81] YIGSR [72, 75, 82, 83]
		<u>Neurotransmitters</u> Acetylcholine [48] Dopamine [84]
		<u>Other</u> Chondroitinase ABC [65, 85] Electrical conduction [86-97] Methylprednisolone [98, 99] Poly-lysine [100-103] Contact guidance [104-110]

1.2.1 Nervous System Biology

1.2.1.1 Central Nervous System Structure and Organization

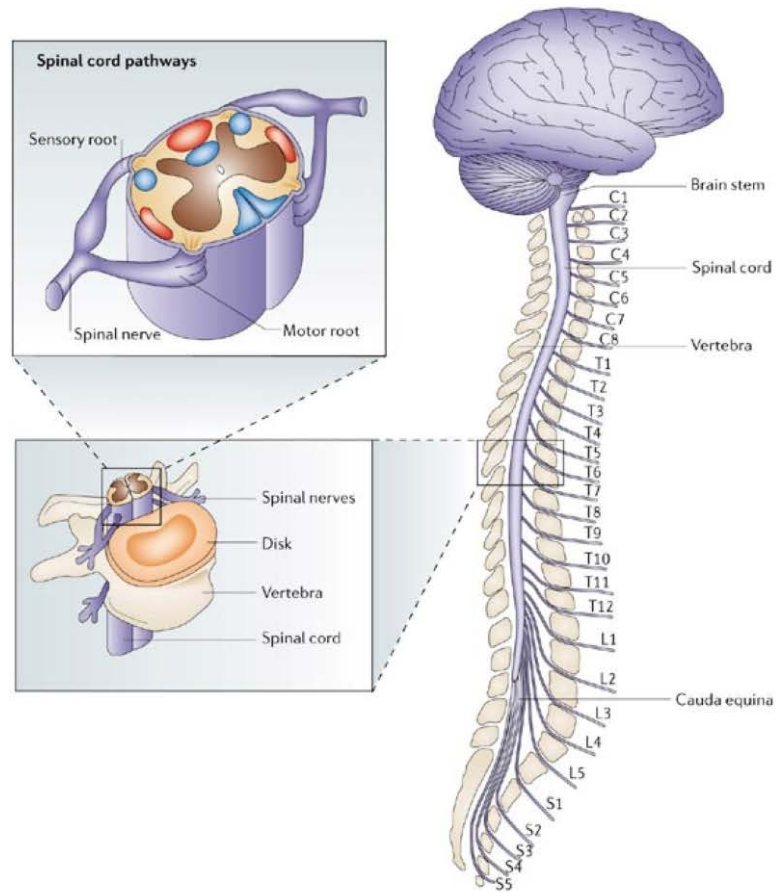
Understanding the organization and biology of the nervous system is essential to formulating materials-based solutions to the challenges in nerve repair and regeneration. The CNS is composed of the brain and spinal cord and is responsible for conducting and interpreting signals between the brain and the body (**Figure 2A**). The PNS connects the CNS to the rest of the body. Though the two systems are intricately connected, each possesses a unique environment which results in drastically different responses to traumatic injury. This difference

is primarily attributable to the presence of Schwann cells in the PNS, which rapidly infiltrate the injury region and secrete growth-promoting cytokines [111], thus rendering the PNS more permissive for regeneration. The lack of Schwann cells, glial scar formation and the presence of growth inhibitory proteoglycans combine to generate an environment that is not conducive to regeneration in the CNS.

There are two primary cell types in the CNS: neurons and glia. Neurons form specific contacts (synapses) with each other via their axons and dendrites to create neuronal networks. They secrete chemical messengers known as neurotransmitters at their synapses, which propagate electrical signals. Glial cells, such as astrocytes and oligodendrocytes, support, nourish and protect neurons. Oligodendrocytes form myelin sheaths around axons, which increase the conduction velocity of action potentials. Myelin contains approximately 70% lipids and 30% proteins [112] including myelin basic protein, myelin oligodendrocyte glycoprotein and myelin-associated glycoprotein. Astrocytes promote oligodendrocyte myelinating activity, form the blood brain barrier, modulate neurotransmitter uptake and release, and maintain synaptic plasticity [113]. Microglial cells are also present in the CNS; they scavenge cell debris and secrete molecules that affect the immune and inflammatory response. In addition to supporting and nurturing neurons, glia also play an important role in the response to trauma and regeneration [114].

The tissue of the CNS is composed of two distinct regions: white matter and grey matter. White matter contains myelinated axon tracts and glial cells, and constitutes the communication networks between grey matter regions. The high lipid content of myelin gives this tissue its white appearance. The grey matter contains neuronal soma, glial cells and has a high capillary density. Its function is to route motor and sensory stimuli to interneurons via chemical synapse activity in

order to generate a response. Interneurons are cells which act as intermediaries between afferent neurons, which conduct impulses from the body toward the CNS, and efferent neurons, which conduct impulses away from the CNS towards the body. The tissue in both the brain and the spinal cord is covered by three layers of connective tissue: the dura mater, arachnoid mater, and pia mater, collectively referred to as the meninges. The subarachnoid space, between the arachnoid and pia mater, is filled with cerebral spinal fluid. The role of the meninges is to protect the CNS (**Figure 2B**). The ECM of the CNS is composed of hyaluronan, adhesive glycoproteins such as tenascin, laminin, netrin and reelin, and proteoglycans such as neurocan, versican and brevican. It serves to organize the CNS structure, guide axon growth and development, and store growth factors and cytokines. Additionally, the ECM modulates the mechanical properties of the CNS.



Copyright © 2006 Nature Publishing Group
Nature Reviews | Neuroscience

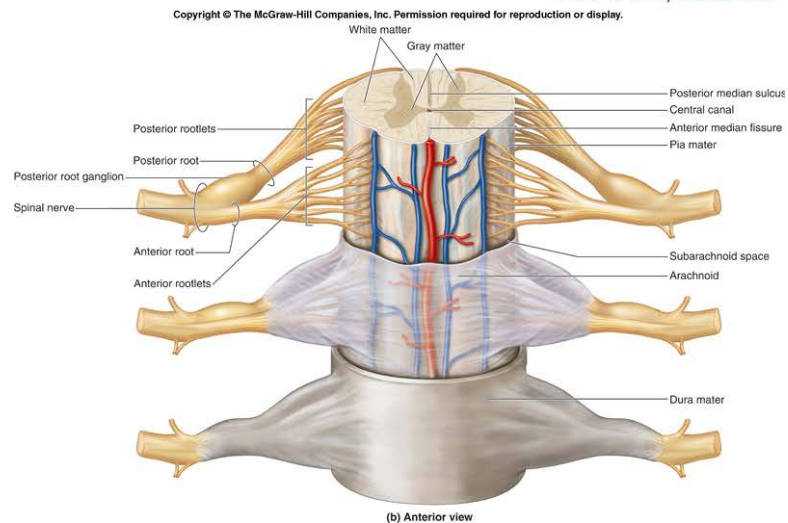


Figure 2. Structure of the CNS. The spinal cord has four segments (C: cervical; T: thoracic; L: lumbar; S: sacral) which connect to discrete body regions. These segments connect to the brain via ascending (red) and descending (blue) pathways which transmit neural impulses to and from the brain, respectively (B).

1.2.1.2 Response to Injury

Traumatic injury and degenerative diseases considerably alter the architecture and function of nerves. The regenerative ability of nervous tissue is highly influenced by glial cells, and permissive and non-permissive cues in the environment (**Figure 3A**). Specifically, the CNS has a limited capacity for spontaneous regeneration following disease or injury compared to the PNS, which may be attributed to the following: 1) mature neurons are post-mitotic and exist in a quiescent, non-dividing state; thus their intrinsic ability to regenerate declines with age; 2) a lack of trophic—or nutritional—support, which is provided by Schwann cells in the PNS [111]; 3) the presence of myelin debris and myelin-associated inhibitors [117]; and 4) the mechanical barrier imposed by the glial scar [118].

Trauma to the CNS occurs in two phases. The primary acute stage is the immediate response to the mechanical insult. It is characterized by cell death at the injury epicenter, disruption of local blood flow, and inflammation. Axons traversing the injury region are severed, leaving connections distal to the injury site isolated from their soma. Disruption of cellular membranes causes leakage of intracellular contents and an increase in the extracellular Ca^{2+} concentration, which contributes to further cell death. Incomplete oxygen metabolism results in the generation of reactive oxygen species, lipid peroxidation and accumulation of endogenous toxins which in turn attack intact membranes on neighboring cells. Vascular damage and inflammation result in edema of the nervous tissue.

The second, chronic phase of injury can span months to even years. Many of the events that occurred in the initial phase continue, resulting in atrophy of the damaged tissue. Reactive astrocytes and meningeal fibroblasts ultimately form a glial scar around the injury epicenter. Reactive astrocytes also secrete inhibitory molecules such as chondroitin sulfate proteoglycans.

Additionally, inhibitory myelin debris, such as myelin-associated glycoprotein and Nogo accumulate due to damaged myelin sheaths and oligodendrocyte death. The scar persists, serving to isolate remaining healthy tissue from damaged tissue.

The cascade of events that occurs following trauma to the CNS is complex, illustrating how many factors inhibit axon regeneration. The glial scar presents a mechanical barrier to growing axons, while myelin debris and proteoglycans constitute biochemical barriers, as illustrated in **Figure 3A**. Utilization of bioactive materials to neutralize the inhibitory environment or encourage the growth of severed axons has enormous potential to improve neural regeneration (**Figure 3B**). More extensive information on the molecular and cellular events following nerve injury and therapeutic interventions in use can be found in several recent reviews [42, 44, 119-122].

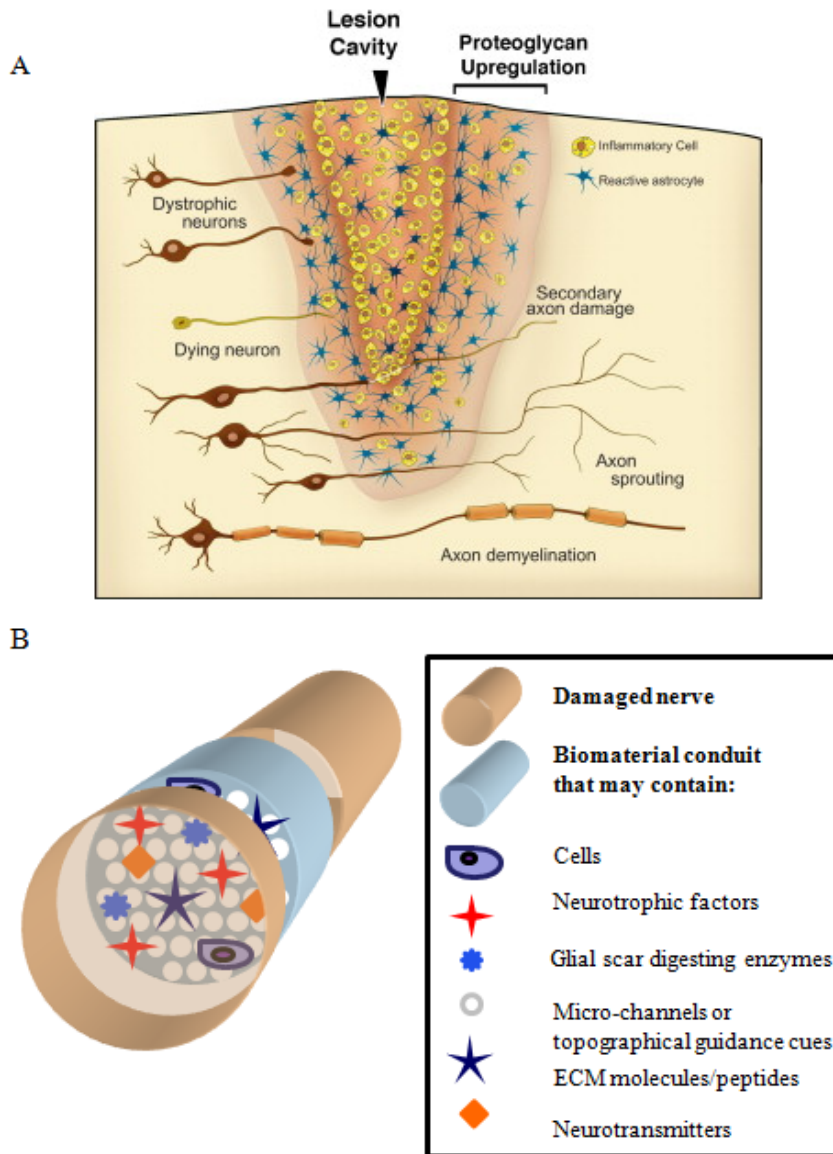


Figure 3. Following trauma, an influx of inflammatory cells and reactive astrocytes causes the lesion cavity to expand (A). Reactive astrocytes secrete inhibitory molecules, resulting in secondary damage to axons spared by the initial insult. This causes demyelination and increased concentrations of myelin-associated inhibitors. Combined, these factors inhibit regeneration [122]. (B) Biomaterials-based therapies can promote neural repair. They can be designed as conduits or lesion-filling scaffolds and can incorporate various bioactive factors which interact with surrounding cells and tissues to elicit a pro-regenerative response.

1.2.2 Materials Used in Nerve Regeneration

A wide range of materials have been studied for use in the CNS, and can be classified based on their physico-chemical properties. These characteristics are cell-independent, and are the basis for defining three categories of base materials – natural, biodegradable synthetic, and bio-stable synthetic.

1.2.2.1 Natural Materials

Naturally-derived materials such as polysaccharides and glycosaminoglycans have been used extensively in tissue engineering applications. They possess good biocompatibility and may exhibit inherent bioactivity that can facilitate cell recognition and tissue integration. Moreover, this class of materials can be degraded by enzymes in the body. Examples of biodegradable natural materials include—but are not limited to—chitosan, collagen, fibronectin, fibrin, hyaluronic acid (HA) and Matrigel.

Chitosan is a polysaccharide derived from the full or partial deacetylation of chitin, found in crustacean shells. By altering the degree of deacetylation and thus the amount of positive charges on chitosan, degradability and cell adhesiveness can be controlled. It exhibits pH sensitivity, forming a highly permeable gel at neutral pH [101]. Its ease of use and long in vivo lifetime make it appealing for nerve regeneration, where long recovery times are typically required. Moreover, culture of hippocampal neurons on chitosan membranes form extensive neural networks by 7 days, comparable to culture on poly-D-lysine-coated controls [123]. Recent evidence also suggests that chitosan itself is neuroprotective, as it has the capacity to seal damaged neuronal cell membranes, and limit the extent of lipid peroxidation and reactive oxygen species formation following injury [124, 125].

Collagen has been widely explored for tissue engineering applications due to its abundance, biocompatibility, and ease of modification. Because it is present in the ECM, collagen is inherently cell-adhesive and is frequently used for three-dimensional cell culture studies [126, 127]. By varying the degree of cross-linking the strength, porosity and degradability of collagen can be controlled. Thus it is used in many different forms such as tubes, gels, membranes and coatings [83, 128-131]. For example a collagen-filament scaffold implanted into a rabbit SCI model resulted in axon growth through the injury epicenter and partial restoration of function as measured by the BBB test [132]. While BBB scores were significantly higher in treated groups, low scores overall (4.7 ± 2.3 , and 2.8 ± 0.5 in controls, out of a total possible score of 21) suggest that functional recovery was limited to modest movement of hind limb joints. This indicates that substantial improvements need to be made to collagen to enhance its regeneration-promoting abilities.

Mats made from the ECM glycoprotein fibronectin have been shown to be neuroprotective and permissive for axonal growth [133]. In addition to supporting repair, the mats integrated into spinal tissue with little cavitation, suggesting fibronectin may inhibit the progression of tissue damage. Much like collagen, fibronectin is present in the ECM and binds integrins on cell surfaces. It has been explored for use in CNS regeneration both as a base material and as a coating for other materials [130, 133]. Matrigel, a gelatinous mixture of proteins secreted by mouse sarcoma cells, forms a hydrogel at room temperature. It is composed of basal membrane extract and includes ECM proteins such as laminin, collagen IV, heparin sulfate proteoglycans and growth factors [134]. It is valuable as an ECM mimicking matrix to study 3-D neural cell culture. Matrigel was also used as a cell delivery vehicle in order to improve the viability of human neural stem cells implanted in a canine model of SCI [135].

Though Matrigel is a powerful research tool, its tumorigenic origin will likely present significant regulatory challenges for translation to human applications.

Fibrin is another material investigated for CNS regeneration. Because it is a natural wound-healing matrix, it can be autologously-obtained, and has tailorable mechanical and degradation properties. Implanting fibrin scaffolds in rats two weeks after SCI resulted in decreased glial scarring and enhanced axon sprouting compared to untreated controls [136]. The most significant work done using fibrin in the CNS is that of Sakiyama-Elbert and colleagues, who have modified fibrin into a versatile and effective drug delivery system (See '1.2.3.1 Neurotrophins') [65, 66, 69-71, 136, 137].

Hyaluronic acid is a long, negatively-charged glycosaminoglycan, and a major component of CNS ECM. A linear copolymer of D-glucuronic and N-acetyl-D-glucosamine, HA has been frequently modified with bioactive agents for drug delivery to the CNS. It has been shown to promote angiogenesis at low molecular weights and inhibit glial scarring at high molecular weights [51]. In vitro, HA hydrogels cross-linked with PEG promoted 50% longer neurite outgrowth from DRGs compared to fibrin gels [138]. Additionally, Shoichet and colleagues [139, 140] developed an injectable blend of HA and methylcellulose in order to create a fast-gelling drug delivery system, which will be discussed further in Section 1.2.3.2.

Agarose, a polysaccharide obtained from agar, has also been studied extensively for CNS regeneration applications. Because it does not evoke a significant inflammatory or immune response, integrates well with CNS tissue and is inherently non-cell adhesive, agarose is useful for guided axon growth. It has been fabricated into nerve guidance scaffolds with uniaxial channels through both freeze-drying and templating techniques [141, 142]. It has also been used as a delivery system for therapeutic biomolecules such as methylprednisolone and chondroitinase

ABC [85, 99]. However, agarose is not biodegradable; thus its ultimate clinical use may be limited. This list of materials is not meant to be exhaustive, but provides an idea of the contribution that naturally-derived biomaterials make to the field of CNS regeneration. Their versatility enables them to be used in a variety of forms, as base materials and as modifications or coatings of other base materials.

1.2.2.2 Biodegradable Synthetic Materials

Batch-to-batch variability and the potential for disease transmission with mammalian-derived materials are two challenges faced when using natural materials. In these aspects, synthetic materials are advantageous because stringent synthesis and manufacturing protocols avoid these complications. Generally, synthetic materials can be processed into a variety of physical structures. Unlike natural materials, however, synthetic materials do not have inherent bioactive cues, and need modification to possess bioactivity. Biodegradable synthetic materials can be degraded, absorbed or remodeled by the body, ideally being replaced by new tissue as the nerve grows to minimize physical interference with the regenerating nerve. Both the material and its degradation products must be non-toxic. The biodegradable synthetic materials described here include PGA, PLA, PLGA, PCL, PHB, PGS and synthetic peptide amphiphiles.

PGA, PLA and their copolymers (PLGA) belong to the family of poly(α -hydroxyacids) that have been used in tissue engineering applications due to their biocompatibility, biodegradability and wide availability. The Neurotube, composed of PGA and manufactured by Synovis, was the first biodegradable synthetic peripheral nerve guide approved by the FDA for clinical use [143]. Moreover, PLGA has been approved by the FDA for use in a wide range of therapies. It is especially beneficial for drug delivery because its degradation rate is easily controlled by varying the ratio of glycolic acid to lactic acid. It has also been used to study the

effects of mechanical properties, topography, and drug and cell delivery on neurite outgrowth [144-152].

Polycaprolactone (PCL), also a component of several FDA-approved devices, has also been used in the CNS. Compared to PLGA, PCL degrades more slowly and results in fewer acidic degradation products. It has been shown to elicit a weaker inflammatory response—as demonstrated by fewer activated macrophages and astrocytes—than PLGA when implanted in the rat brain [146]. PCL is easily manipulated into a variety of shapes and sizes, and is commonly used for studying the effect of material topography on neurite outgrowth [104-106, 110, 153, 154].

Polyhydroxybutyrate (PHB) and poly(glycerol sebacate) (PGS) have been studied for nerve regeneration, albeit less extensively, with good biocompatibility and promising results [155, 156]. PHB is a polyester that is synthesized in microorganisms under nutrient deficiency, and can be produced commercially using a fermentation process [157]. It exhibits good biocompatibility and is capable of supporting axon growth in vivo [155]. PGS is an elastomer that degrades by surface erosion and possesses mechanical properties close to those of nervous tissue. PGS exhibits good biocompatibility in the PNS, where it elicits significantly less inflammation and fibrosis than PLGA [156, 158]. Though PGS hasn't been used in CNS injury models, its properties make it a viable candidate for future study.

Peptide amphiphiles are synthetic molecules containing hydrophobic and hydrophilic domains, enabling them to self-assemble into cylindrical nanofibers when the ionic strength of the environment changes [74, 159]. These molecules were designed such that they display a bioactive peptide sequence at their hydrophilic end. Peptide amphiphiles form a gel-like 3-D

network and have been used both in vitro and in vivo to study the effect of the laminin peptide IKVAV on neural growth and repair (See 2.3.3 ECM Peptides).

Most synthetic materials have little to no inherent biological activity. Therefore current studies using synthetic biodegradable materials involve various types of coatings and/or modifications – either with ECM peptides, growth factors or other therapeutic agents – to impart bioactivity to the material and make it more permissive for neuronal growth. In the following sections, we will highlight select modification strategies in order to elucidate the critical role bioactive cues play in nerve regeneration.

1.2.3 Materials-Based Delivery of Bioactive Agents

The failure of cells to activate regeneration-associated genes and the accompanying lack of neurotrophic support are major factors that hinder nerve repair [160, 161]. Addition of neurotrophins, antibodies or other therapeutic agents after nerve injury can provide neuroprotection and enhance axonal growth. For example, injections of BDNF or NT-3 after SCI significantly increase the survival of rubrospinal neurons [162] and promote axonal growth into the distal spinal cord [54]. Other neurotrophins studied include neurotrophin-4/5, GDNF, and NGF, all of which can preserve CNS tissue [42]. Additionally, NT-3 and BDNF stimulate oligodendrocyte proliferation and increase myelination [163]. Antibodies and other therapeutic agents, such as anti-inflammatory drugs and glial scar digesting enzymes can also suppress the progression of secondary damage and promote neurite sprouting [41, 57, 140, 164].

Utilizing biomaterials to deliver such therapies may enable spatio-temporal control over their presentation, which is important for guiding nerve growth. Moreover, biomaterial delivery matrices protect and stabilize their cargo, which typically have short half lives in the body when

injected alone [165, 166]. Biomaterials achieve local, sustained delivery of therapeutic agents through one of three methods: physical entrapment, non-covalent interactions, or covalent incorporation. In effect, a biomaterial increases the bioavailability of a therapeutic factor by localizing it to the desired site of delivery and preventing its degradation once inside the body. The ability to deliver multiple drugs or growth factors in a controlled manner is also desired, to target the multitude of neural and inflammatory cells involved in nerve injury and regeneration. As such, delivery using biomaterials may modulate the environment of the injury site, provide neuroprotection and induce axon growth. In this section we will discuss biomaterials-mediated delivery of neurotrophins, proteins and drugs.

1.2.3.1 Neurotrophins

It has been shown that a 7 day continuous infusion of neurotrophins reduces axonal degeneration to a greater extent than a single, bolus injection [167]. Since most growth factors have a short half-life in vivo they need to be administered continuously; however continuous infusions are invasive, and cumbersome from a clinical standpoint. Biodegradable materials offer a viable solution to this challenge, for they can protect neurotrophins as well as present them to cells in a favorable manner. Such systems can be implanted in the CNS to release neurotrophins over time via diffusion and material degradation. In order to be effective, neurotrophin delivery systems must be non-toxic and provide a desired delivery profile. Properly-designed delivery systems hold immense promise for improving nerve regeneration.

When neurotrophins are physically embedded within a biomaterial, their release is controlled by the porosity, structure, geometry and degradation rate of the material, and the diffusive properties of the growth factor. A preliminary study using *PLA-block-PEG-block-PLA* copolymer hydrogels delivered NT-3 in vivo for more than two weeks, enhancing behavioral

recovery when compared to the hydrogel alone [168]. Similarly, a PLA tubular scaffold containing BDNF was used to treat acute SCI, enhancing neuronal survival and rapid axonal growth into the implant compared to PLA alone [169]. However a lack of axonal penetration into the distal cord and no behavioral improvement over controls indicate BDNF alone is insufficient to achieve complete neural repair. These studies suggest that combination therapies are necessary, and delivery systems that rely upon physical entrapment offer the advantage of being able to incorporate multiple growth factors or bioactive cues.

Neurotrophins can be incorporated into polymeric carriers such as micro- or nanoparticles to further sustain their release. Chitosan-NT-3 carriers were found to maintain the viability of rat NSCs as well as reduce the dosage of NT-3 required for the survival and differentiation of the cells [67]. When this system was implanted in a rodent model of traumatic brain injury, extensive neuronal fibers were found in the lesion epicenter and glial scarring was reduced compared to untreated controls and treatment with empty chitosan carriers [68]. However, no functional recovery was observed. Another group demonstrated that PLGA nanoparticles delivering GDNF preserved neuronal fibers at the injury site which resulted in significantly better behavioral recovery than empty PLGA microspheres [62]. However, glial activation was not reduced, further suggesting the potential benefit a combination of growth factors would provide.

Non-covalent association is typically achieved by exploiting the electrostatic properties of neurotrophins; negatively-charged polymers such as heparin bind positive molecules and entrap them, thus slowing their release. Sakiyama-Elbert and colleagues modified fibrin gels in order to create a heparin-based delivery system for controlled growth factor release [137]. They synthesized a bifunctional peptide containing a fibrin-binding substrate at its N-terminal and a

heparin-binding sequence at its C-terminal. The peptide in turn binds heparin, which then associates electrostatically with growth factors in the matrix. This system has been used to successfully deliver GDNF, NGF, NT-3 and PDGF to both the CNS and PNS without compromising the bioactivity of the growth factors [64-66, 69-71, 170, 171]. Controlled delivery of NT-3 to spinal cord lesions was particularly effective in the short term, resulting in increased neuronal fiber sprouting and cell migration into the lesion at 2 weeks compared to unmodified fibrin gels (**Figure 4**) [70]. However at 12 weeks there was no significant difference in functional recovery between the experimental groups and saline controls [71]. By improving this drug delivery system such that it has a longer in vivo lifespan, the time period over which neurotrophins are delivered can be extended, and may promote sustained functional recovery. Since many different growth factors bind to heparin, this system also allows delivery of combinations of growth factors, although this has not yet been extensively studied.

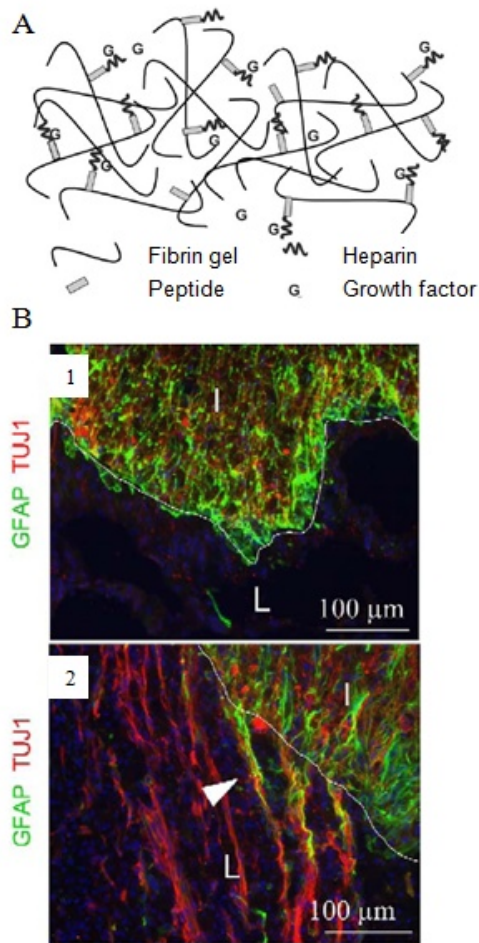


Figure 4. A heparin-based delivery system generated from modified fibrin gels (A) used to deliver NT-3 causes infiltration of neurons (red) and astrocytes (green) into spinal cord lesions (B, 2) NT-3 delivery caused more neuronal growth than TBS-injected controls (B,1). I: intact cord; L: lesion.

These investigations show the utility of growth factor delivery to enhance the regenerative capacity of natural and synthetic biomaterials. Many challenges remain to be overcome, such as increasing the loading efficiency, improving stability and maintaining bioactivity. As new information emerges about specific combinations of growth factors and optimal delivery conditions, materials scientists can design delivery systems specifically tailored towards the CNS environment.

1.2.3.2 Other Therapeutic Agents

In addition to neurotrophic factors, biomaterials can be used to deliver other therapeutic agents, such as antibodies, anti-inflammatory drugs and other biomolecules that provide neuroprotection and inhibit secondary injury progression. Such systems are especially attractive for the delivery of larger molecules to the CNS, because the blood brain barrier inhibits their diffusion from the circulation into nervous tissue. For example the Nogo-66 receptor antagonist is capable of promoting neurite extension by blocking the inhibitory effects of Nogo, a myelin-derived protein [172]. Covalent immobilization of Nogo-66 receptor antibodies to HA gels enhanced neuronal migration and growth in vivo [173, 174]. It even demonstrated the capacity to promote recovery of limb function in a rodent stroke model. Most recently a combination of Nogo antibody and poly-L-lysine in an HA hydrogel enhanced the viability and attachment of primary hippocampal neurons over either modification alone [52]. This latter study once again demonstrates the promise of combination therapies where the best results may be obtained by not one but many factors.

ChABC is another important factor influencing nerve regeneration. It is a bacterial enzyme which digests inhibitory CSPGs, which are upregulated following CNS injury. ChABC promotes sprouting and functional recovery after injury to the CNS, but is limited by its instability at body temperature [164]. To overcome this problem and design a system capable of delivering bioactive chABC for extended periods, Lee and colleagues [85] developed a thermostabilized variation of chABC using the sugar trehalose. By encapsulating chABC/trehalose molecules in hollow lipid microtubes and embedding them in agarose gels, the bioactivity of chABC was preserved for up to 2 weeks in vitro. Additionally, this system effectively digested CSPGs in vivo, as evidenced by immunostaining for CS-56. Using a

biodegradable hydrogel to deliver thermostabilized chABC would further increase its utility for clinical translation.

A number of other therapeutic molecules have been delivered via the HAMC gel system developed by Shoichet's group. HA gives the gel mechanical strength, while methylcellulose enables injectability. Erythropoietin, nimodipine, NBQX (a sodium channel blocker), human IgG (Immunoglobulin G) and several growth factors have all been delivered from HAMC over periods ranging from days to weeks, depending on the drug [57, 61, 140, 175]. This system is also capable of delivering molecules such as nimodipine, which possess limited solubility in aqueous environments. In order to vary the release time, drugs were incorporated into PLGA microparticles, which were then embedded in the HAMC gels. This stabilized the system and prolonged release to more than one month *in vitro* [57]. The HAMC system is a good example of one that is capable of delivering several different types of therapies, and would be particularly suited to study the efficacy of combination treatments. However *in vivo* delivery and degradation needs to be more thoroughly examined, as it should be capable of delivering therapeutics for several weeks.

Similarly, PLGA nanoparticles have been used to deliver a plethora of biomolecules at varying rates, including methylprednisolone [98, 99, 152, 176, 177]. PLGA micro- and nano-particle drug delivery systems are attractive due to their injectability, biocompatibility, and capacity for customized drug release. Additionally, they can be used alone or in combination with other materials, such as nerve conduits [176] or films [152]. The major advantages of degradable biomaterials-based delivery systems are that they (1) only require a single surgery for implantation, (2) can be designed to deliver drugs at a specific dose over a specific period of time, (3) localize delivery to a specific region of interest, and (4) protect their contents from

degradation, thus reducing the required dosage. As such, properly-designed drug delivery systems have huge implications for CNS repair.

Though much progress has been made in developing biomaterials for nerve regeneration, significant functional recovery *in vivo* has been rare. Substantial challenges remain, such as finding the optimal combination of material and bioactive cues that both promote neurite outgrowth and inhibit growth inhibition. Additionally, a better understanding of developmental biology and wound healing will greatly help regenerative efforts. Insights in neurogenesis and the molecular changes after trauma will inspire the design of new biomimetic materials and treatment strategies. Regeneration of the CNS is complex and challenging; the extent to which we are capable of reversing loss of function due to injury or disease remains unknown. What is certain is that nerve regeneration is an exciting area of research which faces great challenges and offers substantial opportunities for materials scientists to improve the lives of patients suffering nerve injuries.

1.3 OBJECTIVES

The objective of this work was to study the formulation and application of polymer-based delivery systems for use in the eye and CNS.

1.3.1 Objective 1: Deliver bevacizumab intravitreally using a biocompatible reverse thermal gel

As previously discussed, the efficacy of intraocular drug delivery is limited by the short half-life of drugs, uptake by the systemic circulation, and diffusive barriers within the eye tissues. To this end, we sought to investigate novel drug delivery formulations which can improve ocular drug delivery. A functionalizable, biodegradable temperature sensitive gel, poly(ethylene glycol)-poly(serinol hexamethylene urethane)(ESHU) is a solution at room temperature and undergoes phase transition to form a physical gel at body temperature. These features render ESHU injectable, and enable it to be combined with a multitude of molecules and proteins for therapeutic sustained drug delivery. Additionally, the potential for hydrogen bond formation between the ESHU backbone and therapeutic molecules may sustain release further. In order to test the hypothesis that ESHU can sustain the release of intravitreal drugs, we chose to focus on bevacizumab (Avastin®), a VEGF antibody that inhibits angiogenesis and is widely used by ophthalmologists to treat choroidal neovascularization. We first sought to successfully formulate the ESHU-bevacizumab delivery system, and determined its ability to release bevacizumab in vitro. Additionally, the cytocompatibility with ocular cells was studied. Next, the delivery system was injected into rabbit eyes to assess the effect of the gel's presence on inflammation, intraocular pressure and retinal integrity. Finally, the ability of ESHU to sustain bevacizumab release in vivo was examined.

1.3.2 Objective 2: Improve the survival of transplanted bone marrow stromal cells in a rat model of spinal cord injury.

Transplanted cells survive poorly in the injured spinal cord. The presence of inflammatory cytokines, reactive oxygen species, and inflammatory cells in the injury environment inhibit the growth and integration of transplanted cells which ultimately results in their death. Consequently, the reparative potential of these cells is eliminated within a few days. We hypothesized that transplanting the cells in ESHU gels would increase their survival, and therefore improve outcomes in injured rats. We tested our hypothesis in vitro by culturing BMSCs under conditions of oxidative stress, and in vivo by utilizing a contusion model of rat SCI.

1.3.3 Objective 3: Study the effect of controlled growth factor release to the injured spinal cord using a coacervate-based protein delivery system.

While improved cell transplant survival does improve outcomes in rats following SCI, we recognize the need for a combinatorial approach to further promote transplant survival and improve outcomes. With this in mind, we hypothesized that growth factor delivery to the injured spinal cord can be more efficacious when delivered via an injectable coacervate. Ultimately, the goal will be to combine growth factor and cell delivery. However, we must first test the growth factor delivery system in vivo. This system is composed of poly(ethylene argininyaspartate diglyceride) (PEAD), a polycation which binds heparin through electrostatic interactions. The PEAD-heparin system in turn is capable of binding a multitude of growth factors, making it attractive for treatment of SCI. We began by investigating sonic hedgehog (Shh), which is a

powerful morphogen involved in many processes in the developing CNS. Shh is not highly expressed in the adult mammalian CNS but is present throughout adulthood in zebrafish, whose nervous systems regenerate after injury. This suggests a potential role of Shh in the ability of the spinal cord to repair itself. We employed the same rat contusion model of SCI and injected the coacervate-Shh system directly into the injury region. We performed exhaustive behavioral and histological analysis in order to assess the effect of controlled Shh release on clinical outcomes.

2.0 FORMULATION AND CHARACTERIZATION OF REVERSE THERMAL GEL FOR OCULAR DRUG DELIVERY

(Note: This chapter was published previously as: Park D, Shah V, Rauck BM, Friberg TR, Wang Y. An anti-angiogenic reverse thermal gel as a drug-delivery system for age-related wet macular degeneration. *Macromolecular bioscience*. 2013;13:464-9 and is reproduced here with permission from the publisher)

2.1 INTRODUCTION

Age-related macular degeneration (AMD) is the leading cause of irreversible vision loss in Americans over the age of 50. The wet—or exudative—form is characterized by abnormal blood vessel growth from the choroid, beneath the sensory retina. These vessels are associated with fluid leakage, which over time results in bleeding, retinal detachment, scarring and ultimately, loss of central vision [178-180].

Intravitreal injection of anti-angiogenic drugs is currently the most widely utilized strategy for preventing choroidal neovascularization, and can decelerate vision loss significantly [181, 182]. More specifically, vascular endothelial growth factor (VEGF) is a major target of such treatments as its expression is elevated in patients with AMD, and is known to promote

blood vessel growth, enhance vascular permeability and stimulate inflammatory leukocyte recruitment [183-186]. While effective, the short half-life of VEGF-inhibiting drugs necessitates frequent painful injections, placing an overwhelming burden on patients and their families [187]. Moreover, such frequent injections increase the risk of retinal detachment, endophthalmitis, intraocular hemorrhage and other ocular complications [8, 9]. Therefore, a controlled release delivery system that reduces injection frequency while maintaining the drug's efficacy would be highly beneficial to those suffering from AMD.

With this goal in mind, we investigated the feasibility of a reverse thermal gel as an intraocular drug delivery vehicle for AMD. Reverse thermal gels are water-soluble and undergo spontaneous phase transition upon temperature elevation; ideally such a material would be in the solution phase at room temperature and form a physical gel when placed at body temperature [188-192]. When designed in this manner the gel can be loaded with bioactive macromolecules such as proteins, independent of their solubility properties. Since the gel forms rapidly in-situ, this system can achieve sustained, localized drug release. Previously we reported synthesis of an ABA type block copolymer, ESHU, as a reverse thermal gel in which A is hydrophilic and B is hydrophobic [193]. In this work, we used ESHU to successfully design an anti-angiogenic reverse thermal gel system by combining ESHU with bevacizumab. Bevacizumab was chosen as a model anti-angiogenic agent because it is the most commonly-used VEGF inhibitor for treatment of AMD, and is also administered intravitreally for other VEGF-mediated diseases such as central retinal vein occlusion and proliferative diabetic retinopathy [194-197]. We assessed the cytocompatibility of ESHU with bovine and human ocular cells, and studied the release kinetics of the bevacizumab-loaded gel in order to gauge the applicability of ESHU as an intraocular drug delivery vehicle.

2.2 MATERIALS AND METHODS

2.2.1 Materials

N-BOC-serinol, hexamethylene diisocyanate (HDI), tetramethyl benzidine, hyaluronic acid from *Streptococcus equi* (M_w : 1.5 million), and bovine serum albumin (BSA) were purchased from Sigma-Aldrich (St. Louis, MO, USA). PEG was obtained from Alfa Aesar (Ward Hill, MA, USA). Anhydrous diethyl ether was obtained from Fisher Scientific (Pittsburgh, PA, USA). Anhydrous chloroform and anhydrous N,N-dimethylformamide (DMF) were purchased from EMD (Gibbstown, NJ, USA). The Spectra/Por dialysis membrane (MWCO: 3,500-5,000) was bought from Spectrum Laboratories (Rancho Domingues, CA, USA). Recombinant human VEGF 165 was obtained from R&D System (Minneapolis, MN, USA). Horseradish peroxidase-goat anti-human IgG (H+L) was purchased from Invitrogen (Carlsbad, CA, USA). Bevacizumab was purchased from Drugstore (Swedesboro, NJ, USA).

2.2.2 Equipment

Proton NMR spectra were recorded on a Bruker Avance 600 NMR. The molecular weight was calculated by gel permeation chromatography (GPC) on a Viscotek GPCmax VE2001 system using a Viscotek I-MBMMW-3078 column and a Viscotek 270 dual detector with THF as the eluent. Polyethylene glycol (American Polymer Standard) was used for calibration. Thermal behavior was studied by a thermostatted oscillating rheometer (AR2000, TA Instruments) equipped with 45 mm aluminum parallel plate geometry. 700 μ l of the polymer solution was used for the measurements. Data was collected at an angular frequency of 1 rad/s with 0.5%

strain. Cell images were obtained on a Nikon TI Fluorescence Microscope. Fluorescence intensity in the images was recorded and analyzed using MetaMorph 7.7.4 software (Molecular Devices Sunnyvale, CA).

2.2.3 Synthesis of ESHU

ESHU was synthesized as described previously with minor modifications [193]. Briefly, the hydrophobic polyurethane block was synthesized by the reaction of N-BOC-serinol (0.5 g, 2.62 mmol) with HDI (0.44g, 2.62 mmol) at 90 °C under nitrogen atmosphere. After reacting for 3 h, it was dissolved in 10 ml anhydrous DMF with excess HDI (0.88 g, 5.24 mmol) and stirred for 24 h at 85 °C. After cooling to ambient temperature, the mixture was poured into excess anhydrous diethyl ether to precipitate the polymer. The precipitate was then dissolved in 2 ml anhydrous DMF and the purification process was carried out twice with diethyl ether. Then the precipitates were washed in 100 ml of anhydrous diethyl ether overnight to remove unreacted HDI. A transparent polyurethane middle block was obtained after drying at 45 °C under vacuum (yield: 98%). To conjugate the hydrophilic block, polyurethane (1 g) and PEG (4g, M_w : 550) were dissolved in 10 ml anhydrous DMF, and stirred for 24 h at 85 °C. After cooling to ambient temperature, the mixture was poured into excess anhydrous diethyl ether to precipitate out the polymer. The polymer was purified by dialysis in water at room temperature for 3 days. Finally, the dialyzed solution was freeze-dried and a transparent solid, ESHU, was obtained (yield: 95%, M_w : 7,244, M_w/M_n : 1.54). ^1H FTNMR (CDCl_3 , δ in ppm): 4.83-5.23 [2H, $-\text{NH}(\text{CH}_2)_6\text{NH}-$]; 4.0-4.2 [4H, $-\text{CH}_2(\text{NH-BOC})\text{CH}_2-$]; 3.66 (4H, $-\text{OCH}_2\text{CH}_2\text{O}-$); 3.19 [4H, $-\text{NHCH}_2(\text{CH}_2)_4\text{CH}_2\text{NH}-$]; 1.41 [9H, $-\text{OC}(\text{CH}_3)_3$]; 1.26 and 1.44 [8H, $-\text{NHCH}_2(\text{CH}_2)_4\text{CH}_2\text{NH}-$].

2.2.4 Cell Culture

To isolate bovine corneal endothelial (CE) cells, fresh whole cow corneas were excised with a scleral rim and then placed endothelium side up in plastic tube caps. The CE cells were enzymatically detached by application of 0.05% trypsin/0.5 mM EDTA with incubation at 37°C and harvested by gentle scraping. The CE cells were separated from Descemet's membrane and cell suspensions were broken up by gentle pipetting and sieved through a 70- μ m nylon mesh. The suspended CE cells were centrifuged, and pelleted cells to be used for the assay were directly re-suspended in 1% low-melting-point (LMP) agarose and used as described below. For culture, CE cells were re-suspended in DMEM (Invitrogen, Carlsbad, CA) supplemented with 10% fetal bovine serum (Hyclone, Logan, UT), gentamicin, penicillin/streptomycin, and amphotericin B and cultured in 25 cm² cell culture flasks at 37°C in 5% CO₂ until 90% confluent.

To test human retinal pigment epithelium (RPE), ARPE-19 (American Type Culture Collection) cells were suspended in 1% low-melting-point (LMP) agarose and centrifuged. The pelleted cells were directly re-suspended in 1% low-melting-point (LMP) agarose, then Dulbecco's Modified Eagle Medium (DMEM) supplemented with 10% fetal bovine serum, gentamicin, penicillin/streptomycin, and amphotericin B and cultured in 25 cm² cell culture flasks at 37°C in 5% CO₂ until 90% confluent.

To test in vitro cytotoxicity, both primary bovine CE and ARPE-19 cells were incubated with 20 wt% ESHU in Glycated Human Serum Albumin (GHSA) medium for 24 and 72h, respectively at 37 °C in 5% CO₂. Cells cultured on tissue culture polystyrene (TCPS) with no exposure to ESHU gel were used as a positive control.

2.2.5 Live-Dead Cytocompatibility Experiment

After incubation with ESHU, cell viability was assessed using the Live/Dead assay. Cells were washed with DMEM containing 50 µg/ml Calcein AM for 20 min at 37 °C. In the final 5 min of incubation, 5 µg/ml propidium iodide (PI) was added, and then cells were washed with DMEM. Finally, nuclei were counterstained with 1µg/ml Hoechst 33342 for 5 minutes. The live and dead cells were analyzed by a fluorescence microscope. Comparative quantification of live cells was assessed using by a cell counting application sensitive to luminescence of Calcein AM, PI, and Hoechst staining in representative photomicrographs.

2.2.6 Immunoassay of Bevacizumab

The concentration of bevacizumab was measured by an enzyme linked immunosorbent assay (ELISA) as previously described with slight modification [198]. Ninety-six-well plates were coated with 1 µg/ml recombinant human VEGF 165 (100 µl/well) and incubated overnight at 4°C. After washing three times with phosphate-buffered saline (PBS) containing 0.05% Tween-20, wells were blocked with 1% bovine serum albumin in PBS for one hour at room temperature (200 µl/well). Wells were then washed five times with PBS containing 0.05% Tween-20 and stored at 4°C until use. Samples diluted in PBS containing 0.1% BSA were added to the plates and incubated for 3 h at room temperature. After washing three times with PBS containing 0.05% Tween-20, 1 µg/ml horseradish peroxidase-goat anti-human IgG (H+L) was added (100 µl/well) and incubated for 3 h at room temperature. After washing five times with PBS containing 0.05% Tween-20, color development was performed with 100 µl of tetramethyl benzidine, and the reaction was stopped by the addition of 100 µl of 1 M hydrogen chloride.

Optical density was measured on a Microplate Reader using Gen5 software (SYNERGY Mx, BioTek) at 450 nm with correction at 570 nm. A standard curve was prepared with bevacizumab concentrations ranging from 0.2 ng/ml to 3.125 µg/ml, and the linear region was used for the calculation. We measured the bevacizumab concentration in each sample thrice.

2.2.7 Release Profile of Bevacizumab

In vitro bevacizumab release studies were carried out in 1% (wt/v) of hyaluronic acid (HA) in PBS (pH 7.4) on a thermal rocker to mimic vitreous fluid composition [199] and eye motion, respectively. Gel solutions (200 µl) of 15 and 20% (wt/v) containing 0.5, 1, 3, and 5 mg of bevacizumab were injected into the HA solution through a 27-gauge needle at 37 °C within 5 seconds. The needle was submerged into the solution completely to mimic clinical injection into the vitreous. The concentrations, 15 and 20%, were chosen in the range that the solution could be easily injected through the 27-gauge needle with a quick sol-gel transition time. At predetermined time points, three samples (20 µl each) were withdrawn from different positions, and the same amounts of fresh HA solution were added. The samples were diluted with PBS containing 0.1% (wt/v) BSA, and released bevacizumab was quantified using ELISA. The cumulative release was calculated based on the theoretical loading amount.

2.3 RESULTS AND DISCUSSION

2.3.1 Cytocompatibility of ESHU with Ocular Cell Types

In a previous study, we demonstrated that ESHU showed good biocompatibility in vitro with smooth muscle cells as well as in vivo when injected subcutaneously [193]. Here we investigated the suitability of ESHU for intraocular drug delivery. We first tested whether ESHU was compatible with intraocular cell lines. We chose two different lines—bovine corneal endothelial cells and human ARPE-19 cells—because these cell types are likely to be exposed to ESHU and its degradation products upon intravitreal injection. First we exposed primary bovine corneal endothelial cells to either control conditions (serum-free DMEM), or ESHU (15% w/v in DMEM). Cells were stained with Calcein AM/PI /Hoechst and viability was evaluated at 1, 12, and 24h. Representative photomicrographs were taken to quantify cell survival at each time point (**Figure 5**), and cell morphology was also assessed. Cells exposed to ESHU exhibited typical polygonal morphology that showed no difference from control conditions, suggesting that ESHU did not affect the growth of CE cells. Cell viability was expressed in terms of percentage cell death (PI nuclei/overall nuclei). There was no significant difference in the survival of CE cells between the control and ESHU groups ($P>0.05$, two- way ANOVA) at any time point (**Figure 6**).

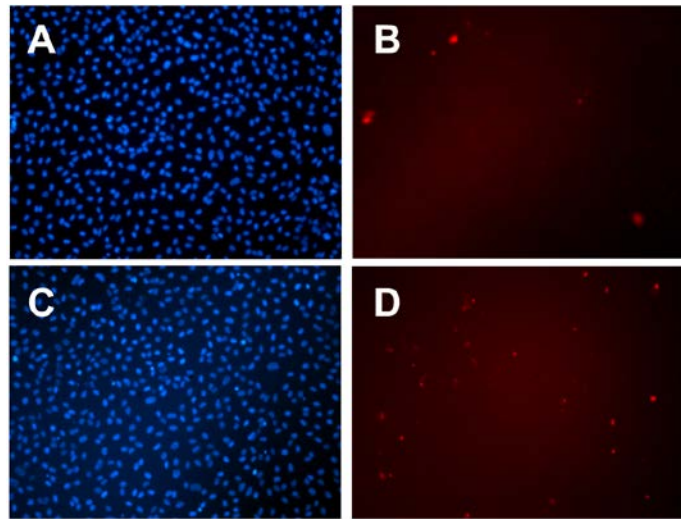


Figure 5. Representative fluorescence micrograph images of bovine CE cells exposed to control (A,B) and ESHU (C,D) at 24h. Both groups show comparable intense nuclei staining (A,C) with scarce red-stained dead cells (B,D) indicating little cell death.

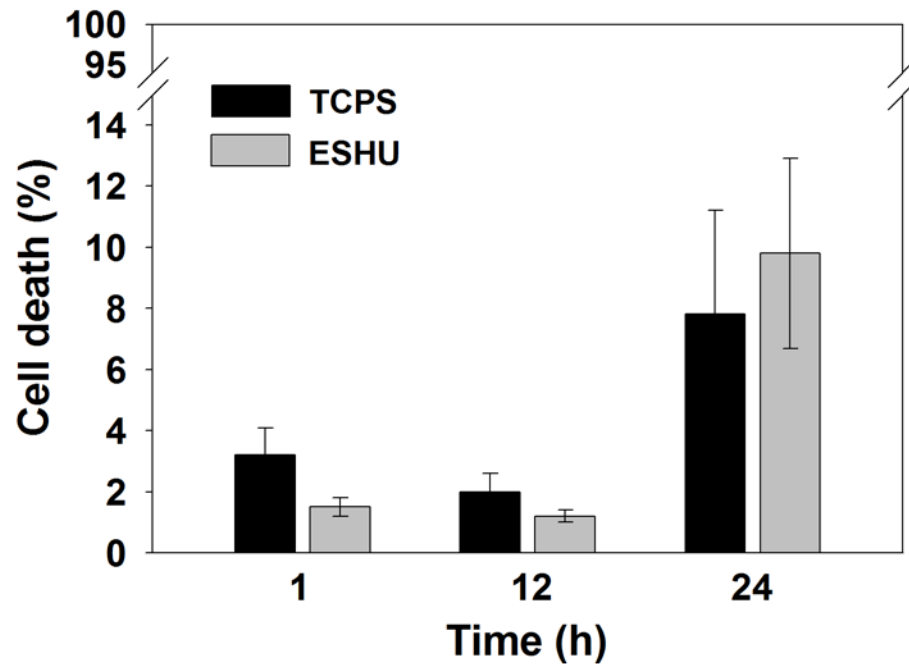


Figure 6. In vitro cytotoxicity of ESHU against bovine CE cells after 1, 12, and 24 hour incubation. The number of dead CE cells was determined by counting the number of PI+ cells, and was expressed as a function of the total number of cells labeled by Hoechst staining. Values are expressed as the means \pm SD (n=3).

ESHU showed good cytocompatibility with bovine CE cells, which are likely to be exposed to ESHU degradation products but not necessarily ESHU itself. Therefore, we needed to assess its compatibility with cells from the posterior segment of the human eye, as these cell types will be more directly exposed to the hydrogel. We used human ARPE-19 cells and exposed them to either DMEM (positive control) or ESHU, as described above. We found no significant cell death as indicated by the small number of PI-dyed dead cells (**Figure 7**). At each time point, total cell death was less than 1%, and statistically there were no differences between control and ESHU groups ($P>0.05$, two-way ANOVA) (**Figure 8**). Taken together, ESHU shows little to no cytotoxicity when cultured with both bovine and human ARPE-19 cells.

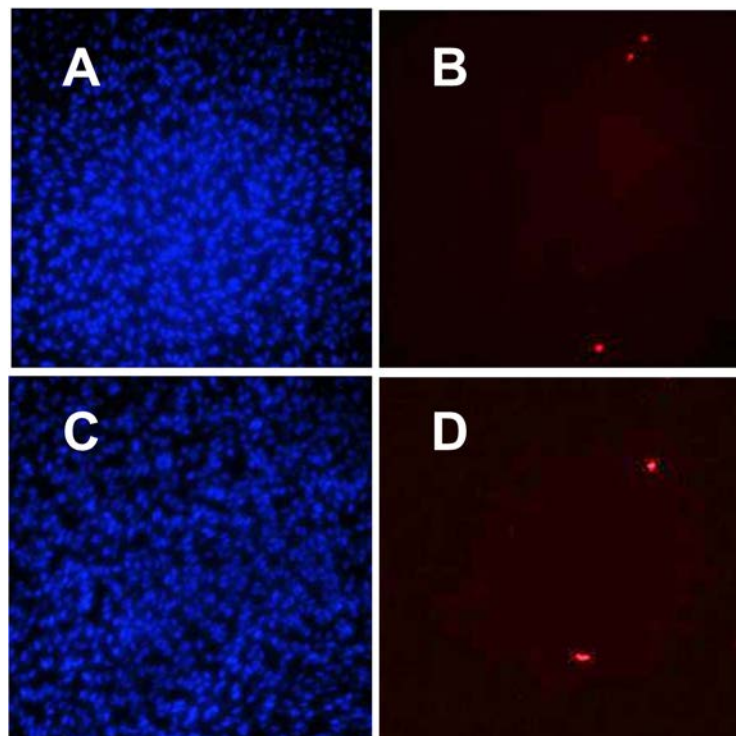


Figure 7. Representative fluorescence micrograph images of human ARPE-19 cells exposed to control (A,B) and ESHU (C,D) at 72h. There was no difference between experimental groups in the total number of viable cells (A,C) and dead cells (B,D).

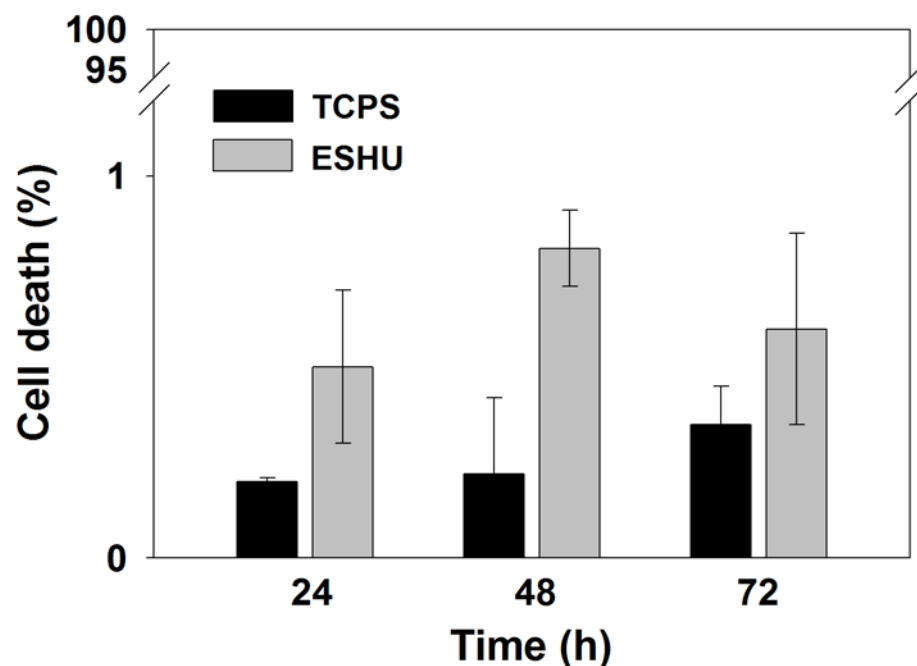


Figure 8. In vitro cytotoxicity of ESHU against human ARPE-19 cells after 24, 48, and 72 hour incubation. The percentage of dead ARPE-19 cells was determined by expressing the number PI+ cells over the total number of cells labeled by Hoechst staining. Values are the means \pm SD (n=3).

2.3.2 Thermal Behavior of Bevacizumab-Loaded ESHU

In order to examine whether bevacizumab-loaded ESHU underwent a phase transition at body temperature, we formulated a 20 wt% ESHU solution containing 1.25 mg of bevacizumab and monitored elastic modulus (G') changes during heating. We used 1.25 mg because it is the standard dose ophthalmologists inject intravitreally to treat AMD [200, 201]. The bevacizumab-loaded ESHU solution underwent phase transition comparable to that of pure ESHU (Figure 9) [193]. The elastic modulus, G' , which is indicative of a material's stiffness and thus its phase, began to increase slightly from 32 °C to 33 °C, corresponding to the initiation of gelation. It then increased dramatically as temperature continued to rise and reached a maximum stiffness at 39

°C, indicating formation of a complete physical gel. Although G' steadily increased until 39 °C, it had reached about 90% of its maximum value at 37 °C, at which point the solution had already visibly formed a gel. Given the phase transition behaviors, bevacizumab-loaded ESHU maintained thermal gelling properties as expected.

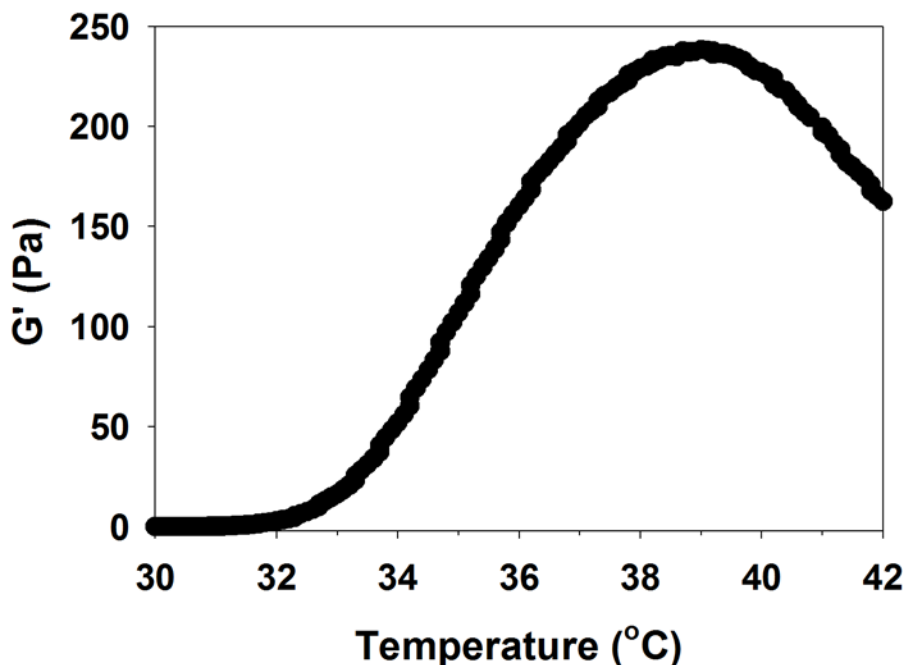


Figure 9. Thermal behavior of bevacizumab-loaded ESHU formulated with 20 wt% ESHU and 1.25 mg bevacizumab. The steep increase in G' from 33 to 39 °C indicated a sol-gel phase transition. The phase transition behavior is similar to pure ESHU [193].

2.3.3 In Vitro Bevacizumab Release

The key challenge of bevacizumab therapy for AMD is to prolong its release because the half-life of free bevacizumab in human eyes after intravitreal injection is on the order of 7 to 10 days [202]. The intraocular concentration depends on local conditions, such as the presence of blood or fluid under the retina, the state of the vitreous gel and other factors. To evaluate the potential

of the ESHU-bevacizumab platform, we performed release tests in 7.5 ml of 1 wt% hyaluronic acid at 37 °C to mimic vitreous fluid, while gyrosopic shaking was conducted to simulate human eye motion. Four formulas, each of 15 and 20 wt% of ESHU containing 0.5, 1, 3, and 5 mg of bevacizumab, gelled immediately upon injection into the 37 °C solution. The resulting sphere quickly sank to the bottom of the vessel, suggesting that the delivery system will sink out of the optical axis of the eye when injected in vivo. In all formulas, release was sustained without reaching plateau during the 17-week observation period (**Figure 10**). Release was more sustained with 20 wt% ESHU because ESHU formed a more rigid gel at the higher concentration [193], which presumably affects the diffusion path of bevacizumab. We also observed a small initial burst release for all the formulations. It is well-documented that burst release from injectable systems is higher than from pre-fabricated architectures such as implants [203]; thus we hypothesize that the observed burst release can be attributed to bevacizumab lost during the phase transition. Larger bursts were observed in the 15 wt% system, as well as with higher bevacizumab doses. This observation can be explained by the theory that at higher drug loading more is likely to be lost during the phase transition; additionally the lower ESHU concentration requires a longer gelation time, allowing for more bevacizumab to be released. This burst release might be helpful clinically, however, so as to provide immediate drug exposure in order to maximize efficiency. Moreover, the ability to control this burst by altering the ESHU concentration is attractive in that it can attenuate potential systemic effects of bevacizumab absorption, some of which can be serious, while still having an immediate therapeutic effect [204]. Thus, the bevacizumab-ESHU delivery system has three advantages over the current practice of direct bevacizumab injection in that the therapeutic window is much longer, release is sustained over 17 weeks in vitro, and injection frequency can be greatly reduced.

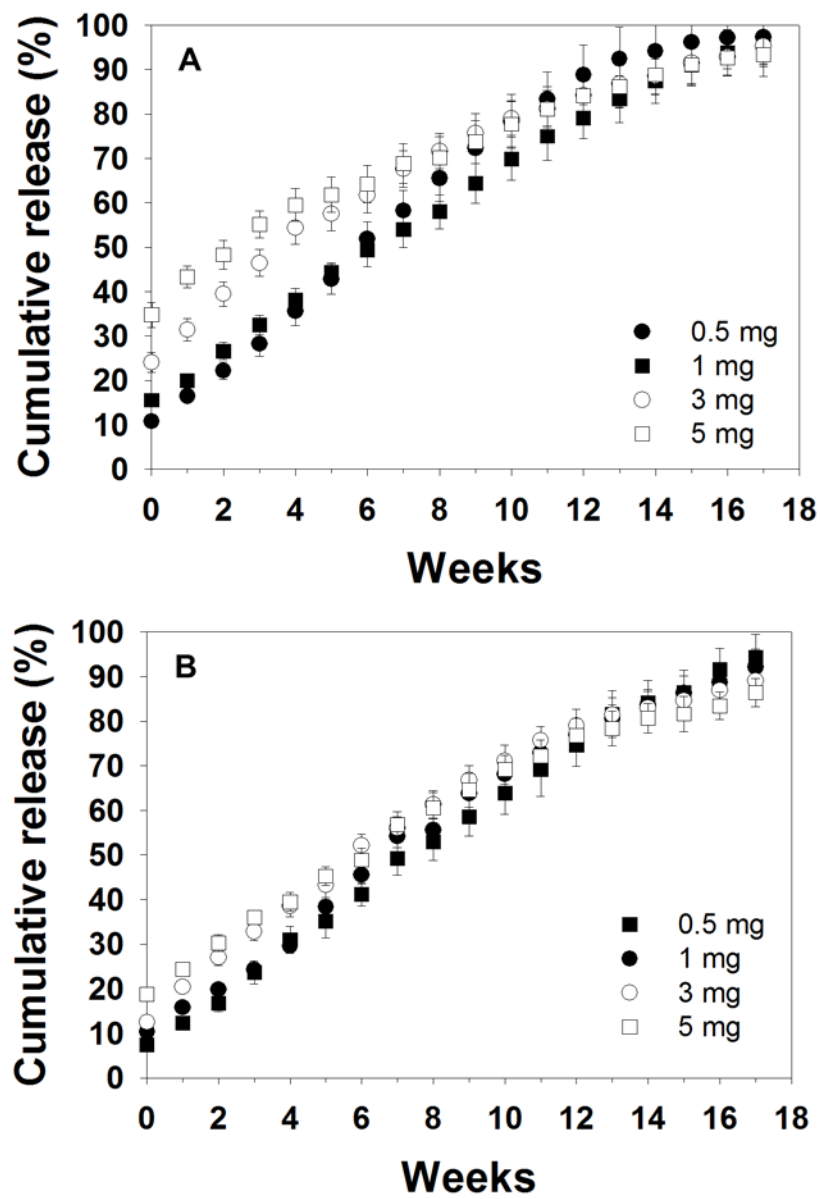


Figure 10. The release profile of bevacizumab from (A) 15 and (B) 20 wt% ESHU systems. The release was sustained over the 17-week period with initial burst releases. The 20 wt% ESHU systems resulted in slower release rates, and smaller burst releases due to its higher concentration.

2.4 CONCLUSIONS

We developed an anti-angiogenic reverse thermal gel system using ESHU and bevacizumab that demonstrates potential as a controlled release drug delivery system for AMD. ESHU appears to be an excellent material for ocular drug delivery, as it shows good cytocompatibility with bovine CE and human ARPE-19 cells, and an in vitro bevacizumab release profile extending to 17 weeks. Moreover, ESHU is not limited to the use of bevacizumab; other water-soluble drugs can be easily loaded into the system as well, enabling multi-faceted treatment approaches. This preliminary work supports the concept that such a strategy may significantly reduce administration frequency, decrease treatment cost, and improve patient compliance.

3.0 INJECTABLE THERMORESPONSIVE HYDROGEL SUSTAINS THE RELEASE OF INTRAVITREAL BEVACIZUMAB IN VIVO

(Note: This chapter was published previously as: Rauck BM, Friberg TR, Medina Mendez CA, Park D, Shah V, Bilonick RA, et al. Biocompatible reverse thermal gel sustains the release of intravitreal bevacizumab in vivo. *Investigative ophthalmology & visual science*. 2014;55:469-76 and is reproduced here with permission from the publisher.)

3.1 INTRODUCTION

Choroidal neovascularization (CNV) is the hallmark of many blinding disorders, most notably wet age-related macular degeneration (AMD) and diabetic retinopathy. It is characterized by pathologic blood vessel growth which originates in the choroid and progresses through the Bruch's membrane into the subretinal space [205]. These vessels are fragile and permeable, causing hemorrhage, retinal detachment, scarring and ultimately, loss of central vision. Elevated levels of vascular endothelial growth factor (VEGF) is a central cause of CNV [206-208], thus intravitreal injection of anti-VEGF medications such as bevacizumab (Avastin®) or ranibizumab (Lucentis®) has emerged as a leading treatment strategy [209-211]. The efficacy of these drugs, however, is severely limited by rapid clearance from the eye; their half-lives are on the order of 7 days [198, 200]. This necessitates frequent injections, imposing a significant burden on patients

and increasing healthcare costs as well as procedure-related complications such as endophthalmitis, retinal detachment, cataract, and uveitis [212-215]. A delivery system that extends the presence of intravitreal drugs in the eye is therefore highly desirable for reducing injection frequency and adverse effects while maximizing therapeutic outcomes.

A number of polymeric delivery systems have been considered by researchers for intravitreal drug delivery, including microparticles, which are well-tolerated in the eye and are capable of delivering drugs over a longer period of time [216, 217]. For example, microparticle-encapsulated or PEGylated bevacizumab are more effective than bevacizumab alone in treating CNV in rats [217]. However, direct intravitreal injection of such microparticle formulations may result in rapid particle dispersion and cause turbidity of the vitreous humor, affecting vision. In situ-forming, injectable hydrogels are thus an attractive alternative for intravitreal delivery as they can be formulated to encapsulate drugs and sustain release locally. Studies with non-degradable, thermally-responsive hydrogels have demonstrated excellent protein encapsulation, minimal toxicity, and easy injectability with no long-term effects on retinal function in vivo [31, 32]. These studies established that thermoresponsive hydrogels are excellent candidates for intraocular drug delivery.

Ideally, hydrogels for intravitreal administration should be biodegradable so as to avoid material accumulation in the vitreous with repeated injections over time. To this end, we investigated the utility of a biodegradable, thermally responsive hydrogel, poly(ethylene glycol)-poly-(serinol hexamethylene urethane), or ESHU, to deliver bevacizumab in rabbit eyes. Previously, we have demonstrated that an aqueous solution of ESHU will undergo a sol-to-gel phase transition when the temperature is increased from room to body temperature, making it attractive for minimally invasive applications [193]. We hypothesized that ESHU would be a

suitable platform for intraocular drug delivery and demonstrated that it is compatible with cells from ocular sources, and capable of releasing bevacizumab over a 17 week period in vitro [218]. The aim of the present study was to demonstrate sustained bevacizumab release in vivo when compared to a standard, bolus injection. Additionally, we compared the cytocompatibility of ESHU to other commonly-used ocular biomaterials and assessed the in vivo biocompatibility of the gel.

3.2 MATERIALS AND METHODS

3.2.1 Materials

N-Boc-serinol, hexamethylene diisocyanate (HDI), tetramethyl benzidine, and bovine serum albumin (BSA) were obtained from Sigma-Aldrich (St. Louis, MO, USA). Polyethylene glycol (PEG) was obtained from Alfa Aesar (Ward Hill, MA, USA). Anhydrous diethyl ether and 10% formalin were obtained from Fisher Scientific (Pittsburgh, PA, USA) and anhydrous *N,N*-dimethylformamide was purchased from EMD (Gibbstown, NJ, USA). The Spectra/Por dialysis membrane (MWCO: 3500–5000) was purchased from Spectrum Laboratories (Rancho Domingues, CA, USA). The Live/Dead cytotoxicity assay kit was purchased from Molecular Probes (Carlsbad, CA, USA). Recombinant human VEGF₁₆₅ was obtained from Peprotech (Rocky Hill, NJ, USA). Horseradish peroxidase-goat anti-human IgG was purchased from Invitrogen (Carlsbad, CA, USA). Bevacizumab was obtained from Genentech (South San Francisco, CA).

3.2.2 Preparation of Bevacizumab-Loaded ESHU

ESHU was prepared as described previously [193, 218]. To prepare bevacizumab-loaded ESHU, the desired amount of polymer was measured out and sterilized via ethylene oxide (12 hour cycle, 20 °C, >35% relative humidity). The sterilized ESHU polymer was then dissolved in a solution of 25 mg/ml bevacizumab, or PBS for control gels, at 4 °C in the dark at a polymer concentration of 15% w/v.

3.2.3 Injection Force Measurements

The injection force of 15% w/v ESHU in bevacizumab was measured using a material testing system (Insight, MTS Systems, Eden Prairie, MN). Water and 1% hyaluronic acid were used as controls. Samples were loaded into syringes containing a 31G needle and the plunger was fixed to the instrument. The syringe was attached to a vial in order to collect the injected liquid, and compression tests were performed at speeds of 0.5, 1 and 3 mm/s. The force measurement at steady-state was considered to be the required injection force. Three separate runs were averaged for each sample at every speed.

3.2.4 In Vitro Cytotoxicity

Bovine corneal endothelial cells were isolated as previously described [218]. Cells were suspended in Dulbecco's Modified Eagle Medium (DMEM, Invitrogen, Carlsbad, CA, USA) supplemented with 10% fetal bovine serum (Hyclone, Logan, UT, USA), penicillin/streptomycin, gentamicin, and amphotericin B, then incubated at 37 °C in 5% CO₂

until cells were 90% confluent. For in vitro cytotoxicity assays, cells were exposed to one of four experimental conditions: serum-free media (control), 15% w/v ESHU in DMEM, perfluorooctane (PFO), or 5000cs silicone oil. As commonly utilized ocular materials, PFO and silicone oil served as control groups, and all conditions were run in triplicate. At 1, 12 and 24 hours, cell viability was assessed using the Live/Dead assay. Cells were stained with 50 µg/ml Calcein AM (in DMEM) at 37 °C for 20 min, and during the last 5 min of incubation, 5 µg/ml propidium iodide (PI) was added. After washing in DMEM, nuclei were stained with 1 µg/ml Hoechst 33342 for 5 min. Representative images were taken of each culture using a fluorescence microscope. Cell viability was expressed as the ratio of PI-positive cells to Hoechst-stained cells in each sample.

3.2.5 Intravitreal Injection

All animal experiments were conducted in compliance with protocols approved by the Institutional Animal Care and Use Committee at the University of Pittsburgh, with strict adherence to guidelines of the National Institutes of Health, United States Department of Agriculture, and the ARVO statement for the Use of Animals in Ophthalmic and Vision Research. Male New Zealand White rabbits (8 weeks old, Charles River Laboratories, Boston, MA) were used for this study. Prior to injection, animals were anesthetized by intramuscular administration of ketamine/xylazine (40 mg/kg). Topical antibiotic (Vigamox, Alcon Laboratories, Fort Worth TX, USA) and anesthetic (Proparacaine, Falcon Pharmaceuticals, Fort Worth TX, USA) eye drops were applied prior to injection. Intravitreal injections were conducted through the pars plana (2.5 mm posterior to the limbus). Eyes received one of three 50

µl injections: 1.25 mg bevacizumab in saline (n=3), 1.25 mg bevacizumab in 15% ESHU (n=4), or 15% ESHU in saline (n=2). Uninjected eyes served as healthy controls (n=2).

3.2.6 Clinical Examination

Clinical evaluations were conducted pre- injection, immediately after injection, 15 minutes post-injection and at 1, 3, and 7 days, and weekly thereafter for ten weeks. Clinical examinations included analysis of inflammatory response via indirect ophthalmoscopy and IOP measurements.

3.2.6.1 Indirect Ophthalmoscopic Observation

To observe the gel in situ and identify potential gross inflammation in the anterior or posterior segments, eyes were dilated using tropicamide 0.5% (Bausch and Lomb, Tampa, FL) and phenylephrine 2.5% (Alcon, Fort Worth, TX) and examined using an indirect ophthalmoscope with a 20 diopter lens (Nikon, Tokyo, Japan).

3.2.6.2 Intraocular Pressure

IOP was monitored using a rebound tonometer (TONOVET, Icare, Helsinki, Finland). Baseline IOP measurements were obtained following anesthesia, prior to injection. Measurements were taken again immediately following injection, 15 minutes later, and at each sampling time point thereafter. Three measurements per eye were averaged.

3.2.7 In Vivo Bevacizumab Release

Aqueous humor samples were obtained via anterior chamber paracentesis with a 30G syringe (approx. 100 μ l sample volume) at 1, 4, and 7 days post injection, and weekly thereafter until sacrifice. The concentration of bevacizumab present in samples was determined using ELISA. Wells of 96-well plates were coated with 100 μ l of 1 μ g/ml recombinant human VEGF₁₆₅ overnight at 4 °C. Following 3x washing with PBS containing 0.05% Tween-20, wells were blocked for 1h at room temperature with 1% BSA in PBS. Samples were diluted with 0.1% BSA and added to the plates following 5x washing. After 1h at room temperature, wells were washed 3 times and horseradish peroxidase-goat anti-human IgG (diluted 1:2000 in 0.1% BSA) was added to each well for 1h at room temperature. Wells were then washed five times and color development was performed using 100 μ l of tetramethyl benzidine. The reaction was stopped by addition of 100 μ l of 1M hydrogen chloride. A standard curve of bevacizumab (linear region: 0.05 ng/ml to 1 ng/ml) was used to determine the concentration of bevacizumab in samples.

3.2.8 Histological Analysis

At 9 weeks, 4 of 5 animals were sacrificed and the eyes were explanted for histological analysis. One animal was sacrificed at 18 weeks to assess long-term compatibility. Eyes were fixed in 10% formalin, embedded in paraffin and sectioned at 5 μ m thickness. Following deparaffinization, sections were then stained with hematoxylin & eosin, Masson's Trichrome, and Periodic Acid Schiff (PAS) stain to assess eye morphology.

3.2.9 Statistical Analysis

Data are expressed as mean \pm standard error of the mean (SEM). One-way analysis of variance (ANOVA) with Tukey post-hoc testing was used to determine statistical differences between groups for IOP and injection force data. Two-way ANOVA was used for the live/dead assay. Differences were considered significant at $p < 0.05$. For in vivo studies, the observed bevacizumab concentrations in anterior chamber samples were modeled as a nonlinear function of time (day) and treatment group using a first order compartment model for power transformed bevacizumab concentrations. To appropriately account for the longitudinal repeated measurements, a nonlinear mixed effects model was used. The R language and environment for statistical computing and graphics (Version 2.15.1) [219] with the nlme (Version 3.1-108) R package [220] were used to compute the maximum likelihood estimates and confidence intervals via the nlme (nonlinear mixed effects model) and SSfol (self-starting first order compartment model) functions. A detailed description of the model and parameter estimates can be found in Appendix A.

3.3 RESULTS

3.3.1 Feasibility of ESHU Injection

The small needle commonly used for intravitreal injection makes viscous materials difficult to inject; therefore the force required to push ESHU through a 31G needle was quantified using compression testing. Water and 1% hyaluronic acid (HA) were used as controls in order to relate

3.3.2 In Vitro Cytotoxicity of ESHU

Cytotoxicity testing was performed using primary bovine corneal endothelial cells. Cells were exposed to either serum-free media (control), ESHU (15% w/v in DMEM), silicone oil, or perfluorooctane (PFO). PFO is used intraoperatively during vitreoretinal surgery, and silicone oil is used commonly as a vitreous substitute for the repair of complex retinal detachments [221, 222]. At 1, 12 and 24 hours, cells were stained with Calcein AM, PI and Hoechst and toxicity was quantified as the number of PI+ cells compared to the total number of Hoechst+ cells. In cultures treated with ESHU and PFO, no significant cell death occurred throughout the 24h culture period (**Figure 12**, $p > 0.05$). Silicone oil treated cultures underwent substantial cell death at each time point compared to both control and ESHU groups, with approximately 76% death at 24h. Qualitatively, cells exposed to ESHU showed little to no evidence of cellular damage and appeared morphologically identical to control groups.

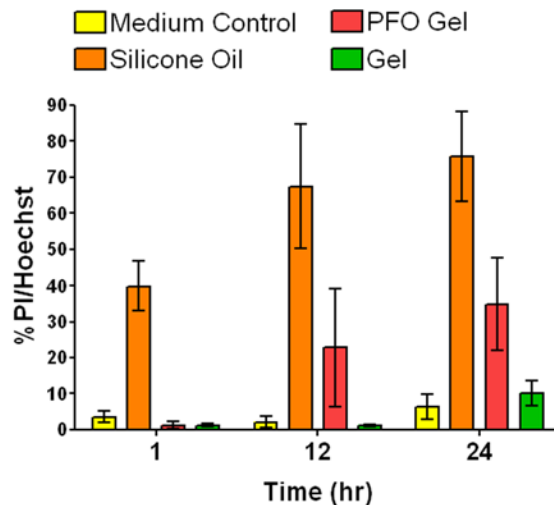


Figure 12. Bovine CE cells survive well over a 24-hour period following exposure to ESHU gels, with no significant difference when compared to TCPS controls. In contrast, silicone oil caused significant cell death compared to all other experimental groups ($p < 0.05$).

3.3.3 Effect of ESHU on Intraocular Pressure

IOP measurements were taken immediately before and after injection and prior to each sampling time point throughout the course of the study. Measurements show that IOP spiked sharply following injection of both ESHU and bevacizumab solutions, and returned to baseline levels within 15 minutes (**Figure 13**). Throughout the remainder of the study, IOP remained at baseline and was not significantly different from control eyes.

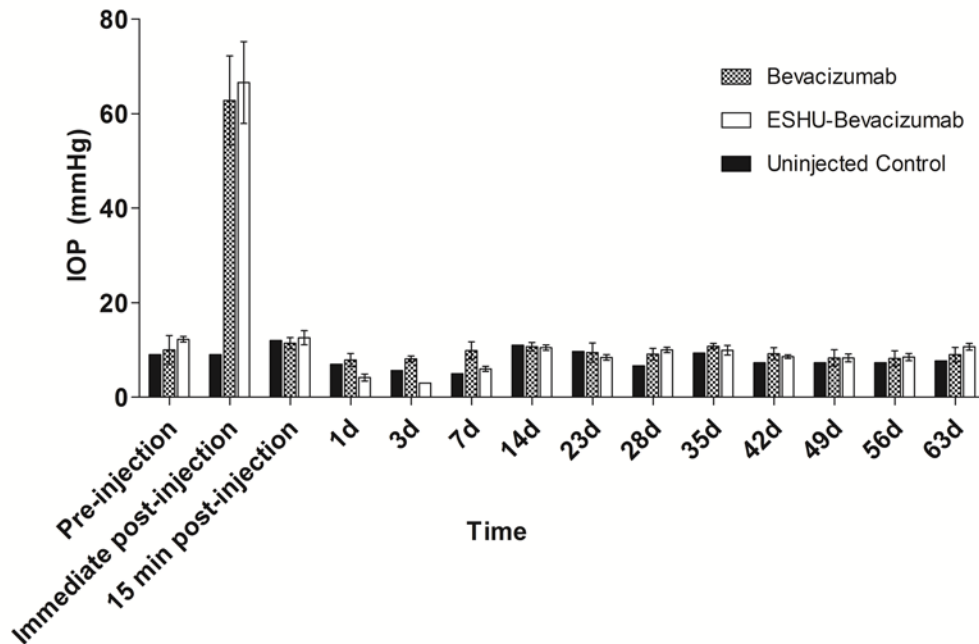


Figure 13. IOP measurements return to baseline values 15 minutes following intravitreal injection.

Throughout the study, IOP was not significantly different between ESHU and control groups ($p>0.05$).

3.3.4 Effect of ESHU on Inflammatory Response

In addition to IOP measurements, gels were observed and photographed in situ through indirect ophthalmoscopy. 24 hours post-injection, injected hydrogels had sunk to the bottom of the

vitreal space. Animals displayed no signs of discomfort or external signs of inflammation (redness or tearing). Throughout the study period, the gels remained translucent and ovoid in shape, with no evidence of inflammation or cellular accumulation on the gel surface (**Figure 14A**). In the animal that was sacrificed at 18 weeks, gels appeared to become more transparent as degradation occurred. Additionally, the long-term presence of the gel did not seem to affect the eye based on indirect observation, or histologically. Though ESHU appears to fill a large portion of the vitreal space from the indirect, it should be noted that the view includes only part of the vitreal space. The gels are typically 3-4 mm in diameter and occupy approximately 3% of the vitreal volume. Following sacrifice, eyes were processed for histological analysis and representative H&E images are shown in Figure 14B. The retinal layers are intact with no evidence of inflammation, corroborating the indirect observations.

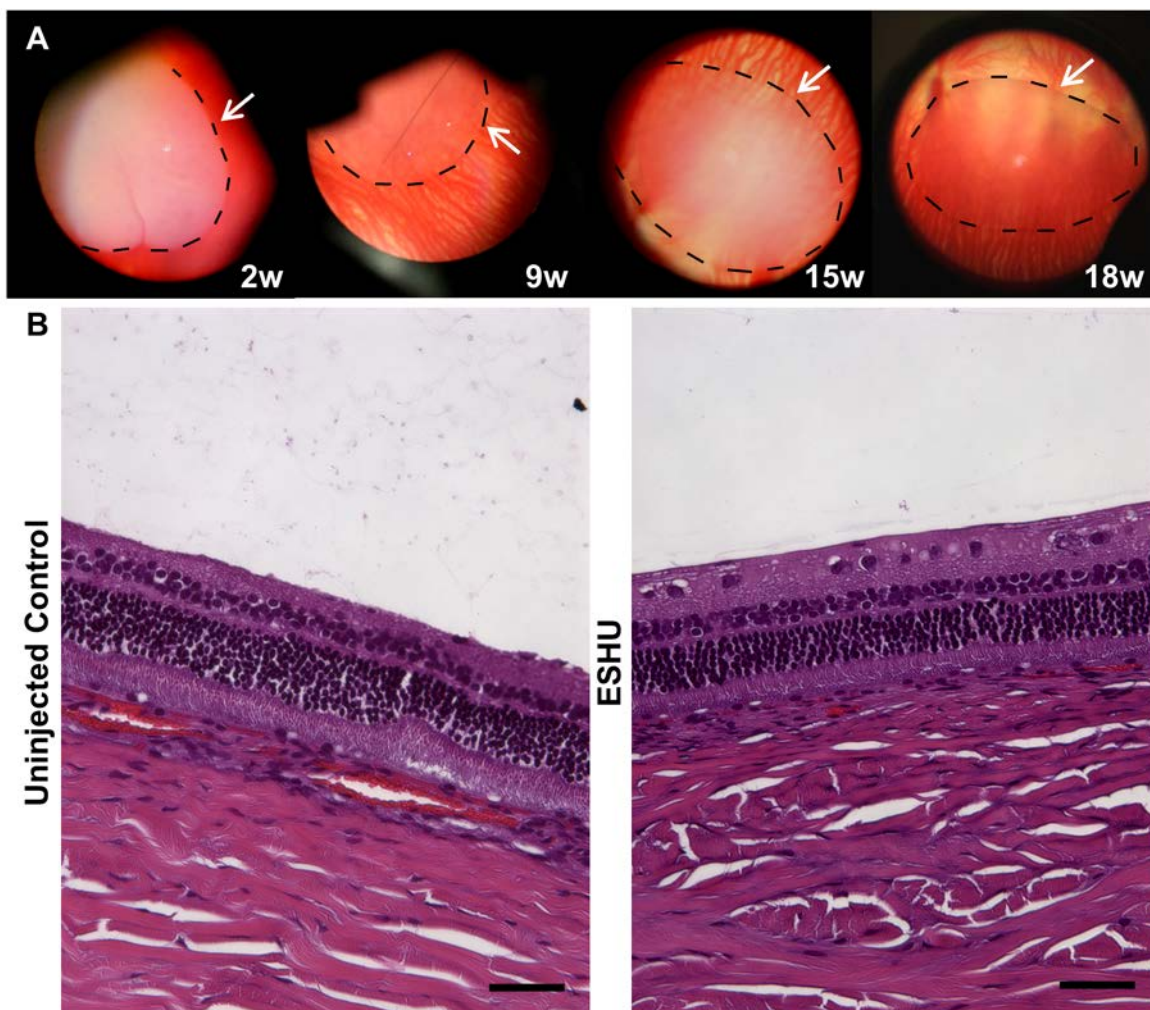


Figure 14. ESHU is biocompatible in the eye. (A) Indirect images of the hydrogel in the vitreous space. The surface of the gel (traced in black) is free of inflammatory cells and the vitreous humor is clear. (B) Hematoxylin and eosin stains comparing the retinal structure of ESHU and control groups. The two groups are morphologically indistinguishable, suggesting that the presence of ESHU did not adversely affect retinal health. Scale bar: 100 μm .

3.3.5 In Vivo Bevacizumab Release

We sought to compare the concentration of bevacizumab in rabbit eyes receiving the ESHU delivery system to a single bolus intravitreal injection. We injected 1.25 mg of bevacizumab (50

μl) in both experimental groups to allow for direct comparison to the clinically administered dose. Anterior chamber (AC) paracentesis was performed to obtain aqueous humor samples, and ELISA was used to quantify the amount of bevacizumab present (**Figure 15**). A first-order compartment model was used to model the bevacizumab concentration in experimental groups over time. The fixed effect parameters were found to be well-estimated by the model (Tables A1 and A2 of Appendix A). The concentration in bevacizumab-only groups peaks earlier and is lower than for ESHU-bevacizumab. The parameters that characterize these differences are highly statistically significant ($p \ll 0.05$). On average, the ESHU maintained a bevacizumab concentration that was 4.7-fold higher than eyes which received a bolus injection. It should be noted that any bevacizumab present in control eyes was below the limit of detection for the ELISA assay and was therefore considered to be negligible. Thus this data is not shown in Figure 15.

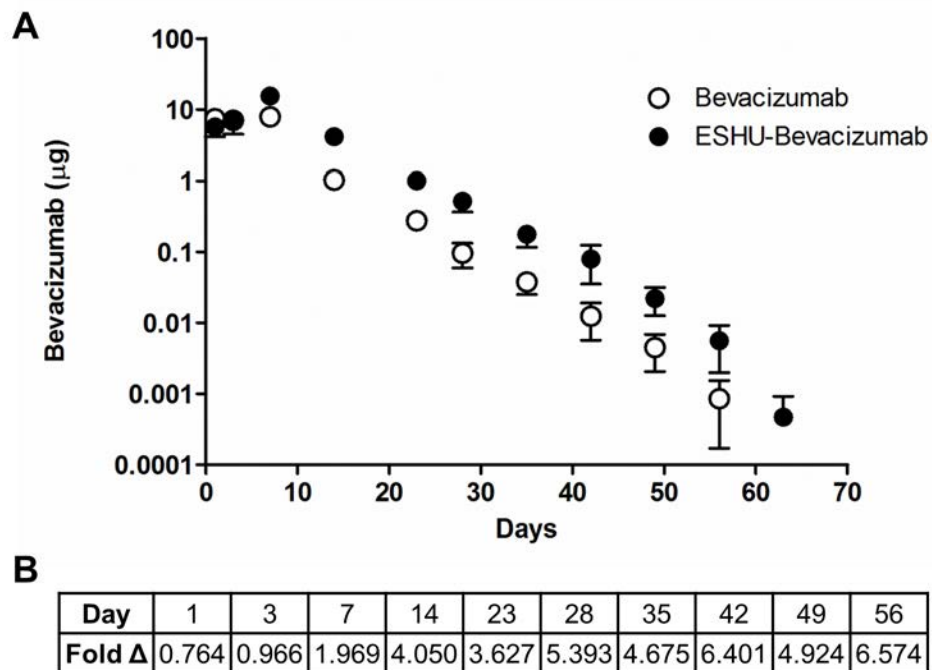


Figure 15. ESHU sustains bevacizumab release for over 9 weeks. The concentration of bevacizumab in AC samples over time is plotted on a semi-log scale (A). On average, animals receiving the delivery system had 4.7-fold more bevacizumab present (B).

3.4 DISCUSSION

The present study demonstrated that ESHU, a thermally responsive hydrogel, is feasible for intravitreal injection, is biocompatible in vitro and in vivo, and can maintain bevacizumab concentrations at levels approximately five times higher than in controls. The force required to inject ESHU is less than that for HA, a highly viscous glycosaminoglycan and major component of the vitreous humor. HA is used extensively in ophthalmic surgery, and cataract surgery in particular as an injectable vitreous substitute [223, 224]. The injection force data indicate that ESHU formulations are suitable for intravitreal injection through small gauge needles without

requiring significant effort to administer. Upon injection into a solution of HA heated to 37 °C, ESHU formulations undergo a rapid sol-gel phase transition and form spherical-to-ovoidal shaped hydrogels. This transition occurs rapidly, yet not instantaneously, enabling time for injection without gelation occurring within the needle. ESHU does not cause significant cell death when cultured with bovine corneal endothelial cells; in previous work we demonstrated ESHU had good cytocompatibility with both bovine corneal endothelial and retinal pigment epithelial cells.[218]. The experiments in this study elaborated upon these results by comparing ESHU to other synthetic materials that are commonly used in retinal surgery – silicone oil and perfluorooctane. The substantial cell death caused by silicone oil treatment, which is commonly used clinically, suggests that ESHU will be well-tolerated in vivo. While ESHU appeared to cause less cell death than PFO at 12 and 24h, this difference was not statistically significant. Taken together, these results indicate that ESHU is less toxic than other, FDA-approved materials for ocular applications and should be biocompatible in the eye.

Next, intravitreal injections of bevacizumab, ESHU dissolved in bevacizumab, or ESHU dissolved in PBS were performed in rabbits. IOP was measured throughout the study as one metric of ocular health. The initial spike following injection is typical and secondary to a small increase in volume of the eye, and is a function of the ocular rigidity [222]. As IOP variations can be indicative of pathologies such as trabeculitis and retinal detachment [225, 226] the normal measurements observed throughout the study suggest that the presence of ESHU did not cause significant damage to the eye. Indirect and histological observation revealed that the gel remained spherical-to-ovoidal in shape throughout the course of the study, sunk to the bottom of the eye within one day of injection, caused no significant inflammatory response to the presence of ESHU and did not affect retinal structures. In one animal that remained under observation for

18 weeks, the gel became more transparent over time, suggesting occurrence of degradation. Previously it was demonstrated that ESHU undergoes approximately 10% and 20% degradation after 45 days in vitro in PBS in the absence and presence of cholesterol esterase respectively [193]. It was hypothesized that in vivo degradation would occur more rapidly; however the immune privileged state of the eye may have protected ESHU from enzyme and cell mediated breakdown, resulting in minimal degradation. Current studies are focused on introducing more rapidly degrading bonds to the ESHU backbone in order to control its degradation rate.

To our knowledge, this is the first study to date which compares the long-term in vivo release of bevacizumab from thermoresponsive biodegradable hydrogels to bolus intravitreal administration. The suitability of thermoresponsive hydrogels for intravitreal applications has previously been explored using non-degradable poly(*N*-isopropylacrylamide) (PNIPAAm)-based hydrogels, as well as biodegradable poly(2-ethyl-2-oxazoline)-*b*-poly(ϵ -caprolactone)-*b*-poly(2-ethyl-2-oxazoline) (PEOz-PCL-PEOz), or ECE gels [31-34]. These studies demonstrated that intravitreal injection of synthetic hydrogels caused no long-term (up to 2 months) changes to retinal function, IOP or histomorphology in rabbits, corroborating our observations. However, PNIPAAm gels are non-degradable, and therefore would require surgical removal. Additionally, their synthesis protocol requires free radical polymerization and involves the use of potentially toxic initiators, whereas ESHU synthesis requires no catalysts. ESHU polymer is biodegradable, and would thus disappear with time. Compared to the biodegradable ECE gel, we previously demonstrated that ESHU releases bevacizumab for approximately 17 weeks in vitro, compared to less than 3 weeks in the ECE gel [218]. A potential reason for this is hydrogen bond formation between the ESHU gel backbone and bevacizumab, which would sustain the release of the drug. These prior studies have elegantly demonstrated the benefit that minimally invasive hydrogels

may provide; however did not demonstrate sustained release in an animal model. We built upon their work to show that intravitreal injection of a clinically-relevant volume of bevacizumab-containing hydrogel sustains bevacizumab release in vivo and does not elicit a chronic inflammatory response. Though the eye displays immune privilege and is generally less susceptible to foreign body responses, [227] chronic inflammation can manifest itself as alterations in retinal morphology, which was not observed in this study. The nearly five-fold increase in bevacizumab concentration in ESHU-injected eyes suggests that the polymer functions to protect bevacizumab from degradation and should therefore be more effective in treating CNV. Future work will focus on optimizing the drug release kinetics by varying drug dose, polymer concentration, molecular weight and degradation, as well as confirming the efficacy of the drug delivery system in a non-human primate model of CNV. According to some researchers, such efficacy studies should be done in primates, as bevacizumab is humanized and its effect on CNV can be species-specific [228].

3.5 CONCLUSIONS

We have studied the feasibility of a unique thermally-responsive hydrogel, ESHU, as an intraocular drug delivery vehicle. ESHU is easily injectable and from a clinical standpoint, its administration would be no different than the current practice of injecting bevacizumab. In vivo, ESHU gels are well tolerated with little to no evidence of inflammation, and are capable of sustaining bevacizumab release over 9 weeks. Because the polymer is an injectable solution, it can be used to sustain the release of many different medications and can be useful for other ocular diseases as well as diseases in other tissues.

4.0 INJECTABLE THERMORESPONSIVE HYDROGELS ENHANCE CELLULAR TRANSPLANT SURVIVAL AND IMPROVE OUTCOMES FOLLOWING TRAUMATIC SPINAL CORD INJURY

(Note: This chapter was published previously as: Ritfeld GJ, Rauck BM, Novosat TL, Park D, Patel P, Roos RA, et al. The effect of a polyurethane-based reverse thermal gel on bone marrow stromal cell transplant survival and spinal cord repair. *Biomaterials*. 2014;35:1924-31 and is reproduced here with permission from the publisher)

4.1 INTRODUCTION

Cell therapy is promising for repair of the damaged nervous system [229-231]. Bone marrow stromal cells (BMSCs) are candidate cells for such therapies because of their repair proficiency and relative accessibility [232-235]. BMSCs support repair of a myriad of other ailments including cardiomyopathy, muscle dystrophy, and wound healing [236-238]. Intraneural BMSC transplants are thought to elicit repair through paracrine effects [239-242]. However, these effects are likely limited due to low transplant survival in damaged nervous tissue [243-246].

Cell transplants may be lost due to various events including inflammation [247] and oxidative stress [248-252], which are initiated rapidly after injury. Thus, measures to protect cell transplants against these death-mediating mechanisms may increase transplant survival and

potentially improve their reparative effects. One strategy to improve transplanted cell survival is by using the synthetic poly(ethylene glycol)–poly(serinol hexamethylene urethane) or ESHU, which is a reverse thermal gel with good biocompatibility and degradability [193, 218]. ESHU is a copolymer with two hydrophilic poly(ethylene glycol) blocks flanking a hydrophobic poly(serinol hexamethylene urethane) block [193]. The presence of polyurethane [253, 254] may provide ESHU with antioxidant capacity. ESHU dissolves in water and undergoes phase transition with increasing temperatures to form a physical gel at 37 °C, which makes it especially practical for treatment of closed injuries [255].

ESHU was shown to have good biocompatibility with nervous tissue in the ocular system [218, 256]. A beneficial feature of ESHU is that the repeating units of the polymer contain protected amine groups, providing an easy path to functionalization using biomolecules or other signaling molecules that can offer enhanced bioactivity of the gel *in vivo*. One example is to functionalize ESHU through these amine groups with the pentapeptide, IKVAV, which in pilot experiments was shown to produce a neural interface similar to laminin.

We hypothesized that ESHU protects intraneural BMSC transplants from death leading to improved repair. This premise was tested *in vivo* using an adult rat model of spinal cord contusion [235, 243, 244] assessing BMSC transplant survival, inflammation, anatomical restoration, and functional recovery and *in vitro* using BMSC cultures determining the effects of ESHU on survival of BMSCs under oxidative stress.

4.2 MATERIALS AND METHODS

4.2.1 Ethics and Surgical Approval

Before and after surgery, rats were housed following guidelines of the National Institutes of Health and the United States Department of Agriculture. The rats were kept within a double-barrier facility in standard rat cages with continuous supply of fresh air, water, and food. All procedures were approved by the Institutional Animal Care and Use Committee at the University of Pittsburgh.

4.2.2 Transplant Preparation

We harvested BMSCs from femurs of harvested BMSCs from femurs of female adult Sprague Dawley rats according to a previously described protocol (Figure 1a) [235, 243, 257]. Isolated cells were grown in Dulbecco's Modified Eagle Medium (DMEM, Sigma–Aldrich, Allentown, PA, USA) with 10% fetal bovine serum (Mediatech, Manassas, VA, USA) and 1% penicillin/streptomycin (Invitrogen, Grand Island, NY, USA). To enable detection after transplantation, first passage cells were transduced to express green fluorescent protein (GFP) using lentiviral vectors (**Figure 16a**) [235, 243, 244]. Fourth passage cells positive for the BMSC markers, CD90 and CD105 and negative for blood cell markers, CD34, CD45 and HLA-DR [244, 258, 259] were used for the experiments.

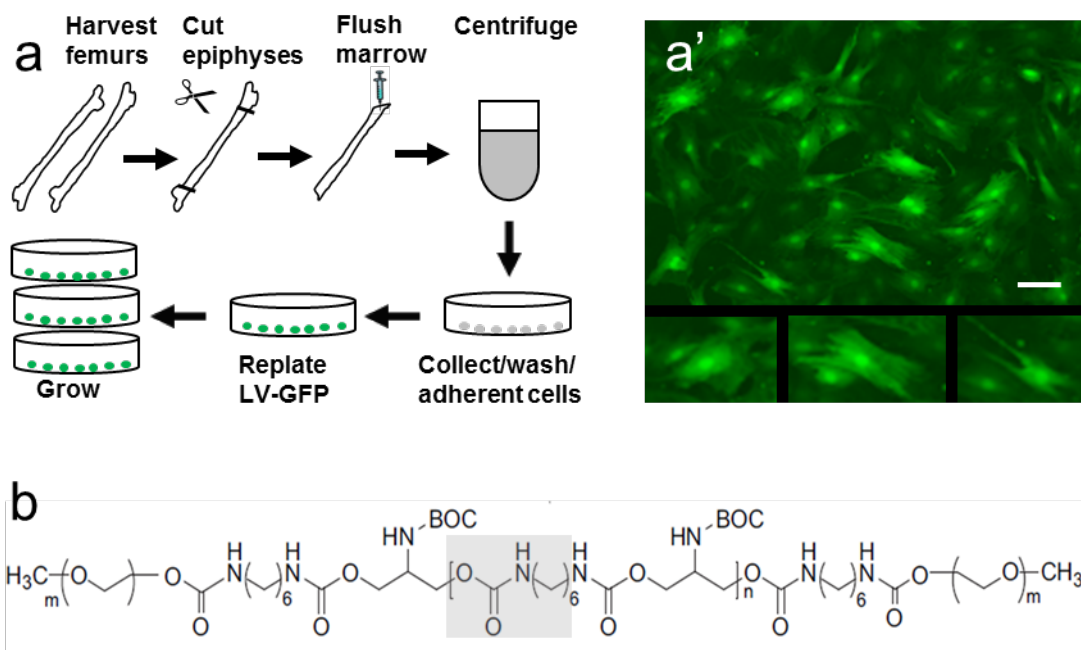


Figure 16. Schematic representations of transplant preparation and ESHU. (a) Isolation and transduction of bone marrow stromal cells. Plastic-adherent cells from femurs of adult Sprague-Dawley rats were collected, lentivirally transduced with green fluorescent protein, and passaged four times before used for transplantation. (a') Green fluorescent protein-expressing BMSCs in culture. Smaller panels show examples of cultured BMSC morphologies. (b) Structural formula of ESHU with the urethane bond in gray box. Bar = 50 μm in a' and 25 μm in panels below.

4.2.3 ESHU

The preparation of ESHU (**Figure 16b**) was previously described [193]. In brief, polyurethane blocks were synthesized by melting N-BOC-serinol (Sigma–Aldrich) under nitrogen and slowly adding hexamethylene diisocyanate (HDI; TCI America, Wellesley Hills, MA, USA) to initiate polymerization via urethane bonds. Both ends of polyurethane were capped with an isocyanate group using additional HDI and then dissolved in anhydrous dimethylformamide. Diethyl ether (Fisher Scientific, Pittsburgh, PA, USA) was used to precipitate out the polymer and remove

unreacted hexamethylene diisocyanate. Polyethylene glycol (Alfa Aesar, Ward Hill, MA, USA) was coupled onto the polyurethane blocks under nitrogen, dissolved in dimethylformamide (EMD, Gibbstown, NJ, USA), and precipitated in and washed with diethyl ether. For purification, ESHU was dissolved in water and dialyzed (3500 MWCO) for 48 h and finally freeze-dried. In our experiments, a 16% w/v ESHU solution in phosphate-buffered saline (PBS; pH 7.4) was prepared and sterile-filtered before use.

4.2.4 Surgical Procedures

A model of adult rat spinal cord contusion [260, 261] was used to test our hypothesis. Female adult Sprague Dawley rats (200 g, $n = 80$; Charles Rivers Laboratory, Wilmington, MA, USA) were anaesthetized using intraperitoneal injection of ketamine (60 mg/ml; Butlerschein, Dublin, OH, USA) and dexdomitor (0.5 mg/kg; Pfizer, New York, NY, USA). The tenth thoracic spinal cord segment was contused using a force of 200 kDyne (Infinite Horizon IH-0400 impactor; Precision Systems and Instrumentation, LLC, Versailles, KY, USA) [235, 243, 244]. The wound site was rinsed with sterile PBS with 0.1% gentamicin (VWR, Radnor, PA), the muscles were sutured in layers, and the skin was closed with Michel wound clips (Fine Science Tools, Foster City, CA, USA). All rats included in the studies had an impact within 5% of the intended force, resulting in a 0.9–1.8 mm spinal cord compression and a Basso-Beattie–Bresnahan (BBB) [262, 263] score ≤ 1 at day 1 and ≤ 5 at day 3 post-impact. Three days post-injury, rats were sedated and injected into the contusion with 5 μ l ESHU or PBS with 5×10^5 BMSCs, or ESHU or PBS only.

4.2.5 Post-Surgery Procedures

Antisedan (1.5 mg/kg; Pfizer) was injected subcutaneously to reverse the effects of dexdomitor. An intramuscular injection of gentamicin (6 mg/kg; VWR), a subcutaneous injection of Rimadyl (5 mg/kg; Pfizer), and a subcutaneous injection of Ringer's solution (10 ml on surgery day, 5 ml thereafter; Butlerschein) were administered daily for the first three days post-injury. After the intraspinal injection at three days post-injury, the rats received gentamicin for four days and Ringer's and Rimadyl for three days. Bladders were manually emptied twice daily until reflex voiding occurred [235, 243]. Rats were monitored daily throughout the experiments. Rats were fixed at 15 min, one, four, or six weeks after injection. All rats survived without requiring pain or distress treatment.

4.2.6 Motor Function Assessment

Overground walking ability was assessed using the BBB test [262, 263] weekly for six weeks post-injection ($n = 10/\text{group}$). Rats were tested for 4 min by two testers unaware of the treatments. Rats were familiarized with the open field and baseline values were determined before surgery. Scores were averaged per experimental group. Higher motor functions were assessed at six weeks post-injury using the BBB sub-score [264, 265] as previously described ($n = 10/\text{group}$). Scores were averaged per experimental group. Sensorimotor function of the hindlimbs was assessed before (baseline) and at six weeks post-injection using horizontal ladder walking ($n = 10/\text{group}$) [266, 267]. Slips of the foot and part of lower leg and slips of the full leg were counted and expressed as a percentage of the total number of steps. Scores were averaged per experimental group.

4.2.7 Histological Procedures

Rats were anaesthetized and transcardially perfused with 300 ml PBS followed by 400 ml 4% paraformaldehyde (Sigma–Aldrich) in PBS. Spinal cords were dissected, post-fixed overnight in the same fixative, and transferred to 30% sucrose (Fisher Scientific) in PBS for 48 h. A 12 mm-long spinal cord segment centered at the injury epicenter was cut in 20 µm-thick horizontal cryostat sections (CM 1950; Leica Biosystems, Buffalo Grove, IL, USA). Every twelfth section was stained with cresyl violet (0.5%; Sigma–Aldrich) for cytoarchitecture analysis and spared tissue volume assessment. Other section series were used for immunocytochemistry. Sections were analyzed using an Axio Observer Z1 fluorescent microscope (Zeiss, Thornwood, NY, USA) with StereoInvestigator[®] (MicroBrightField, Inc., Williston, VT, USA).

4.2.8 Immunocytochemistry

Tissue sections were incubated in 5% normal goat serum (Vector Labs, Burlingame, CA, USA) and 0.03% Triton X-100 (Sigma–Aldrich) in PBS for 1 h followed by the primary antibody for 2 h at room temperature and then overnight at 4 °C. Rabbit polyclonal antibodies against glial-fibrillary acidic protein (GFAP) were used to detect astrocytes (1:200; Dako North America, Inc., Carpinteria, CA). Mouse monoclonal antibodies against ED1 were used to detect macrophages (1:100; Millipore, Temecula, CA). BMSCs in vitro on 8-chamber culture slides (BD Falcon, Franklin Lakes, NJ; see also below) were fixed with 4% paraformaldehyde in PBS for 10 min and stained with monoclonal antibodies against caspase 3 (rabbit, clone D3E9) to detect apoptotic cells (1:100; Millipore) and 8-oxo-2'-deoxyguanosine (8-oxo-dG; mouse, clone 483.15) to detect cells with DNA damage (1:200; Millipore). After washing twice in PBS for

20 min, sections or cells were incubated with goat-anti-rabbit and goat anti-mouse Alexa Fluor 594 (1:200; Life Technologies, Grand Island, NY, USA) for 2 h at room temperature. DAPI (0.2 µl/ml; Sigma–Aldrich) was used to stain nuclei. Sections were covered with glass slips in fluorescent mounting medium (Dako North America, Inc.) and stored at 4 °C. Sections were analyzed using an Axio Observer Z1 fluorescent microscope (Zeiss, Thornwood, NY, USA) with StereoInvestigator® (MicroBrightField, Inc., Williston, VT, USA).

4.2.9 Cell Quantification

StereoInvestigator® (MicroBrightField, Inc.) was used to determine the numbers of GFP-positive BMSCs in the injury site [243, 268] at seven days post-transplantation ($n = 6/\text{group}$) in every twelfth section and the numbers of caspase 3- and 8-oxo-dG-positive BMSCs in cultures (see below). All assessments were done by personnel blinded to the treatment groups. For GFP-positive BMSCs in the contusion, sections were 240 µm apart spanning the width of the spinal cord. In every section the area containing GFP-positive cells was outlined manually at 2.5× magnification and covered with a 250 × 250 µm grid. At 60× magnification with oil immersion, GFP-positive cells with a discernible DAPI-stained nucleus were marked using the optical fractionator with a 60 × 60 µm counting frame [235, 243, 268]. The numbers of immunostained cells in cultures were similarly determined. The numbers of GFP-positive cells were expressed as a percentage of the number of transplanted cells ($\pm\text{SEM}$). The numbers of caspase 3- and 8-oxo-dG-positive cells were expressed as a percentage of the number of seeded cells ($\pm\text{SEM}$). The numbers were averaged per experimental group.

Image J Software was used to determine the number of ED1-immunoreactive macrophages in the injury site at one and four weeks post-transplantation in every twelfth section by persons blinded to the treatment groups. Numbers were averaged per experimental group.

4.2.10 Measurement of Nervous Tissue Sparing

Cresyl violet-stained sections of rats that survived for four weeks post-injection were used to determine the volume of spared tissue in the damaged spinal cord segment using the Cavalieri estimator function of StereoInvestigator[®] (MicroBrightField, Inc.) [235, 268]. Analysis was performed by personnel blinded to the experimental groups ($n = 6/\text{group}$). The Gundersen Coefficient of Error was <0.05 for all measurements. Spared tissue volume was expressed as a percentage of the volume ($\pm\text{SEM}$) of an equally-sized comparable uninjured spinal cord segment and averaged per experimental group.

4.2.11 In Vitro Assessment of the Protective Effect of ESHU

To assess ESHU's cell protective ability we kept BMSCs in vitro under oxidative stress, which is known to contribute to intraneural cell transplant loss [251, 252]. A total of 4×10^5 cells were incubated in 100 μl ESHU or PBS with 200 μM hydrogen peroxide (H_2O_2 ; Sigma–Aldrich) for 24 h at 37 °C. Then, 100 μl Trypan Blue (Sigma–Aldrich) was added and viable (Trypan Blue-negative) cells were quantified in a hemacytometer and expressed as a percentage of all counted cells. Results from nine samples from three independent experiments were averaged. In nine samples from three independent experiments, the average number of BMSCs expressing caspase 3, a marker for apoptosis, and 8-oxo-2'-deoxyguanosine (8-oxo-dG), a marker for DNA

damage, were determined (see above). Details on caspase 3 and 8-oxo-dG staining are described in 4.2.8. Immunocytochemistry.

4.2.12 Quantification of ESHU's Antioxidant Ability

ESHU's ability to scavenge H₂O₂ relative to PBS was measured using a H₂O₂ quantification kit (National Diagnostics, Atlanta, GA, USA) which colorimetrically measures Xylenol Orange–Ferric iron complex resulting from H₂O₂-mediated oxidation of ferrous iron. The linear standard curve of this assay is 15–100 ng/ml. We added 30 ng/ml H₂O₂ (Sigma–Aldrich) to ESHU or PBS which was kept in reagent buffer for 30 min following the manufacture's guidelines. Absorbance was measured (Victor 2V 1420; Perkin–Elmer, Waltham, MA, USA) and the values from three independent experiments were averaged.

4.2.13 Statistical Analysis

Two-tailed Student's *T*-test was used to determine differences in cell numbers in vivo and in vitro and in H₂O₂ concentrations in vitro. One-way ANOVA with Tukey's post-hoc test was used to assess differences in macrophages and nervous tissue sparing. Repeated measures ANOVA with Tukey's post-hoc test determined differences in functional performances. Differences between groups were considered significant when $p < 0.05$.

4.3 RESULTS

4.3.1 BMSC Transplant Survival

We investigated whether ESHU protects transplanted BMSCs from death in damaged nervous tissue using a spinal cord contusion model. At 15 min post-injection, rounded BMSCs were present in the injury when mixed in either ESHU (**Figure 17a**) or PBS (**Figure 17b**). One week post-injection, in both groups many spindle-shaped cells were also found (**Figure 17c, d**). At 4 and 6 weeks, hardly any cells could be found in or near the contusion site after injection of BMSCs in ESHU (**Figure 17e**) or in PBS (**Figure 17f**). The temporal morphological profile of the grafted cells is in accordance with earlier observations [243]. Also, GFAP staining (**Figure 17a-f**) was similar as previously described [235, 243]. We found that $73 \pm 17\%$ (SEM; $n = 6$) of transplanted cells had survived in ESHU while $21 \pm 8\%$ (SEM; $n = 6$) survived in PBS (**Figure 17g**), which represents a significant ($p < 0.05$) 3.5-fold increase in survival in ESHU compared with PBS. At four weeks post-injection, in both groups $<1\%$ of the cells has survived in the injury site. The data show that ESHU does not affect BMSC transplant morphology and protects against early death resulting in increased transplant presence at one week post-injection.

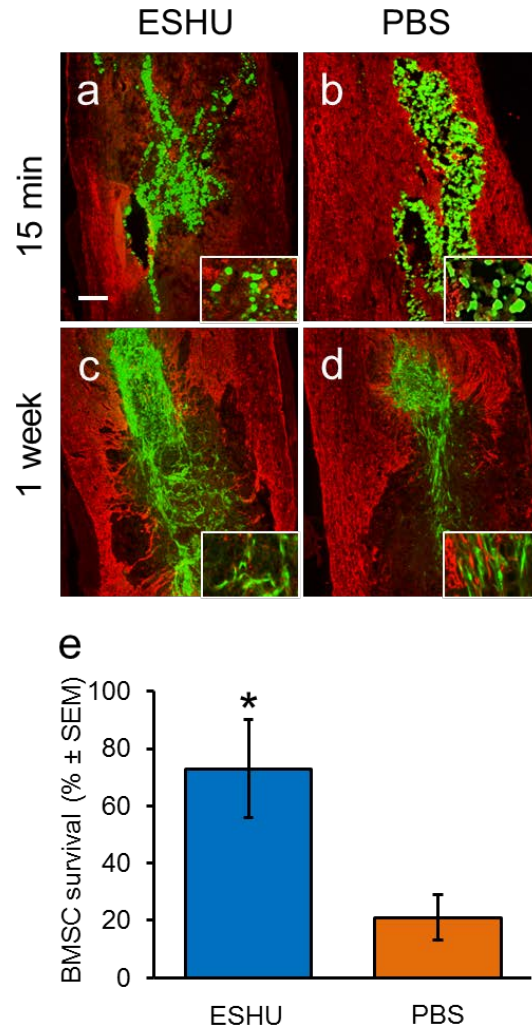


Figure 17. ESHU improves survival of BMSC transplants in a spinal cord contusion. 15 minutes after injection, transplanted cells (green) occupy most of the contusion regardless of whether they were suspended in ESHU (a) or PBS (b). Staining for GFAP (red) was used to outline the contusion. Transplanted cells (green) were mostly rounded in ESHU (inset a) and PBS (inset b). 1 week after injection, the transplant occupies only part of the contusion site but more so when suspended in ESHU (c) than PBS (d). Transplanted cells at this time point were mostly elongated with bipolar morphologies. 4 weeks after injection, hardly any cells were detected in the contusion in either group. Similar results were observed after 6 weeks (not shown). (g) More transplanted cells survive in the contusion site 1 week after injection when suspended in ESHU than PBS. Survival rate was measured against total number of injected cells. Error bars in graph display standard error of the mean (SEM). Asterisk = $p < 0.05$. Bar in a = 350 μm in a-d and 30 μm in insets.

4.3.2 Effect of BMSC Transplant Survival on Neuroprotection

Because BMSC transplant survival is associated with neuroprotection [243] we assessed whether ESHU-promoted transplant survival rendered enhanced tissue sparing (**Figure 18a-d**). The results demonstrated that the volume of spared tissue in rats with the transplant in ESHU is 66% larger ($p < 0.05$; $n = 6/\text{group}$) than in rats with the transplant in PBS at four weeks post-transplantation (**Figure 18e**). ESHU only had no effect on spared tissue volume in the damaged area (**Figure 18e**). The data suggest that increased survival of intraneural BMSC transplants early after injection enhances neuroprotection of nervous tissue.

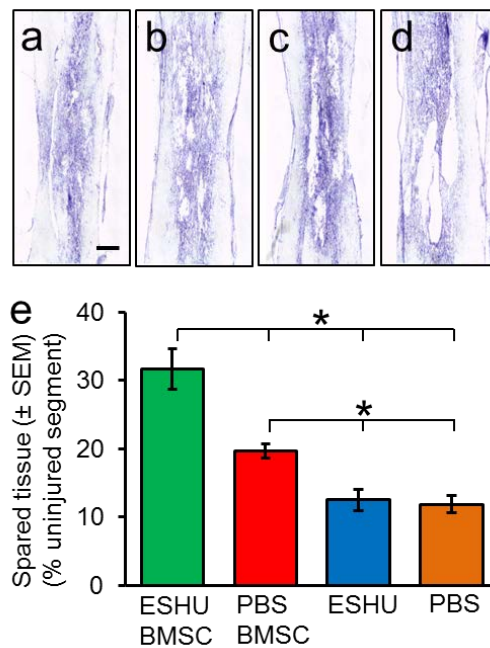


Figure 18. ESHU augments neuroprotection by BMSC transplants in the contused spinal cord. Damage and loss of nervous tissue were observed 4 weeks after a BMSC transplant in ESHU (a) or PBS (b), or ESHU (c) or PBS (d) alone into the contused spinal cord. (e) Spared tissue volume was larger with the transplant in ESHU compared with all other groups. Error bars represent SEM, and asterisks = $p < 0.05$. Bar in = 600 μm in a-d.

4.3.3 Effect of BMSC Transplant Survival on Motor Recovery

After spinal cord contusion, motor performance depends in part on the amount of nervous tissue at the injury site [235]. We examined whether augmented neuroprotection by BMSC transplants with ESHU-enhanced survival affected motor function recovery. We found that rats with the transplant in ESHU performed significantly ($p < 0.05$; $n = 10/\text{group}$) better in overground walking than rats with BMSC in PBS at 4–6 weeks post-injury (**Figure 19a**). Rats with BMSC in ESHU performed better than rats with ESHU or PBS alone at 1–6 weeks post-injury and rats with BMSCs in PBS walked better overground than rats with ESHU or PBS alone only at 1–3 weeks post-injury (**Figure 19a**). At 6 weeks, rats with BMSCs in ESHU showed consistent (>95%) weight-supported plantar steps with frontlimb–hindlimb coordination. The control transplanted rats were less consistent (50–95%) making such steps, whereas rats with ESHU or PBS only were less consistent and lacked frontlimb–hindlimb coordination. During the 4th–6th week after injection, overground walking was increased by 1.7 ± 0.4 points on the BBB scale in rats with the transplant in ESHU which was significantly ($p < 0.05$; $n = 10/\text{group}$) higher than the increase in the other groups (**Figure 19b**). Higher motor functions of the hindlimbs were significantly improved ($p < 0.05$; $n = 10/\text{group}$) by 74% in rats with BMSC in ESHU compared with BMSCs in PBS at 6 weeks post-injury (**Figure 19c**). Sensorimotor function was significantly increased ($p < 0.05$; $n = 10/\text{group}$) in rats with the transplant in ESHU compared with the other three groups at 6 weeks post-injury (**Figure 19d**). Rats receiving the transplant in PBS had significantly improved sensorimotor function compared with rats with ESHU or PBS alone (**Figure 19d**).

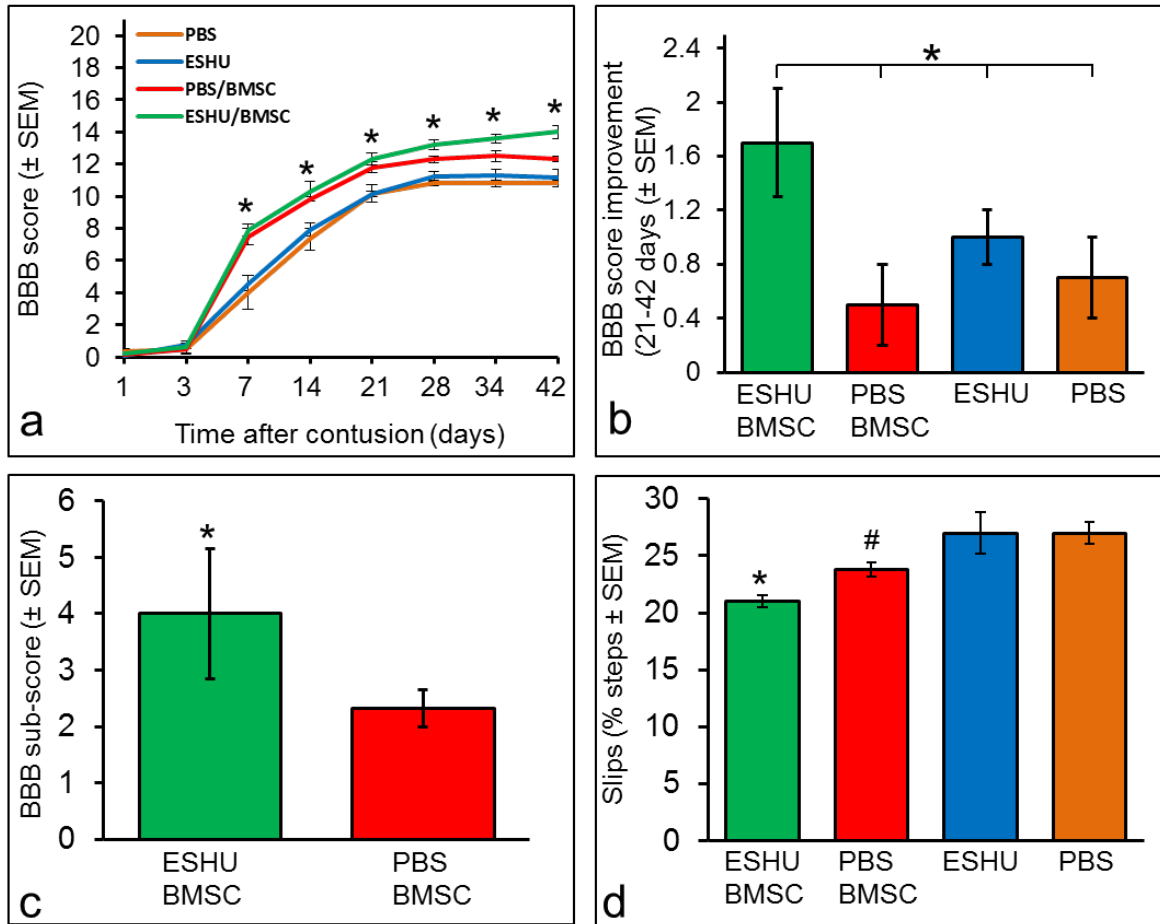


Figure 19. ESHU leads to enhancement of motor function recovery by a BMSC transplant in the contused spinal cord. (a) Overground walking ability was significantly improved in rats with a BMSC transplant in ESHU compared with BMSCs in PBS 4-6 weeks post-injury. Rats with BMSC in ESHU performed better than rats with ESHU or PBS alone at 1-6 weeks post-injury. Rats with BMSCs in PBS walked better overground than rats with ESHU or PBS alone only at 1-3 weeks post-injury. (b) Improvement in overground walking ability during the 4th-6th week post-injury was significantly improved in rats with a transplant in ESHU compared with all over groups. (c) Improved higher motor function in rats with BMSCs in ESHU compared with PBS at 6 weeks post-injury. (d) Improved sensorimotor recovery in rats with the transplant in ESHU over all other groups and in rats with BMSCs in PBS over the control groups without BMSCs at 6 weeks post-injury. Error bars in bar graph display SEM. Asterisks signify $p < 0.05$. Pound sign signifies $p < 0.05$.

4.3.4 Inflammatory Response

Macrophages invade damaged nervous tissue and contribute to cell death [247]. ESHU breakdown products could carry negative charges and so affect macrophage presence [269]. We tested the possible influence of macrophages on ESHU's protective capacity by assessing their presence in the injury after injection of BMSCs in ESHU (**Figure 20a-c**) or PBS (**Figure 20d-f**), or ESHU or PBS only. The results demonstrated similar macrophage presence between all groups at one (**Figure 20g**) and four (**Figure 20h**) weeks post-injection, suggesting that ESHU is non-immunogenic. The data indicate that macrophages are not implicated in ESHU-mediated transplant survival.

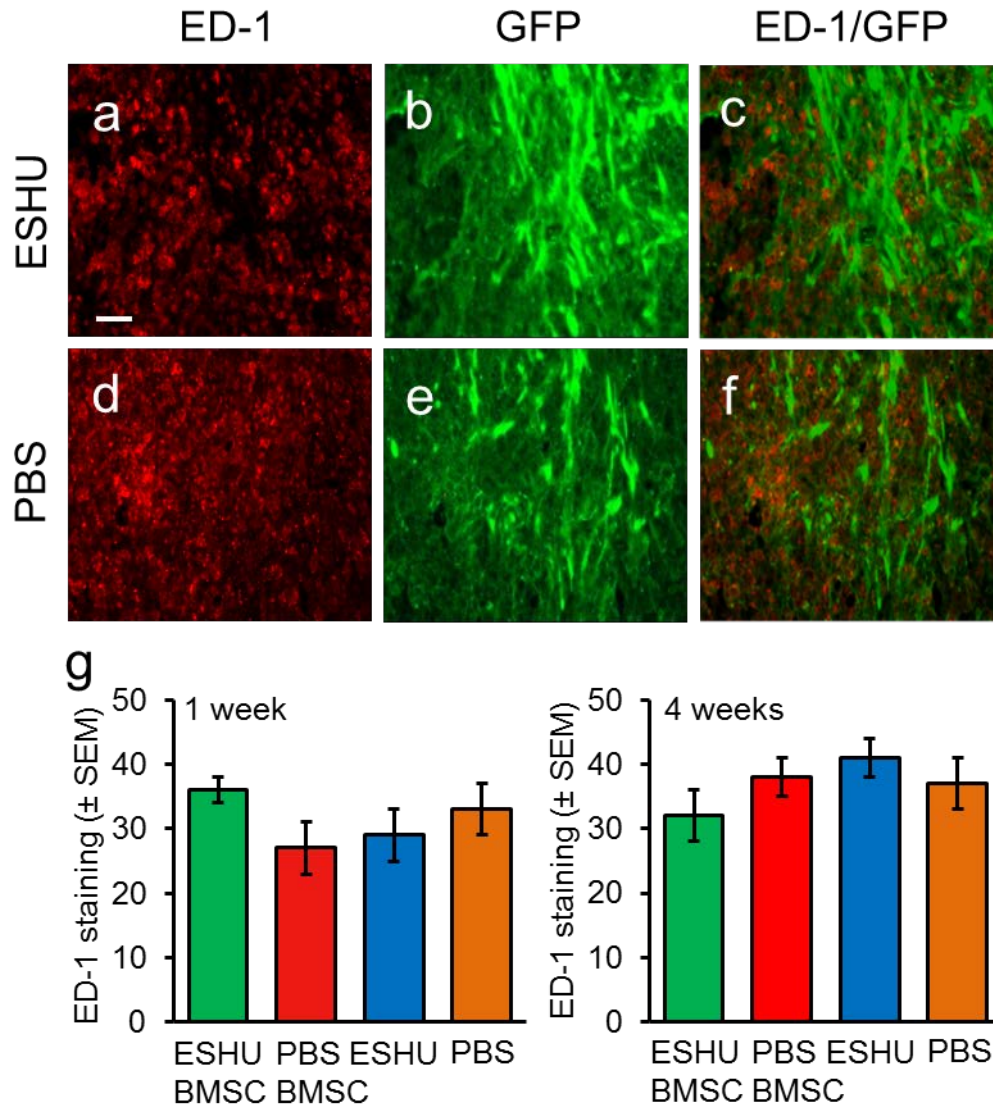


Figure 20. ESHU does not affect the injury-induced macrophage response. Macrophages (ED-1+, red) were found in the contusion with transplanted BMSC (green) in ESHU (a-c) or PBS (d-f). (g) ESHU as a transplant matrix or alone did not affect the presence of macrophages in the contusion at one and four weeks after transplantation. Error bars display SEM. Bar in a = 15 μ m in a-f.

4.3.5 Oxidative Stress-Mediated Cell Death In Vitro

We tested whether ESHU protects BMSCs from H₂O₂-mediated death in vitro (**Figure 21a**) and found that survival was increased four-fold in ESHU ($62 \pm 6\%$, SEM; $n = 9$) compared with PBS ($15 \pm 2\%$, $p < 0.05$, $n = 9$; **Figure 21b**). ESHU resulted in an almost two-fold decrease in BMSCs positive for caspase 3 or 8-oxo-dG ($p < 0.05$, $n = 9$; **Figure 21c**). To explore ESHU's cell protective effects, we assessed its proficiency in scavenging H₂O₂. We found that ESHU decreased the amount of H₂O₂ by 10% (3 ng/ml) in 30 min compared with PBS ($p < 0.05$, $n = 9$; **Figure 6d**), suggesting ESHU-mediated oxidation of H₂O₂. The data show that ESHU scavenges H₂O₂ and protects against oxidative stress-mediated cell death.

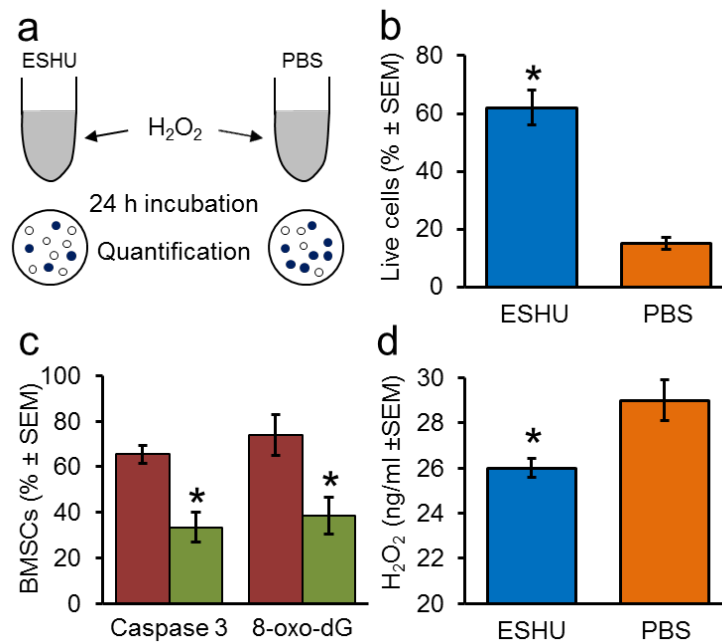


Figure 21. ESHU protects BMSCs in suspension and scavenges hydrogen peroxide in vitro. (a) Schematic representation of in vitro assay of ESHU's ability to protect BMSCs from H₂O₂-induced death. (b) Cell survival from H₂O₂-induced oxidative stress is better in ESHU than PBS. (c) Fewer BMSCs positive for caspase 3 and 8-oxo-dG with ESHU (red) than with PBS (green). (d) ESHU scavenges H₂O₂ in PBS. Error bars in bar graphs display SEM. Asterisks represent $p < 0.05$.

4.4 DISCUSSION

We show that ESHU, a synthetic injectable reverse thermal gel, protects transplanted BMSCs from death thereby prolonging their presence in damaged nervous tissue and leading to enhanced tissue sparing accompanied by improved motor function recovery. Our study demonstrates that improved intraneural BMSC transplant survival enhances their effects on repair, which may have widespread impact on BMSC-based therapies for tissue repair.

The inclusion of ESHU enhanced BMSC presence in a contusion in the adult rat spinal cord. This effect was transient possibly due to degradation of ESHU [193]. When mixed in culture medium, BMSC presence was significantly lower in the contusion site [243-246, 270]. Possibly ESHU retains BMSCs better in the contusion (i.e., the site of injection) compared with culture medium, resulting in the higher numbers. Previously we showed that about 2.4% of GFP-expressing BMSCs in culture medium leaked or migrated away from a contusion [243]. Therefore, the present results suggest that ESHU protects transplants in the contused spinal cord tissue during the first week post-injection, which is a critical time period for BMSC-mediated neuroprotection [243].

The ESHU-mediated increase in BMSC survival in the contused spinal cord resulted in anatomical (tissue sparing) and functional (motor/sensorimotor) improvements. Spared tissue volume was not affected by ESHU alone, indicating that the neuroprotection was elicited by the increased survival of the transplant. Previously, we showed that the neuroprotective effects of BMSC transplants are greatest during the first week post-injury [243]. The current finding demonstrates that the efficacy of an intraspinal BMSC transplant to elicit neuroprotection depends on its degree of survival and that increased survival leads to increased spared tissue volumes. Neuroprotection by intraneural BMSC transplants is thought to result from paracrine

effects [239-242]. Our finding that increased transplant survival results in increased tissue sparing may imply that the magnitude of neuroprotection elicited by the transplants depends on the concentration and/or availability of secreted growth factors mediating paracrine actions.

Overground walking and higher motor and sensorimotor functions of the paralyzed hindlimbs were further improved in rats that received BMSCs in ESHU. The improvements in overground walking were particularly evident during the second half of the 6-week period. It was demonstrated that BMSC transplant-mediated improvements in motor function recovery after spinal cord [232-235, 246] and brain [271-273] injury are correlated with the amount of spared nervous tissue [235, 274]. Thus, in our study, neuroprotection elicited by BMSC transplants with ESHU-increased survival likely contributes to the observed improved motor function recovery. At present the anatomical correlates underlying improved motor recovery are not completely known but may involve increased numbers of descending axons conducting the actual motor activity [235] and/or increased myelination providing better signal conduction [274, 275], which both could result from neuroprotection.

In search of potential mechanisms underlying ESHU-mediated BMSC protection, we assessed macrophage presence in the contusion. Macrophages are naturally present in damaged nervous tissue and contribute to the death of neural and transplanted cells [244, 245, 247]. Oxidation of ESHU could lead to carboxylates whose negative charges might inhibit adhesion of macrophages [269] thereby limiting their contribution to cell death. We found that the number of macrophages in the contusion was similar with or without the presence of ESHU. BMSCs are hypoimmunogenic, lacking MHC class II and co-stimulatory molecules for effector T cell induction [276], and suppress T cell proliferation [277]; thus the adaptive immune response is unlikely to be largely involved in allogeneic BMSC death. Our data suggest that the protective

effects of ESHU result from direct effects on the transplant rather than indirect effects involving macrophages.

Another possible mechanism underlying ESHU-promoted BMSC survival is antioxidation. Reactive oxygen species (ROS) accumulate rapidly in damaged nervous tissue, and induce oxidative stress, leading to cell death [248-252]. We used H₂O₂ to determine whether ESHU has the ability to scavenge ROS and thus mediate antioxidant effects. H₂O₂ is amply present in damaged nervous tissue [278]. We found that a 16% ESHU solution removed 3 ng H₂O₂ in a 30 min time period. Assuming continuous activity at 3 ng/30 min, ESHU removed ~20% of added H₂O₂ in our in vitro assay of ESHU's ability to protect BMSCs, which elicited a 47% increase in their survival relative to PBS. The ability to scavenge ROS may be exerted through its urethane groups [253, 254]. Possibly ESHU's antioxidant effects may be increased with higher concentrations [279]. Our observations point at antioxidation as a potential mechanism of ESHU-promoted BMSC transplant survival. ROS are known to contribute to transplanted cell death [251, 252]. Future studies need to define molecular factors in ESHU's protective actions and whether the protection by ESHU in vivo is concentration-dependent.

4.5 CONCLUSIONS

We demonstrate that the reparative effects of a BMSC transplant are enhanced by promoting their survival. This finding critically impacts current and future BMSC-based therapies for the central nervous system. ESHU's ability to gel at body temperature allows for injection (i.e., minimally invasive) into closed injuries. Besides reducing oxidative stress and serving as a matrix for cells, ESHU can also be used to deliver drugs and/or functionalized with bioactive

molecules to affect targeted biological events. These benefits render ESHU an important candidate in future therapies for the traumatized or degenerated nervous system. Furthermore, because oxidative stress is part of many diseases where BMSCs can be effective, such as cardiac myopathy and peripheral arterial disease, ESHU may have wide therapeutic relevance.

5.0 INJECTABLE COACERVATE FOR GROWTH FACTOR DELIVERY TO THE CONTUSED SPINAL CORD

5.1 INTRODUCTION

The complex progression of events following traumatic spinal cord injury (SCI) poses a significant challenge for providing effective treatment. Cell death, disruption of local blood flow, inflammation, reactive oxygen species and myelin debris contribute to an inhibitory environment that severely limits the regenerative potential of the central nervous system (CNS) [1]. Many strategies such as cell transplantation and biomaterials-based scaffolds have been employed to engineer a favorable environment for neuronal repair; despite some promising results however, most have demonstrated limited success. Controlled drug delivery directly to the injured spinal cord is one promising strategy for promoting neural repair; however its efficacy is limited by the short half-life of free proteins in the body, the highly inflammatory environment which can neutralize administered therapies, and the need for an injectable, biodegradable and biocompatible delivery system that will release drugs slowly over time while simultaneously protecting their bioactivity.

Here we explore a novel growth factor delivery system to deliver sonic hedgehog (Shh) to the injured spinal cord. The delivery system is composed of a synthetic polycation, poly(ethylene argininy laspartate diglyceride), or PEAD. The arginine moieties on the PEAD

backbone impart positive charge to the polymer, which enables it to bind heparin electrostatically [280]. When PEAD and heparin are combined they interact to form small sub-micron sized aggregates referred to as a “coacervate”. This system can deliver heparin-binding growth factors and morphogens with enhanced bioactivity [281, 282] and has been studied in the context of wound healing, cardiac repair, bone regeneration and therapeutic angiogenesis [283-286]. The attractiveness of the coacervate system lies in its injectability, the ability to deliver multiple growth factors, and its demonstrated ability to deliver growth factors with enhanced bioactivity [281].

Because it is generally accepted that a combinatorial approach to treating SCI will likely yield the best results, we chose to deliver a pleiotropic molecule to the injured spinal cord using the coacervate system and investigate anatomical and functional outcomes. Shh is heavily involved in neural development, influencing motor neuron and oligodendrocyte specification, axon guidance, and neural precursor proliferation [287]. It has also been implicated in angiogenesis, blood-brain barrier homeostasis and proliferation of adult neural precursors in the subventricular zone of the brain [288-290]. In the more regenerative peripheral nervous system (PNS), Shh is upregulated in Schwann cells adjacent to the injured sciatic nerve, which results in subsequent expression of brain-derived neurotrophic factor (BDNF). Inhibition of Shh with cyclopamine suppressed BDNF expression and decreased motor neuron survival in lumbar spinal cord, which suggests a potential neuroprotective role of Shh in the PNS [291]. Interestingly, in non-mammalian vertebrates such as zebrafish who are capable of CNS regeneration, Shh is expressed at high levels throughout adulthood, and inhibiting its signaling following SCI impairs motor neuron regeneration [292]. Moreover, regenerating newt limbs express Shh, and inhibition

of Shh signaling with cyclopamine inhibits regeneration [293, 294]. This information suggests that the presence of Shh signaling is involved in successful regeneration.

A handful of studies have discussed the potential for exogenous Shh administration to influence outcomes following CNS trauma. For example, Shh administration induces diffuse proliferation of nestin-positive precursors following SCI as well as ischemic stroke [295-297]. When transplanted in combination with oligodendrocyte precursors, substantial white matter sparing and functional recovery was observed [298]. Finally, delivery of Shh-loaded PLGA microspheres resulted in functional recovery, decreased glial scarring and proliferation of NG2-positive cells following administration in both contusion and dorsal over-hemisection models of SCI in mice [299]. The precise mechanisms for the effects of Shh are unclear, though it is obvious that Shh is a promising candidate for CNS therapy. Therefore, we hypothesized that controlled Shh delivery from a heparin-based coacervate delivery system would improve outcomes after contusion in adult rats. The objective of this work was to evaluate the biocompatibility of the coacervate in the injured spinal cord, and assess the effectiveness of Shh in promoting repair.

5.2 MATERIALS AND METHODS

5.2.1 Coacervate Preparation

The cationic polymer, poly(ethylene argininy laspartate diglyceride) (PEAD), was synthesized as previously described [280]. PEAD and clinical-grade heparin (Scientific Protein Labs, Waunakee, WI) were each dissolved in 0.9% saline, and sterilized via filtration through 0.22 μm

filters. To prepare the coacervate, heparin was first complexed with Shh (Peprotech) then PEAD was added. Self-assembly of the PEAD and heparin:Shh complexes resulted in immediate precipitation to form the coacervate. Solutions were prepared at a final Shh concentration of 100 ng/ μ l. For controls, heparin was directly complexed with PEAD without the addition of Shh.

5.2.2 Spinal Cord Contusion Model

All animal experiments were conducted in compliance with protocols approved by the Institutional Animal Care and Use Committee at the University of Pittsburgh, with strict adherence to guidelines of the National Institutes of Health and United States Department of Agriculture. Female Sprague Dawley rats (225-250g, n=10/group; Charles River Laboratory, Wilmington, MA, USA) were anesthetized via intraperitoneal injection of ketamine (60 mg/kg Butlerschein, Dublin, OH, USA) and dexdomitor (0.5 mg/kg, Pfizer, New York, NY, USA). Following laminectomy, an Infinite Horizon impactor (Precision Systems and Instrumentation, LLC, Versailles, KY, USA) was used to generate a 200 kDyne contusion injury at the tenth thoracic segment of the spinal cord. The injury was then rinsed with sterile 0.9% saline containing 0.1% gentamicin (VWR, Radnor, PA, USA), the muscles were sutured and the skin closed with Michel wound clips (Fine Science Tools, Foster City, CA, USA). Three days post-injury, animals were sedated for a second time, the injury site was exposed and animals were injected with 5 μ l of one of four treatments: PEAD:Heparin:Shh, PEAD:Heparin, Shh only, or PBS only. For groups receiving Shh, the total administered dose was 500 ng.

5.2.3 Post-Surgical Care

Antisedan (1.5 mg/kg; Pfizer, New York, NY, USA) was injected subcutaneously to wake the animals following both procedures. Intramuscular administration of gentamicin (6 mg/kg; VWR, Radnor, PA, USA), was administered for 7 days following injury, and subcutaneous administration of Rimadyl (5 mg/kg; Pfizer, New York, NY, USA) and Ringer's solution (5 ml; Butlerschein, Dublin, OH, USA) were administered for 6 days post-injury. Bladders were manually expressed twice daily until the ability to urinate was regained (approximately 2 weeks post-injury).

5.2.4 Motor Function Assessment

5.2.4.1 BBB

Overground walking ability of the animals was assessed using the Basso, Beattie and Bresnahan (BBB) open field test [262]. Animals were assessed at 1, 3, 7, 14, 21, 28, 35 and 42 days post-injury. Experimenters blinded to treatment groups observed the animals for 4 minutes and assigned a score between 0 and 21, signifying the hindlimb locomotor capability of the animal.

5.2.4.2 Horizontal Ladder Walk

Sensorimotor function was assessed using the horizontal ladder test. Rats were recorded walking across a ladder with irregularly-spaced rungs, and slips of the foot up to the ankle (small) and whole leg (large) were counted and expressed as a percentage of the total number of steps taken. Three runs were analyzed per animal.

5.2.4.3 Gait Analysis

The DigiGait Analysis System (MouseSpecifics, Boston, MA, USA) was used to analyze specific parameters of hindlimb locomotion before and after injury. The DigiGait system consists of a clear treadmill with a camera located underneath which records and digitizes the animal's footprints. Animals were acclimated to the treadmill for four days prior to taking baseline (pre-injury) and endpoint (6 weeks post-injury) video recordings at a speed of 20 cm/s. The videos were then analyzed for a number of gait indices such as paw area, paw angle, stride length and coordination. 6 week data were compared to baselines and values averaged per experimental group.

5.2.5 Histological Analysis

Six weeks post-injury, rats were anesthetized, then transcardially perfused with 300 mL PBS, followed by 400 mL 4% paraformaldehyde (Sigma-Aldrich, Allentown, PA, USA) in PBS. Spinal cords were dissected and post-fixed in 4% paraformaldehyde overnight, followed by cryoprotection in 30% sucrose for at least 48h. A spinal cord segment measuring 12 mm centered on the lesion was cut into serial sections at a thickness of 14 μ m. Histological stains included cresyl violet for general morphology and tissue sparing analysis. Immunohistochemical stains included GFAP (1:400, DAKO), ED1 (1:250, Millipore), 5-HT (1:2000, Immunostar), RT-97 (1:200, DSHB), and Nestin (1:100, BD Biosciences). Briefly, sections were blocked for 1h at room temperature with 10% normal goat serum (NGS) with 0.1% Triton, then incubated overnight in 1^o antibody solutions diluted in 2% NGS with 0.1% Triton. After washing, samples were incubated in 2^o solutions (goat anti-mouse 488 or goat anti-rabbit 594, 1:200, Invitrogen) for 2h at room temperature, washed and counter-stained with DAPI, then coverslipped.

5.2.6 Quantitative Immunofluorescence Analysis

Images were analyzed using Nikon NIS Elements software. For macrophage quantification, the number of ED1 positive cells was quantified on large image composites of the entire lesion and expressed as a function of the tissue area. GFAP intensity was assessed on images taken rostral, caudal, and at the lesion epicenter, and total intensity was considered to be the average intensity of all regions. 5HT and RT97 were quantified similarly, and the total amount of positive fiber staining was expressed as a function of the tissue area.

5.2.7 Statistical Analysis

Data are expressed as mean \pm standard error of the mean (SEM). Statistical analyses for endpoint outcomes such as Digigait, tissue sparing and immunohistochemistry were performed using one-way ANOVA with Fisher pairwise comparisons when significance ($p < 0.05$) was indicated. Repeated measures analysis was used for time-dependent studies (BBB, horizontal ladder walk) with Fisher pairwise comparisons when significance was indicated. All data were analyzed using Minitab 17 software.

5.3 RESULTS AND DISCUSSION

5.3.1 Biocompatibility of PEAD in the Injured Spinal Cord

Because PEAD is untested in the injured spinal cord, we sought to assess its biocompatibility by quantifying the inflammatory response and the extent of glial scarring. Following traumatic injury, there is a large influx of macrophages to the spinal cord both at the lesion epicenter and in more distant regions of the cord which is sustained for several weeks [300]. Introduction of a foreign material may worsen this response; therefore the density of ED1+ macrophages was quantified within the lesion. The macrophage density was similar in all experimental groups tested ($p>0.05$), suggesting that PEAD injection does not exacerbate inflammation (**Figure 22A, D**). Similarly, analysis of glial fibrillary acidic protein (GFAP) revealed that PEAD injection did not increase glial scarring (**Figure 22B, C, D**). Glial scar formation is part of the highly complex cascade of reactive processes which occurs following injury and serves to preserve still healthy tissue from injury progression. Many of the cell types that compose the scar, such as astrocytes and meningeal fibroblasts, produce inhibitory molecules which prevent axon regeneration and therefore it is critical that an increase in scar formation is not observed [301]. Additionally, the Shh-coacervate group saw a significant reduction in total glial scar formation as well as scarring at the lesion epicenter compared to PBS and empty coacervate groups. Free Shh also had significantly less scarring compared to empty coacervate groups at the lesion epicenter. This data suggests that Shh may play a role in reducing astrocyte activation and subsequent scar formation. While the effects of Shh administration on glial scar formation have not been explicitly studied, it has been reported that hedgehog pathway activation in astrocytes can alter their phenotypic behavior following injury [302]. Specifically, Shh induces phenotypic plasticity in activated

astrocytes both in vitro and in vivo following middle cerebral artery occlusion and stab wound injuries in the brain. When isolated and cultured in vitro, these cells can differentiate into neurons, oligodendrocytes and astrocytes with the proper cues. It is possible that exogenous Shh administration alters the typical behavior of the activated astrocytes and thus reduces their contribution to scar formation, though more exhaustive mechanistic studies would need to be performed to confirm this hypothesis.

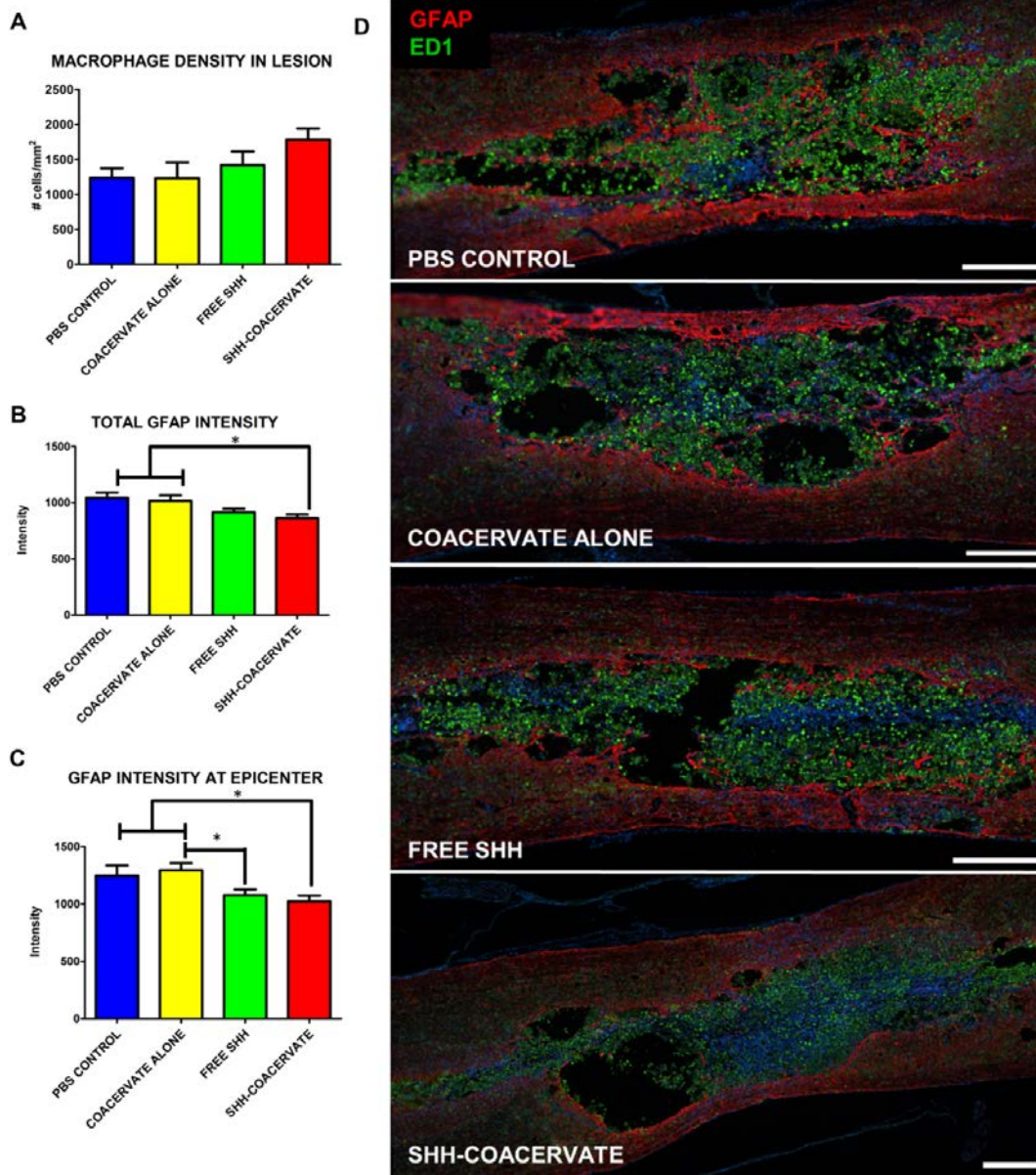


Figure 22. Effect of PEAD injection on the inflammatory response. PEAD does not increase the macrophage density at the lesion epicenter (A, D). Glial scarring, as measured by the intensity of GFAP staining, was also not different in groups receiving the coacervate compared to PBS controls. The intensity of the entire glial scar was quantified (B) as well as at the lesion epicenter, where presumably scarring would be the most prominent (C). In both cases, animals receiving the Shh coacervate had a significant ($p < 0.05$) reduction in GFAP intensity compared to PBS and empty coacervate groups, indicating a possible effect of Shh delivery on scar formation. (Scale bar = 500 μm)

5.3.2 Effect of Controlled Shh Delivery on Nervous Tissue Sparing

It has previously been reported that intrathecal Shh administration results in tissue sparing following ischemic stroke in rats, presumably due to the recruitment of nestin-positive progenitor cells which may exert a neuroprotective effect [295]. Therefore, the volume of spared nervous tissue was quantified stereologically to determine whether local Shh delivery will have a similar effect in spinal cord injured animals. Figure 23 shows the nervous tissue volume expressed as a percentage of healthy spinal cord tissue. The Shh coacervate group had the largest volume of spared tissue ($32.23 \pm 10.08\%$ compared to $28.78 \pm 9.07\%$ in PBS, $26.31 \pm 6.24\%$ in empty coacervate and $28.47 \pm 9.18\%$ in free Shh groups) suggesting a potential effect of Shh delivery on tissue preservation, though the differences are not statistically significant. Future Shh dose optimization may result in more substantial tissue sparing compared to controls.

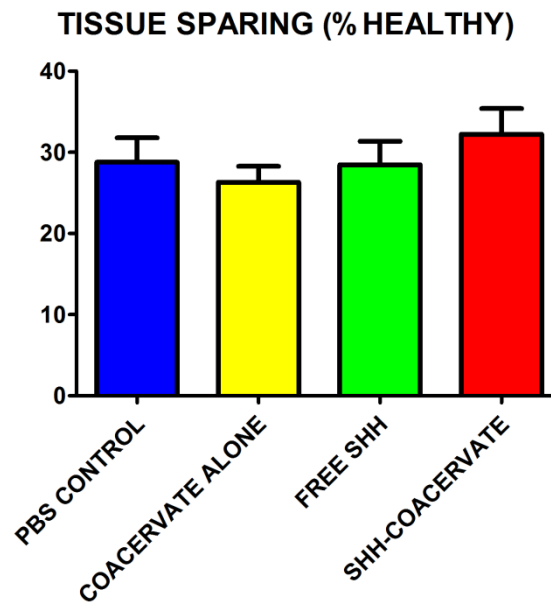


Figure 23. Effect of Shh administration on nervous tissue sparing. Nervous tissue sparing was not statistically significant between experimental groups; however Shh-coacervate treatment did result in the largest percentage of tissue sparing.

5.3.3 Neuronal Fiber Density

To assess whether controlled Shh delivery had an effect on neural cell populations or axon growth beyond the lesion we quantified neurofilament presence with the antibody RT97, and serotonergic fibers with 5HT. The relative density of positive staining was determined both rostral and caudal to the lesion and results are shown in Figure 24. There appear to be trends towards increased 5HT and RT97 staining in Shh coacervate groups, especially rostral to the lesion. This suggests that Shh may be playing a role in limiting neuronal dieback and preserving neuronal viability. These data are in agreement with previously reported results that found Shh administration increased the length of serotonergic fibers [299].

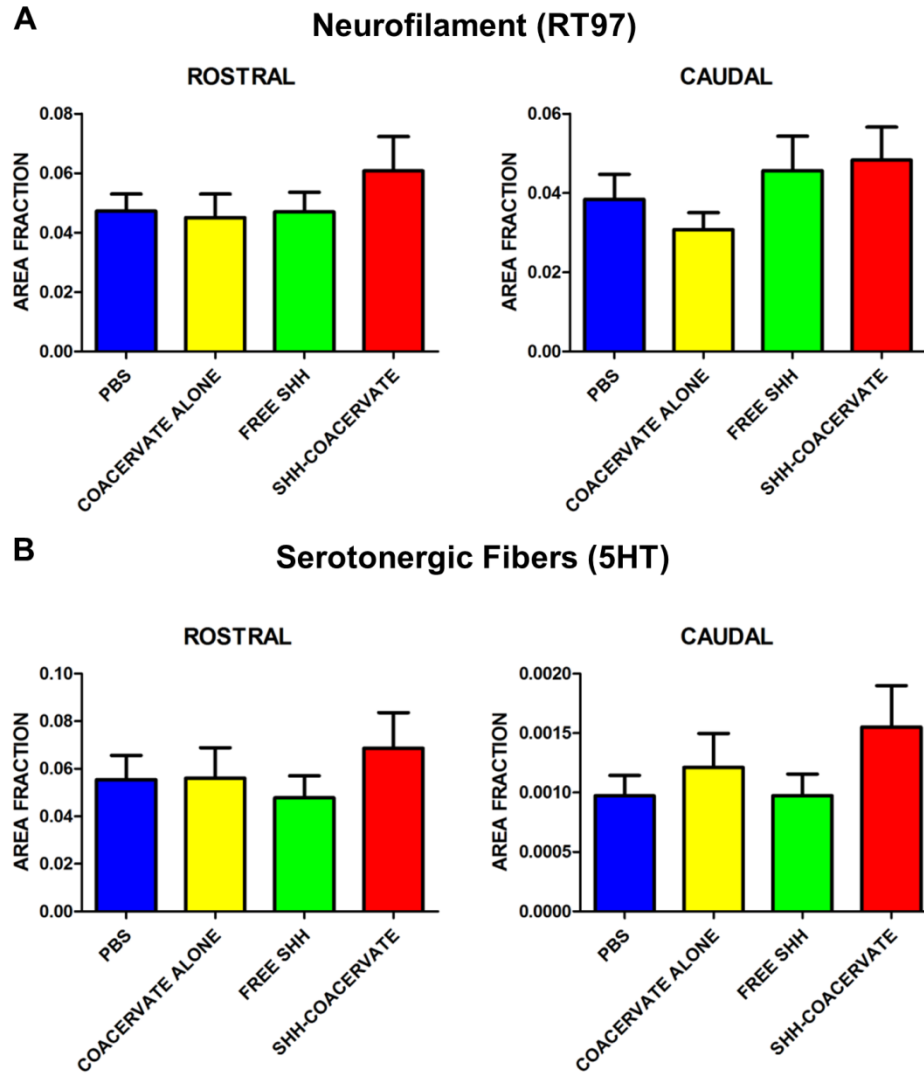


Figure 24. Density of axons and serotonergic fibers rostral and caudal to the lesion. The amount of positive neurofilament (A) and serotonergic fiber (B) staining was determined by calculating the area of positive staining as a fraction of total tissue area.

5.3.4 Motor Function Outcomes

The BBB test was performed weekly throughout the study period. In order to account for variability between animals, BBB scores for each animal were normalized by their 1 day post-injury values (**Figure 25**). The free Shh group has an early increase in BBB score that plateaus at

around 28 days, while the Shh-coacervate animals exhibited slowly improving scores throughout the study period. Perhaps this suggests an early improvement in motor function following exposure to a large dose of Shh whose effects wear off after a few weeks, whereas controlled release of Shh causes a steady, gradual improvement. Statistically, there were no differences between free Shh, Shh-coacervate groups and PBS controls; however, the empty coacervate group had significantly lower scores than the other three groups when the effect of day was removed.

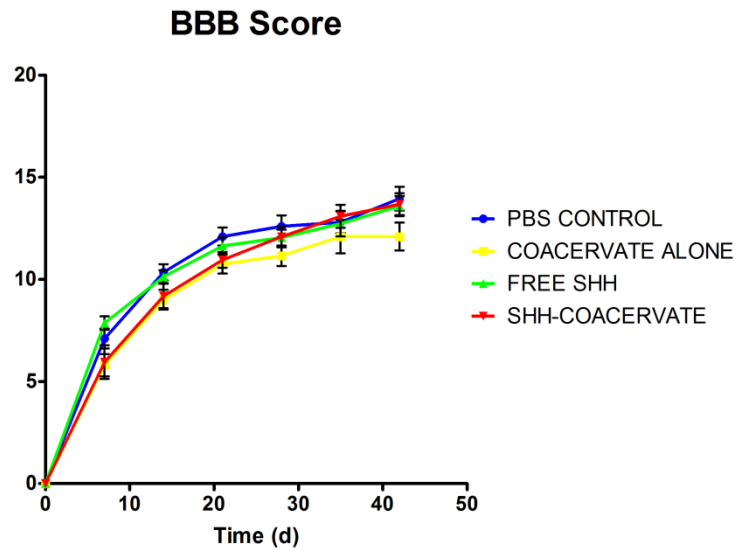


Figure 25. BBB results. Free Shh groups performed well early, whereas Shh-coacervate groups had steadily increasing BBB scores throughout the study.

Similar phenomena could be observed in the horizontal ladder results. Looking at the improvement in slips over time (**Figure 26**) shows that Shh-coacervate animals had the highest reduction in the number of slips made from 2 to 4 weeks post injury, 4 to 6 weeks post injury, as well as 2 to 6 weeks post injury. However the high variability observed between animals for this particular assessment means that none of these results were statistically significant.

SLIP IMPROVEMENT

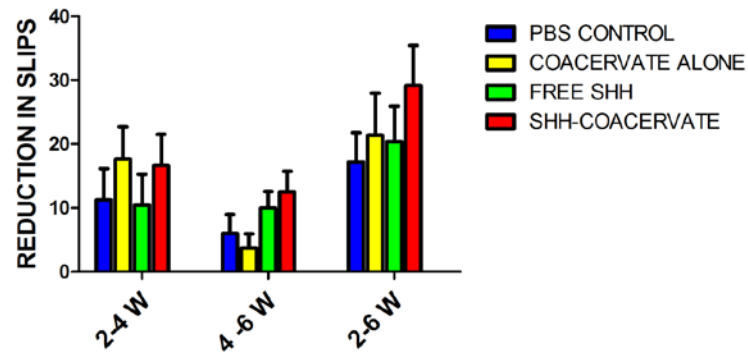


Figure 26. Improvement in hindlimb stepping over time. Shh-coacervate groups had the largest decrease in the number of slips made over the time course of the study period. This indicates that improvements in sensorimotor function were the largest in the controlled delivery groups.

Finally, Digigait analysis indicated slight differences between experimental groups (**Figure 27**). 100% of animals in free Shh and Shh-coacervate groups were physically capable of walking on the treadmill at a speed of 20 cm/s. However, in the empty coacervate and PBS control groups, 80% and 90% of animals respectively were unable to walk and therefore data could not be obtained. This suggests that animals receiving Shh performed better at higher walking speeds than animals receiving control injections. Additionally, stride length was measured and compared to that of healthy animals. Shh-coacervate stride length was the only group whose stride length was not significantly different from healthy animals. Injured animals had a longer stride length as it takes more time for them to lift and swing the hindlimb through to the top of the step; therefore, animals receiving the Shh-coacervate had regained a stride length comparable to healthy animals. Additionally, Shh-coacervate and free Shh animals had a significantly lower paw angle than PBS or empty coacervate groups, though these values were still significantly larger than the paw angle of healthy animals. The increased paw angle is a

result of attempted stability following injury. Hindlimb weakness prevents the animals from adopting a normal stance and thus their paws turn out in order to provide more stability. The significant reduction seen in Shh groups suggests an increased stability in the overground walking ability of these animals.

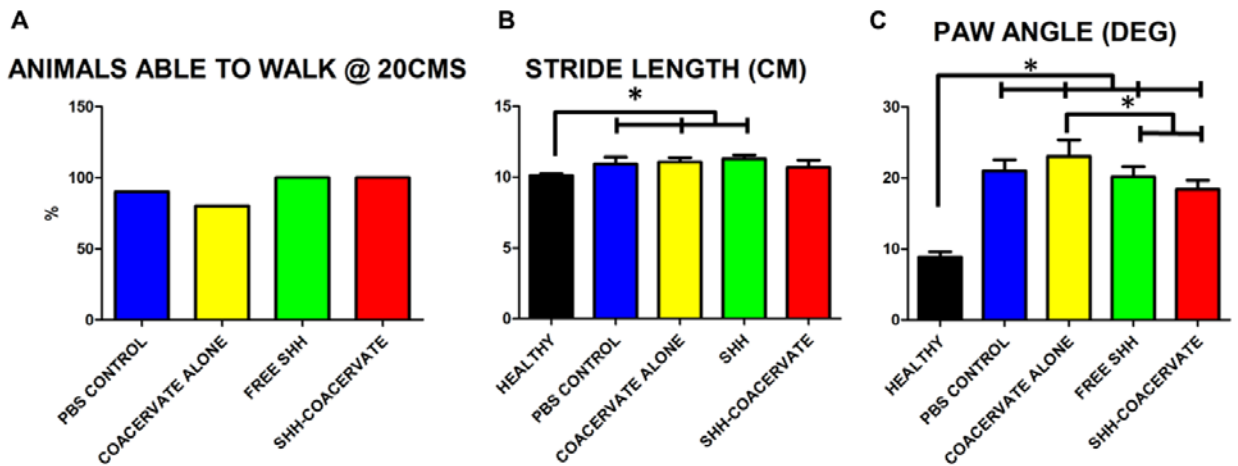


Figure 27. Gait analysis reveals slight improvements in overground walking ability of Shh-coacervate animals. In control groups, three animals were unable to walk at the recording speed of 20 cm/s. All animals in free Shh and Shh-coacervate groups were capable of walking (A). The stride length of Shh-coacervate animals was not significantly different than healthy animals, suggesting an improvement in stepping (B). The paw angle of free Shh and Shh-coacervate animals was significantly less than in controls, suggesting an improved stability when stepping, though the paw angles were still significantly different than in uninjured controls (C).

Slight trends toward improved functional recovery, axon density and tissue sparing in Shh-coacervate groups can be potentially be explained by a few factors. The first is that dose optimization was not performed in this study; because little work has been done in exploring exogenous Shh administration to the injured spinal cord, we chose 500ng based on what available information there was, combined with the dose that was demonstrated to elicit a significant response in cardiac cells in vitro [284]. Additionally, it is possible that the 3-day

delayed injection, while more clinically relevant, is unsuitable for growth factor administration. The high level of inflammation at that time period may have speeded up Shh release from the coacervate and limited its controlled release capabilities. In the future, dose and treatment time optimization may further enhance the efficacy of this system in treating contusive SCI.

5.4 CONCLUSIONS

The present work demonstrated the utility of an injectable, affinity-based growth factor delivery system to the injured spinal cord. PEAD is compatible with CNS tissues and does not negatively impact the typical course of injury progression. Controlled release of sonic hedgehog resulted in decreased glial scarring, and may potentially be involved in neuronal survival and nervous tissue sparing. Future work will focus on dosage optimization and combinatorial approaches, such as multiple growth factor delivery, or cell transplantation combined with growth factors to sustain transplant survival.

6.0 FINAL SUMMARY

Efficient and effective treatment of CNS injury and disease remains a significant challenge due to the intricate structure and function of the CNS, barriers to effective diffusion and unfavorable environments for regeneration. Achieving desired release characteristics while simultaneously protecting the activity of therapeutic biomolecules is critical for the success of controlled drug delivery. The present work describes the formulation, characterization and in vivo evaluation of two novel injectable drug delivery systems that are ideally suited for CNS applications. The biomaterials systems discussed herein can be utilized as minimally invasive neural therapeutics either alone or in combination with other strategies to enhance clinical outcomes. This work lays the foundation for the continued use of these platform technologies for a myriad of applications that span several tissue and organ systems.

6.1 OCULAR DRUG DELIVERY USING REVERSE THERMAL GELS – MAJOR FINDINGS, LIMITATIONS AND FUTURE WORK

In the eye, we studied the viability of an bevacizumab-containing reverse thermal gel system for intravitreal drug delivery. The major findings of this work are:

- ESHU gels are compatible with ocular cell types in vitro, and cause minimal cell death. Compared to commonly-used clinical materials such as silicone, ESHU is relatively non-toxic. This indicates that ESHU should display good biocompatibility in the eye.
- When dissolved in bevacizumab solutions, ESHU gels form an anti-angiogenic drug delivery system that sustains bevacizumab release for over 17 weeks in vitro.
- ESHU-bevacizumab delivery systems are easily injectable through 31G needles and instantaneously form spherical hydrogels upon injection to rabbit eyes.
- ESHU is biocompatible in the eye – intraocular pressure and retinal integrity are unaffected by the presence of the gels and there is little observed inflammatory response.
- Bevacizumab release from hydrogels is sustained for over 9 weeks in vivo at levels approximately 4 times higher than drug alone, indicating that ESHU delivery systems can prolong bevacizumab presence in the eye as hypothesized.

These findings demonstrate the promise of reverse thermal gels for intravitreal drug delivery. Such a strategy has distinct advantages, such as direct exposure of posterior segment tissues to the released drug, minimally invasive administration, and no need for surgical removal of the delivery system. There are two major limitations to this work which are currently being addressed and will be reported in future studies:

- Confirmation of maintained bioactivity of the released bevacizumab over time, both in vitro and in vivo.
- Optimization of bevacizumab degradation time with drug release.

The released bevacizumab was detected using a VEGF ELISA, which indicates that detected drug is still capable of binding its target, providing evidence that bioactivity is maintained. However, limited stability of bevacizumab posed significant complications when performing assays to assess bioactivity. Due to a lack of reliable, well-controlled animal models for choroidal neovascularization and because bevacizumab is a humanized antibody [228], in vivo efficacy of the ESHU delivery system was not assessed in rabbits. Future work will focus on testing this delivery system in an actual animal model of CNV. Two experimental models are currently being considered: the first is a transgenic mouse that is engineered to overexpress humanized VEGF in the retina [303], and the second is a non-human primate model of CNV induced by laser photocoagulation [304].

Finally, our in vivo work showed that all drug was released from the hydrogels several weeks before the gels had degraded. Because the eye is considered immune-privileged, there are few enzymatic or cellular factors affecting degradation of the gel. Therefore, hydrolysis is the principle degradation mechanism, which is known to be slow in degrading polyurethanes [305]. A significant challenge in translating this technology will be successful degradation of the gel at a rate that is in line with drug release and, therefore, injection frequency. Therefore, the chemical structure of ESHU is currently being adjusted by the introduction of polyester bonds in order to increase the rate of hydrolytic degradation of gels in vivo.

6.2 IMPROVED TRANSPLANT SURVIVAL USING REVERSE THERMAL GELS FOR TREATMENT OF SPINAL CORD INJURY – MAJOR FINDINGS, LIMITATIONS AND FUTURE WORK

To demonstrate the versatility of ESHU as a platform delivery technology, we assessed its effect on transplant survival in spinal cord injured rats. Major findings from this work include:

- ESHU protects transplanted BMSCs from oxidative stress-induced death in vitro. Physical protection of the cells as well as oxidation of urethane bonds in the gel by reactive oxygen species are two potential protective mechanisms behind this effect.
- This protective effect is translated in vivo, where BMSCs transplanted in ESHU had 3.5-fold increased survival 1 week post-injury. Long term (28d) survival of the cells, however, was not observed.
- Increased cell survival in the first week after injury was associated with a 66% increase in nervous tissue sparing and enhanced hindlimb motor and sensorimotor recovery.

The most significant finding of this work is that the reparative potential of transplanted cells can be directly linked to their survival – a long-hypothesized theory that had not previously been demonstrated. The most significant limitation of this work is a lack of precise understanding of the mechanisms behind which BMSC transplants promote repair and the major contributors to their fate. Though paracrine effects are thought to play a role, a more precise understanding of the mechanisms of BMSC-promoted repair will help drive the evolution of new transplant strategies. Even a small, one week increase in transplant survival resulted in significant functional and anatomical improvement. Future work should include further

enhancement of BMSC survival in the injured spinal cord, either by co-administration of survival-promoting factors, or by improved protection strategies.

6.3 COACERVATE-BASED PROTEIN DELIVERY TO THE INJURED SPINAL CORD – MAJOR FINDINGS, LIMITATIONS AND FUTURE WORK

The final chapter of this dissertation discusses the safety and efficacy of a coacervate-based growth factor delivery system to treat SCI. Because we recognize the eventual need for a combinatorial strategy for effective treatment of SCI, we wished to assess the feasibility of this delivery system, with the ultimate goal of utilizing it in combination with other treatment strategies. We chose to study sonic hedgehog protein, due to its well-known pleiotropic effects in the CNS and throughout the body. Major findings of this study are:

- The PEAD coacervate is safe to use in the spinal cord; it does not exacerbate the inflammatory response following injury, nor does it increase glial scar formation.
- Though the effects of controlled Shh delivery are inconclusive, slight improvements in tissue sparing, serotonergic fiber density and overground walking ability suggest that Shh administration does have an effect in the injured spinal cord that needs to be further evaluated.

These findings demonstrate that the PEAD delivery system is a viable option for delivery of heparin-binding molecules to the spinal cord; however the inconclusive functional and anatomical results suggest that it will be best-suited for combinatorial treatment strategies. The major limitations of this work include:

- A lack of information about the effects of Shh administration to the injured spinal cord – a handful of reports exist that argue Shh could be beneficial, however dose optimization must be performed in order to maximize its therapeutic potential.
- The time course of injury progression and treatment administration is critical for maximizing outcomes. A 3-day delayed injection of the PEAD-Shh delivery system may be sub-optimal. Evaluation of the best treatment time is necessary.

Future work will focus on dose and intervention time optimization, as well as maximizing therapeutic outcomes by delivering multiple growth factors, further sustaining Shh release by utilizing the ESHU gel, or co-transplantation with BMSCs or other progenitor transplants.

6.4 OVERALL CONCLUSIONS

In summary, this work sets the foundation for easily implantable biomaterials-based treatment systems for CNS repair. These materials are platform technologies that can be utilized to deliver most types of drugs, biomolecules, and cells to promote repair and slow disease progression. The complexity of CNS injury and disease in many cases will necessitate multi-faceted strategies and the biomaterials described in this work are ideally designed for inclusion in such an approach.

APPENDIX A

DETAILED ANALYSIS OF BEVACIZUMAB CONCENTRATIONS

Methods: The observed concentrations were modeled using a first order compartment model for the 0.25 power of the bevacizumab concentration $y(t)$:

$$y(t) = \frac{\exp(\phi_{e_0} + \phi_{e_1} T) \exp(\phi_{a_0} + (\phi_{a_1} + a_{1i}) T)}{\exp(\phi_{c_0} + \phi_{c_1} T) [\exp(\phi_{a_0} + (\phi_{a_1} + a_{1i}) T) - \exp(\phi_{e_0} + \phi_{e_1} T)]} [\exp[-\exp(\phi_{e_0} + \phi_{e_1} T) x] - \exp[-\exp(\phi_{a_0} + (\phi_{a_1} + a_{1i}) T) x]] + \epsilon$$

where x denotes the time in days, T denotes the treatment (coded 0 for bevacizumab and 1 for ESHU-bevacizumab) ϕ_{e_0} denotes the natural logarithm of the elimination rate constant for treatment A, ϕ_{e_1} the difference in the elimination rate constant between treatment EA and A, ϕ_{a_0} denotes the natural logarithm of the absorption rate constant for treatment A, ϕ_{a_1} the difference in the elimination rate constant between treatment EA and A, ϕ_{c_0} denotes the natural logarithm of the absorption rate constant for treatment A, ϕ_{c_1} the difference in the clearance rate constant between treatment EA and A, a_{1i} is a random effect for the absorption rate difference, and ϵ is a random error.

Raising the bevacizumab concentration to the 0.25 power (taking the 4th root) was necessary to ensure homoskedasticity (constant variance) of the random errors (ϵ) and to guarantee convergence to the maximum likelihood parameter estimates for the nonlinear mixed effects model. This transformation was used instead of a logarithmic transformation because

several measured concentrations were recorded as zeroes. The effect of taking the 4th root is otherwise similar to the use of a logarithmic transformation.

Results: Bevacizumab and ESHU-bevacizumab treatments had similar elimination rate constants so the model was refitted with ϕ_{el} constrained to zero. With only seven eyes, the random effects were not well estimated. The fixed effects, however, were well estimated as shown in Tables S1 and S2. Figure S1 compares the difference in effect for the treatments. For the fixed effects estimates (Table S1) and the corresponding fixed effects 95% confidence intervals (Table S2), the rate constants for the bevacizumab group are statistically significant (their confidence intervals exclude 0), and the differences with ESHU-bevacizumab treatment are statistically significant (their confidence intervals exclude 0). The widths of the confidence intervals (and correspondingly, the standard errors and t-statistics) indicate that the clearance rate constant between bevacizumab and ESHU-bevacizumab treatments, and the elimination rate constant for bevacizumab treatment were the most precisely estimated parameters (that is, their confidence intervals were narrow, their standard errors small relative to the parameter estimate, and consequently their t-statistics were very large).

Table A1: Fixed effects parameter estimates for the fourth root of bevacizumab concentrations based on the fitted nonlinear mixed effects model.

<i>Model Parameter</i>	<i>Estimate</i>	<i>Standard Error</i>	<i>Degrees of Freedom</i>	<i>t-statistic</i>	<i>P</i>
ϕ_{e0}	-3.232	0.046	66	-69.637	<0.0001
ϕ_{a0}	0.911	0.290	66	3.145	0.0025
ϕ_{a1}	-0.957	0.297	66	-3.216	0.0020
ϕ_{c0}	-4.187	0.042	66	-99.503	<0.0001
ϕ_{c1}	-0.216	0.040	66	-5.389	<0.0001

Table A2: 95% confidence intervals for fixed effect model parameters.

<i>Model Parameter</i>	<i>Lower Bound</i>	<i>Estimate</i>	<i>Upper Bound</i>
ϕ_{e0}	-3.322	-3.232	-3.143
ϕ_{a0}	0.352	0.911	1.469
ϕ_{a1}	-1.531	-0.957	-0.382
ϕ_{c0}	-4.268	-4.187	-4.106
ϕ_{c1}	-0.294	-0.216	-0.139

BIBLIOGRAPHY

- [1] Gumerá C, Rauck B, Wang Y. Materials for central nervous system regeneration: bioactive cues. *Journal of Materials Chemistry*. 2011;21:7033-51.
- [2] Access Economics, prepared for AMD Alliance International: The Global Economic Cost of Visual Impairment. 2010.
- [3] Prevent Blindness America. Vision problems in the US: Prevalence of adult vision impairment and age-related eye disease in America. Prevent Blindness America; 2012.
- [4] Geroski DH, Edelhauser HF. Drug Delivery for Posterior Segment Eye Disease. *Investigative Ophthalmology & Visual Science*. 2000;41:961-4.
- [5] Urtti A. Challenges and obstacles of ocular pharmacokinetics and drug delivery. *Advanced drug delivery reviews*. 2006;58:1131-5.
- [6] Hornof M, Toropainen E, Urtti A. Cell culture models of the ocular barriers. *European Journal of Pharmaceutics and Biopharmaceutics*. 2005;60:207-25.
- [7] Cunha-Vaz JG. The blood-retinal barriers. *Documenta ophthalmologica Advances in ophthalmology*. 1976;41:287-327.
- [8] Shah CP, Garg SJ, Vander JF, Brown GC, Kaiser RS, Haller JA. Outcomes and Risk Factors Associated with Endophthalmitis after Intravitreal Injection of Anti-Vascular Endothelial Growth Factor Agents. *Ophthalmology*. 118:2028-34.
- [9] Day S, Acquah K, Mruthyunjaya P, Grossman DS, Lee PP, Sloan FA. Ocular Complications After Anti-Vascular Endothelial Growth Factor Therapy in Medicare Patients With Age-Related Macular Degeneration. *American Journal of Ophthalmology*. 152:266-72.
- [10] Prausnitz MR, Noonan JS. Permeability of cornea, sclera, and conjunctiva: a literature analysis for drug delivery to the eye. *Journal of pharmaceutical sciences*. 1998;87:1479-88.
- [11] Ambati J, Gragoudas ES, Miller JW, You TT, Miyamoto K, Delori FC, et al. Transscleral Delivery of Bioactive Protein to the Choroid and Retina. *Investigative Ophthalmology & Visual Science*. 2000;41:1186-91.

- [12] Pitkänen L, Ranta V-P, Moilanen H, Urtti A. Permeability of Retinal Pigment Epithelium: Effects of Permeant Molecular Weight and Lipophilicity. *Investigative Ophthalmology & Visual Science*. 2005;46:641-6.
- [13] Lowder C, Belfort R, Jr, Lightman S, et al. Dexamethasone intravitreal implant for noninfectious intermediate or posterior uveitis. *Archives of ophthalmology*. 2011;129:545-53.
- [14] Haller JA, Bandello F, Belfort R, Blumenkranz MS, Gillies M, Heier J, et al. Dexamethasone Intravitreal Implant in Patients with Macular Edema Related to Branch or Central Retinal Vein Occlusion: Twelve-Month Study Results. *Ophthalmology*. 2011;118:2453-60.
- [15] Haller JA, Bandello F, Belfort R, Blumenkranz MS, Gillies M, Heier J, et al. Randomized, Sham-Controlled Trial of Dexamethasone Intravitreal Implant in Patients with Macular Edema Due to Retinal Vein Occlusion. *Ophthalmology*. 2010;117:1134-46.e3.
- [16] Haghjou N, Soheilian M, Abdekhodaie MJ. Sustained release intraocular drug delivery devices for treatment of uveitis. *Journal of ophthalmic & vision research*. 2011;6:317-29.
- [17] Shelke NB, Kadam R, Tyagi P, Rao VR, Kompella UB. Intravitreal Poly(L-lactide) Microparticles Sustain Retinal and Choroidal Delivery of TG-0054, a Hydrophilic Drug Intended for Neovascular Diseases. *Drug delivery and translational research*. 2011;1:76-90.
- [18] Cardillo JA, Souza-Filho AA, Oliveira AG. Intravitreal Bioerudivel sustained-release triamcinolone microspheres system (RETAAC). Preliminary report of its potential usefulness for the treatment of diabetic macular edema. *Archivos de la Sociedad Espanola de Oftalmologia*. 2006;81:675-7, 9-81.
- [19] Moritera T, Ogura Y, Yoshimura N, Honda Y, Wada R, Hyon SH, et al. Biodegradable microspheres containing adriamycin in the treatment of proliferative vitreoretinopathy. *Investigative ophthalmology & visual science*. 1992;33:3125-30.
- [20] Carrasquillo KG, Ricker JA, Rigas IK, Miller JW, Gragoudas ES, Adamis AP. Controlled delivery of the anti-VEGF aptamer EYE001 with poly(lactic-co-glycolic) acid microspheres. *Investigative Ophthalmology & Visual Science*. 2003;44:290-9.
- [21] He Y, Liu Y, Liu Y, Wang J, Zhang X, Lu W, et al. Cyclosporine-loaded microspheres for treatment of uveitis: in vitro characterization and in vivo pharmacokinetic study. *Investigative ophthalmology & visual science*. 2006;47:3983-8.
- [22] He Y, Wang JC, Liu YL, Ma ZZ, Zhu XA, Zhang Q. Therapeutic and toxicological evaluations of cyclosporine a microspheres as a treatment vehicle for uveitis in rabbits. *Journal of ocular pharmacology and therapeutics : the official journal of the Association for Ocular Pharmacology and Therapeutics*. 2006;22:121-31.
- [23] de Kozak Y, Andrieux K, Villarroya H, Klein C, Thillaye-Goldenberg B, Naud MC, et al. Intraocular injection of tamoxifen-loaded nanoparticles: a new treatment of experimental autoimmune uveoretinitis. *European journal of immunology*. 2004;34:3702-12.

- [24] Silva NC, Silva S, Sarmiento B, Pintado M. Chitosan nanoparticles for daptomycin delivery in ocular treatment of bacterial endophthalmitis. *Drug delivery*. 2013.
- [25] Zhou W, Wang Y, Jian J, Song S. Self-aggregated nanoparticles based on amphiphilic poly(lactic acid)-grafted-chitosan copolymer for ocular delivery of amphotericin B. *International journal of nanomedicine*. 2013;8:3715-28.
- [26] Bochot A, Fattal E. Liposomes for intravitreal drug delivery: A state of the art. *J Control Release*. 2012;161:628-34.
- [27] Lajavardi L, Bochot A, Camelo S, Goldenberg B, Naud MC, Behar-Cohen F, et al. Downregulation of endotoxin-induced uveitis by intravitreal injection of vasoactive intestinal Peptide encapsulated in liposomes. *Investigative ophthalmology & visual science*. 2007;48:3230-8.
- [28] Mufamadi MS, Pillay V, Choonara YE, Du Toit LC, Modi G, Naidoo D, et al. A review on composite liposomal technologies for specialized drug delivery. *Journal of drug delivery*. 2011;2011:939851.
- [29] Widjaja LK, Bora M, Chan PNPH, Lipik V, Wong TTL, Venkatraman SS. Hyaluronic acid-based nanocomposite hydrogels for ocular drug delivery applications. *J Biomed Mater Res Part A*. 2013:n/a-n/a.
- [30] Hao J, Wang X, Bi Y, Teng Y, Wang J, Li F, et al. Fabrication of a composite system combining solid lipid nanoparticles and thermosensitive hydrogel for challenging ophthalmic drug delivery. *Colloids and Surfaces B: Biointerfaces*. 2014;114:111-20.
- [31] Kang Derwent JJ, Mieler WF. Thermoresponsive hydrogels as a new ocular drug delivery platform to the posterior segment of the eye. *Transactions of the American Ophthalmological Society*. 2008;106:206-13; discussion 13-4.
- [32] Turturro SB, Guthrie MJ, Appel AA, Drapala PW, Brey EM, Perez-Luna VH, et al. The effects of cross-linked thermo-responsive PNIPAAm-based hydrogel injection on retinal function. *Biomaterials*. 2011;32:3620-6.
- [33] Wang C-H, Hwang Y-S, Chiang P-R, Shen C-R, Hong W-H, Hsiue G-H. Extended Release of Bevacizumab by Thermosensitive Biodegradable and Biocompatible Hydrogel. *Biomacromolecules*. 2011;13:40-8.
- [34] Hwang YS, Chiang PR, Hong WH, Chiao CC, Chu IM, Hsiue GH, et al. Study in vivo intraocular biocompatibility of in situ gelation hydrogels: poly(2-ethyl oxazoline)-block-poly(epsilon-caprolactone)-block-poly(2-ethyl oxazoline) copolymer, matrigel and pluronic F127. *PloS one*. 2013;8:e67495.
- [35] Lu C, Zahedi P, Forman A, Allen C. Multi-arm PEG/Silica Hydrogel for Sustained Ocular Drug Delivery. *Journal of pharmaceutical sciences*. 2014;103:216-26.

- [36] Xu X, Weng Y, Xu L, Chen H. Sustained release of avastin® from polysaccharides cross-linked hydrogels for ocular drug delivery. *International Journal of Biological Macromolecules*. 2013;60:272-6.
- [37] Spinal cord injury facts and figures at a glance. National Spinal Cord Injury Statistical Center; 2010.
- [38] Berkowitz M, O'Leary P, Kruse D, Harvey C. *Spinal cord injury: An analysis of medical and social costs*. New York: Demos Medical Publishing Inc.; 1998.
- [39] National Institute of Neurological Disorders and Stroke NIH. *Spinal cord injury: hope through research*. 2008.
- [40] Anderson KD. Targeting recovery: priorities of the spinal cord-injured population. *J Neurotrauma*. 2004;21:1371-83.
- [41] Bracken MB, Shepard MJ, Holford TR, Leo-Summers L, Aldrich EF, Fazl M, et al. Methylprednisolone or tirilazad mesylate administration after acute spinal cord injury: 1-year follow up. Results of the third National Acute Spinal Cord Injury randomized controlled trial. *Journal of neurosurgery*. 1998;89:699-706.
- [42] Katz JS, Burdick JA. Hydrogel mediated delivery of trophic factors for neural repair. *Wiley Interdiscip Rev Nanomed Nanobiotechnol*. 2009;1:128-39.
- [43] Straley KS, Foo CWP, Heilshorn SC. Biomaterial Design Strategies for the Treatment of Spinal Cord Injuries. *Journal of Neurotrauma*. 2010;27:1.
- [44] Zhong Y, Bellamkonda RV. Biomaterials for the central nervous system. *J R Soc Interface*. 2008;5:957-75.
- [45] Willerth SM, Sakiyama-Elbert SE. Cell therapy for spinal cord regeneration. *Advanced drug delivery reviews*. 2008;60:263-76.
- [46] Ritfeld GJ, Rauck BM, Novosat TL, Park D, Patel P, Roos RA, et al. The effect of a polyurethane-based reverse thermal gel on bone marrow stromal cell transplant survival and spinal cord repair. *Biomaterials*. 2014;35:1924-31.
- [47] Belkas JS, Munro CA, Shoichet MS, Johnston M, Midha R. Long-term in vivo biomechanical properties and biocompatibility of poly(2-hydroxyethyl methacrylate-co-methyl methacrylate) nerve conduits. *Biomaterials*. 2005;26:1741-9.
- [48] Gumera CB, Wang Y. Modulating neuronal responses by controlled integration of acetylcholine-like functionalities in biomimetic polymers. *Advanced Materials*. 2007;19:4404-9.
- [49] Schense JC, Bloch J, Aebischer P, Hubbell JA. Enzymatic incorporation of bioactive peptides into fibrin matrices enhances neurite extension. *Nature biotechnology*. 2000;18:415-9.

- [50] Hou S, Xu Q, Tian W, Cui F, Cai Q, Ma J, et al. The repair of brain lesion by implantation of hyaluronic acid hydrogels modified with laminin. *J Neurosci Methods*. 2005;148:60-70.
- [51] Kim J, Park Y, Tae G, Lee KB, Hwang SJ, Kim IS, et al. Synthesis and characterization of matrix metalloprotease sensitive-low molecular weight hyaluronic acid based hydrogels. *J Mater Sci Mater Med*. 2008;19:3311-8.
- [52] Wei YT, Sun XD. Hyaluronic Acid Hydrogel Modified with Nogo-66 Receptor Antibody and Poly (L-Lysine) Enhancement of Adherence and Survival of Primary Hippocampal Neurons. *Journal of Bioactive and Compatible Polymers*. 2009;24:205.
- [53] Wei YT, Tian WM, Yu X, Cui FZ, Hou SP, Xu QY, et al. Hyaluronic acid hydrogels with IKVAV peptides for tissue repair and axonal regeneration in an injured rat brain. *Biomed Mater*. 2007;2:S142-6.
- [54] Bamber NI, Li H, Lu X, Oudega M, Aebischer P, Xu XM. Neurotrophins BDNF and NT-3 promote axonal re-entry into the distal host spinal cord through Schwann cell-seeded mini-channels. *Eur J Neurosci*. 2001;13:257-68.
- [55] Jain A, Kim YT, McKeon RJ, Bellamkonda RV. In situ gelling hydrogels for conformal repair of spinal cord defects, and local delivery of BDNF after spinal cord injury. *Biomaterials*. 2006;27:497-504.
- [56] Park J, Lim E, Back S, Na H, Park Y, Sun K. Nerve regeneration following spinal cord injury using matrix metalloproteinase-sensitive, hyaluronic acid-based biomimetic hydrogel scaffold containing brain-derived neurotrophic factor. *J Biomed Mater Res A*. 93:1091-9.
- [57] Baumann MD, Kang CE, Stanwick JC, Wang Y, Kim H, Lapitsky Y, et al. An injectable drug delivery platform for sustained combination therapy. *J Control Release*. 2009;138:205-13.
- [58] Goraltchouk A, Scanga V, Morshead CM, Shoichet MS. Incorporation of protein-eluting microspheres into biodegradable nerve guidance channels for controlled release. *J Control Release*. 2006;110:400-7.
- [59] Hamann J, Maria C, Tator CH, Shoichet MS. Injectable intrathecal delivery system for localized administration of EGF and FGF-2 to the injured rat spinal cord. *Experimental neurology*. 2005;194:106-19.
- [60] Nomura H, Katayama Y, Shoichet MS, Tator CH. Complete spinal cord transection treated by implantation of a reinforced synthetic hydrogel channel results in syringomyelia and caudal migration of the rostral stump. *Neurosurgery*. 2006;59:183-92; discussion -92.
- [61] Kang CE, Tator CH, Shoichet MS. Poly(ethylene glycol) modification enhances penetration of fibroblast growth factor 2 to injured spinal cord tissue from an intrathecal delivery system. *J Control Release*. 144:25-31.

- [62] Wang YC, Wu YT, Huang HY, Lin HI, Lo LW, Tzeng SF, et al. Sustained intraspinal delivery of neurotrophic factor encapsulated in biodegradable nanoparticles following contusive spinal cord injury. *Biomaterials*. 2008;29:4546-53.
- [63] Moore K, MacSween M, Shoichet M. Immobilized concentration gradients of neurotrophic factors guide neurite outgrowth of primary neurons in macroporous scaffolds. *Tissue Eng*. 2006;12:267-78.
- [64] Sakiyama-Elbert SE, Hubbell JA. Controlled release of nerve growth factor from a heparin-containing fibrin-based cell ingrowth matrix. *J Control Release*. 2000;69:149-58.
- [65] Johnson PJ, Parker SR, Sakiyama-Elbert SE. Controlled release of neurotrophin-3 from fibrin-based tissue engineering scaffolds enhances neural fiber sprouting following subacute spinal cord injury. *Biotechnol Bioeng*. 2009;104:1207-14.
- [66] Johnson PJ, Tataru A, Shiu A, Sakiyama-Elbert SE. Controlled release of neurotrophin-3 and platelet-derived growth factor from fibrin scaffolds containing neural progenitor cells enhances survival and differentiation into neurons in a subacute model of SCI. *Cell Transplant*. 19:89-101.
- [67] Li X, Yang Z, Zhang A. The effect of neurotrophin-3/chitosan carriers on the proliferation and differentiation of neural stem cells. *Biomaterials*. 2009;30:4978-85.
- [68] Mo L, Yang Z, Zhang A, Li X. The repair of the injured adult rat hippocampus with NT-3-chitosan carriers. *Biomaterials*. 2010;31:2184-92.
- [69] Taylor SJ, McDonald JW, 3rd, Sakiyama-Elbert SE. Controlled release of neurotrophin-3 from fibrin gels for spinal cord injury. *J Control Release*. 2004;98:281-94.
- [70] Taylor SJ, Rosenzweig ES, McDonald JW, 3rd, Sakiyama-Elbert SE. Delivery of neurotrophin-3 from fibrin enhances neuronal fiber sprouting after spinal cord injury. *J Control Release*. 2006;113:226-35.
- [71] Taylor SJ, Sakiyama-Elbert SE. Effect of controlled delivery of neurotrophin-3 from fibrin on spinal cord injury in a long term model. *J Control Release*. 2006;116:204-10.
- [72] Suzuki M, Itoh S, Yamaguchi I, Takakuda K, Kobayashi H, Shinomiya K, et al. Tendon chitosan tubes covalently coupled with synthesized laminin peptides facilitate nerve regeneration in vivo. *J Neurosci Res*. 2003;72:646-59.
- [73] Tashiro K, Sephel GC, Weeks B, Sasaki M, Martin GR, Kleinman HK, et al. A synthetic peptide containing the IKVAV sequence from the A chain of laminin mediates cell attachment, migration, and neurite outgrowth. *J Biol Chem*. 1989;264:16174-82.
- [74] Tysseling-Mattiace VM, Sahni V, Niece KL, Birch D, Czeisler C, Fehlings MG, et al. Self-assembling nanofibers inhibit glial scar formation and promote axon elongation after spinal cord injury. *The Journal of neuroscience : the official journal of the Society for Neuroscience*. 2008;28:3814-23.

- [75] Yu LM, Kazazian K, Shoichet MS. Peptide surface modification of methacrylamide chitosan for neural tissue engineering applications. *J Biomed Mater Res A*. 2007;82:243-55.
- [76] Cheng H, Huang YC, Chang PT, Huang YY. Laminin-incorporated nerve conduits made by plasma treatment for repairing spinal cord injury. *Biochem Biophys Res Commun*. 2007;357:938-44.
- [77] Stabenfeldt SE, Garcia AJ, LaPlaca MC. Thermoreversible laminin-functionalized hydrogel for neural tissue engineering. *J Biomed Mater Res A*. 2006;77:718-25.
- [78] Cui FZ, Tian WM, Hou SP, Xu QY, Lee IS. Hyaluronic acid hydrogel immobilized with RGD peptides for brain tissue engineering. *J Mater Sci Mater Med*. 2006;17:1393-401.
- [79] Musoke-Zawedde P, Shoichet MS. Anisotropic three-dimensional peptide channels guide neurite outgrowth within a biodegradable hydrogel matrix. *Biomed Mater*. 2006;1:162-9.
- [80] Meiners S, Nur-e-Kamal MS, Mercado ML. Identification of a neurite outgrowth-promoting motif within the alternatively spliced region of human tenascin-C. *J Neurosci*. 2001;21:7215-25.
- [81] Ahmed I, Liu HY, Mamiya PC, Ponery AS, Babu AN, Weik T, et al. Three-dimensional nanofibrillar surfaces covalently modified with tenascin-C-derived peptides enhance neuronal growth in vitro. *Journal of Biomedical Materials Research Part A*. 2006;76A:851-60.
- [82] Dhoot NO, Tobias CA, Fischer I, Wheatley MA. Peptide-modified alginate surfaces as a growth permissive substrate for neurite outgrowth. *J Biomed Mater Res A*. 2004;71:191-200.
- [83] Fukushima K, Enomoto M, Tomizawa S, Takahashi M, Wakabayashi Y, Itoh S, et al. The axonal regeneration across a honeycomb collagen sponge applied to the transected spinal cord. *J Med Dent Sci*. 2008;55:71-9.
- [84] Gao J, Kim YM, Coe H, Zern B, Sheppard B, Wang Y. A neuroinductive biomaterial based on dopamine. *Proc Natl Acad Sci U S A*. 2006;103:16681-6.
- [85] Lee H, McKeon RJ, Bellamkonda RV. Sustained delivery of thermostabilized chABC enhances axonal sprouting and functional recovery after spinal cord injury. *Proc Natl Acad Sci U S A*. 107:3340-5.
- [86] Bryan DJ, Tang JB, Doherty SA, Hile DD, Trantolo DJ, Wise DL, et al. Enhanced peripheral nerve regeneration through a poled bioresorbable poly(lactic-co-glycolic acid) guidance channel. *J Neural Eng*. 2004;1:91-8.
- [87] Collier JH, Camp JP, Hudson TW, Schmidt CE. Synthesis and characterization of polypyrrole-hyaluronic acid composite biomaterials for tissue engineering applications. *J Biomed Mater Res*. 2000;50:574-84.
- [88] Durgam H, Sapp S, Deister C, Khaing Z, Chang E, Luebben S, et al. Novel degradable copolymers of polypyrrole support cell proliferation and enhance neurite out-growth with electrical stimulation. *J Biomater Sci Polym Ed*. 21:1265-82.

- [89] Kim DH, Richardson-Burns S, Hendricks J, Sequera C, Martin D. Effect of Immobilized Nerve Growth Factor on Conductive Polymers: Electrical Properties and Cellular Response. *Advanced functional materials*. 2007;17:79-86.
- [90] Lee JY, Bashur CA, Goldstein AS, Schmidt CE. Polypyrrole-coated electrospun PLGA nanofibers for neural tissue applications. *Biomaterials*. 2009;30:4325-35.
- [91] Rivers T, Hudson T, Schmidt C. Synthesis of a Novel, Biodegradable Electrically Conducting Polymer for Biomedical Applications. *Advanced functional materials*. 2002;12:33-7.
- [92] Runge MB, Dadsetan M, Baltrusaitis J, Knight AM, Ruesink T, Lazcano EA, et al. The development of electrically conductive polycaprolactone fumarate-polypyrrole composite materials for nerve regeneration. *Biomaterials*. 31:5916-26.
- [93] Schmidt CE, Shastri VR, Vacanti JP, Langer R. Stimulation of neurite outgrowth using an electrically conducting polymer. *Proc Natl Acad Sci U S A*. 1997;94:8948-53.
- [94] Stauffer WR, Cui XT. Polypyrrole doped with 2 peptide sequences from laminin. *Biomaterials*. 2006;27:2405-13.
- [95] Wadhwa R, Lagenaur CF, Cui XT. Electrochemically controlled release of dexamethasone from conducting polymer polypyrrole coated electrode. *J Control Release*. 2006;110:531-41.
- [96] Wan Y, Wu H, Wen D. Porous-conductive chitosan scaffolds for tissue engineering, 1. Preparation and characterization. *Macromolecular bioscience*. 2004;4:882-90.
- [97] Zelikin AN, Lynn DM, Farhadi J, Martin I, Shastri V, Langer R. Erodible Conducting Polymers for Potential Biomedical Applications. *Angewandte Chemie International Edition*. 2002;41:141-4.
- [98] Kim YT, Caldwell JM, Bellamkonda RV. Nanoparticle-mediated local delivery of Methylprednisolone after spinal cord injury. *Biomaterials*. 2009;30:2582-90.
- [99] Chvatal SA, Kim YT, Bratt-Leal AM, Lee H, Bellamkonda RV. Spatial distribution and acute anti-inflammatory effects of Methylprednisolone after sustained local delivery to the contused spinal cord. *Biomaterials*. 2008;29:1967-75.
- [100] Tian WM, Hou SP, Ma J, Zhang CL, Xu QY, Lee IS, et al. Hyaluronic acid-poly-D-lysine-based three-dimensional hydrogel for traumatic brain injury. *Tissue Eng*. 2005;11:513-25.
- [101] Crompton KE, Goud JD, Bellamkonda RV, Gengenbach TR, Finkelstein DI, Horne MK, et al. Polylysine-functionalised thermoresponsive chitosan hydrogel for neural tissue engineering. *Biomaterials*. 2007;28:441-9.
- [102] Nisbet DR, Moses D, Gengenbach TR, Forsythe JS, Finkelstein DI, Horne MK. Enhancing neurite outgrowth from primary neurones and neural stem cells using thermoresponsive hydrogel scaffolds for the repair of spinal cord injury. *J Biomed Mater Res A*. 2009;89:24-35.

- [103] Nisbet DR, Rodda AE, Horne MK, Forsythe JS, Finkelstein DI. Implantation of functionalised thermally gelling xyloglucan hydrogel within the brain: Associated neurite infiltration and inflammatory response. *Tissue Eng Part A*.
- [104] Horne MK, Nisbet DR, Forsythe JS, Parish CL. Three-dimensional nanofibrous scaffolds incorporating immobilized BDNF promote proliferation and differentiation of cortical neural stem cells. *Stem cells and development*.19:843-52.
- [105] Nisbet DR, Rodda AE, Horne MK, Forsythe JS, Finkelstein DI. Neurite infiltration and cellular response to electrospun polycaprolactone scaffolds implanted into the brain. *Biomaterials*. 2009;30:4573-80.
- [106] Nisbet DR, Yu LM, Zahir T, Forsythe JS, Shoichet MS. Characterization of neural stem cells on electrospun poly(epsilon-caprolactone) submicron scaffolds: evaluating their potential in neural tissue engineering. *J Biomater Sci Polym Ed*. 2008;19:623-34.
- [107] Shen Y, Qian Y, Zhang H, Zuo B, Lu Z, Fan Z, et al. Guidance of olfactory ensheathing cell growth and migration on electrospun silk fibroin scaffolds. *Cell Transplant*.19:147-57.
- [108] Yang F, Murugan R, Wang S, Ramakrishna S. Electrospinning of nano/micro scale poly(L-lactic acid) aligned fibers and their potential in neural tissue engineering. *Biomaterials*. 2005;26:2603-10.
- [109] Krsko P, McCann TE, Thach TT, Laabs TL, Geller HM, Libera MR. Length-scale mediated adhesion and directed growth of neural cells by surface-patterned poly (ethylene glycol) hydrogels. *Biomaterials*. 2009;30:721-9.
- [110] Bechara SL, Judson A, Popat KC. Template synthesized poly(epsilon-caprolactone) nanowire surfaces for neural tissue engineering. *Biomaterials*.31:3492-501.
- [111] Fu SY, Gordon T. The cellular and molecular basis of peripheral nerve regeneration. *Mol Neurobiol*. 1997;14:67-116.
- [112] Baumann N, Pham-Dinh D. Biology of oligodendrocyte and myelin in the mammalian central nervous system. *Physiol Rev*. 2001;81:871-927.
- [113] Vernadakis A. GLIA-NEURON INTERCOMMUNICATIONS AND SYNAPTIC PLASTICITY. *Progress in Neurobiology*. 1996;49:185-214.
- [114] Rolls A, Shechter R, Schwartz M. The bright side of the glial scar in CNS repair. *Nat Rev Neurosci*. 2009;10:235-41.
- [115] Bradbury EJ, McMahon SB. Spinal cord repair strategies: why do they work? *Nature reviews Neuroscience*. 2006;7:644-53.
- [116] McKinley M, O'Loughlin, V.D. *Human Anatomy*. 1 ed: McGraw-Hill Higher Education; 2006.

- [117] Filbin MT. Myelin-associated inhibitors of axonal regeneration in the adult mammalian CNS. *Nature Reviews Neuroscience*. 2003;4:703-13.
- [118] Stichel CC, Muller HW. The CNS lesion scar: new vistas on an old regeneration barrier. *Cell and Tissue Research*. 1998;294:1-9.
- [119] Vargas ME, Barres BA. Why is Wallerian degeneration in the CNS so slow? *Annu Rev Neurosci*. 2007;30:153-79.
- [120] Yiu G, He Z. Glial inhibition of CNS axon regeneration. *Nat Rev Neurosci*. 2006;7:617-27.
- [121] Thuret S, Moon LD, Gage FH. Therapeutic interventions after spinal cord injury. *Nat Rev Neurosci*. 2006;7:628-43.
- [122] Fitch MT, Silver J. CNS injury, glial scars, and inflammation: Inhibitory extracellular matrices and regeneration failure. *Exp Neurol*. 2008;209:294-301.
- [123] He Q, Zhang T, Yang Y, Ding F. In vitro biocompatibility of chitosan-based materials to primary culture of hippocampal neurons. *J Mater Sci Mater Med*. 2009;20:1457-66.
- [124] Cho Y, Shi R, Ben Borgens R. Chitosan nanoparticle-based neuronal membrane sealing and neuroprotection following acrolein-induced cell injury. *J Biol Eng*. 2010;4:2.
- [125] Cho Y, Shi R, Borgens RB. Chitosan produces potent neuroprotection and physiological recovery following traumatic spinal cord injury. *J Exp Biol*. 2010;213:1513-20.
- [126] Gingras M, Beaulieu MM, Gagnon V, Durham HD, Berthod F. In vitro study of axonal migration and myelination of motor neurons in a three-dimensional tissue-engineered model. *Glia*. 2008;56:354-64.
- [127] Dewitt DD, Kaszuba SN, Thompson DM, Stegemann JP. Collagen I-matrigel scaffolds for enhanced Schwann cell survival and control of three-dimensional cell morphology. *Tissue Eng Part A*. 2009;15:2785-93.
- [128] Sundararaghavan HG, Monteiro GA, Firestein BL, Shreiber DI. Neurite growth in 3D collagen gels with gradients of mechanical properties. *Biotechnol Bioeng*. 2009;102:632-43.
- [129] Madaghiele M, Sannino A, Yannas IV, Spector M. Collagen-based matrices with axially oriented pores. *J Biomed Mater Res A*. 2008;85:757-67.
- [130] De Laporte L, Yan AL, Shea LD. Local gene delivery from ECM-coated poly(lactide-co-glycolide) multiple channel bridges after spinal cord injury. *Biomaterials*. 2009;30:2361-8.
- [131] Hu J, Deng L, Wang X, Xu XM. Effects of extracellular matrix molecules on the growth properties of oligodendrocyte progenitor cells in vitro. *J Neurosci Res*. 2009;87:2854-62.

- [132] Yoshii S, Ito S, Shima M, Taniguchi A, Akagi M. Functional restoration of rabbit spinal cord using collagen-filament scaffold. *J Tissue Eng Regen Med.* 2009;3:19-25.
- [133] King VR, Hewazy D, Alovskaya A, Phillips JB, Brown RA, Priestley JV. The neuroprotective effects of fibronectin mats and fibronectin peptides following spinal cord injury in the rat. *Neuroscience.* 168:523-30.
- [134] Thonhoff JR, Lou DI, Jordan PM, Zhao X, Wu P. Compatibility of human fetal neural stem cells with hydrogel biomaterials in vitro. *Brain research.* 2008;1187:42-51.
- [135] Lee SH, Chung YN, Kim YH, Kim YJ, Park JP, Kwon DK, et al. Effects of human neural stem cell transplantation in canine spinal cord hemisection. *Neurol Res.* 2009;31:996-1002.
- [136] Johnson PJ, Parker SR, Sakiyama-Elbert SE. Fibrin-based tissue engineering scaffolds enhance neural fiber sprouting and delay the accumulation of reactive astrocytes at the lesion in a subacute model of spinal cord injury. *J Biomed Mater Res A.* 92:152-63.
- [137] Sakiyama-Elbert SE, Hubbell JA. Development of fibrin derivatives for controlled release of heparin-binding growth factors. *J Control Release.* 2000;65:389-402.
- [138] Horn EM, Beaumont M, Shu XZ, Harvey A, Prestwich GD, Horn KM, et al. Influence of cross-linked hyaluronic acid hydrogels on neurite outgrowth and recovery from spinal cord injury. *J Neurosurg Spine.* 2007;6:133-40.
- [139] Gupta D, Tator CH, Shoichet MS. Fast-gelling injectable blend of hyaluronan and methylcellulose for intrathecal, localized delivery to the injured spinal cord. *Biomaterials.* 2006;27:2370-9.
- [140] Wang Y, Lapitsky Y, Kang CE, Shoichet MS. Accelerated release of a sparingly soluble drug from an injectable hyaluronan-methylcellulose hydrogel. *J Control Release.* 2009;140:218-23.
- [141] Stokols S, Sakamoto J, Breckon C, Holt T, Weiss J, Tuszynski MH. Templated agarose scaffolds support linear axonal regeneration. *Tissue Eng.* 2006;12:2777-87.
- [142] Stokols S, Tuszynski MH. Freeze-dried agarose scaffolds with uniaxial channels stimulate and guide linear axonal growth following spinal cord injury. *Biomaterials.* 2006;27:443-51.
- [143] Weber RA, Breidenbach WC, Brown RE, Jabaley ME, Mass DP. A randomized prospective study of polyglycolic acid conduits for digital nerve reconstruction in humans. *Plast Reconstr Surg.* 2000;106:1036-45; discussion 46-8.
- [144] Nisbet DR, Pattanawong S, Ritchie NE, Shen W, Finkelstein DI, Horne MK, et al. Interaction of embryonic cortical neurons on nanofibrous scaffolds for neural tissue engineering. *J Neural Eng.* 2007;4:35-41.

- [145] He L, Zhang Y, Zeng C, Ngiam M, Liao S, Quan D, et al. Manufacture of PLGA multiple-channel conduits with precise hierarchical pore architectures and in vitro/vivo evaluation for spinal cord injury. *Tissue Eng Part C Methods*. 2009;15:243-55.
- [146] Wong DY, Hollister SJ, Krebsbach PH, Nosrat C. Poly(epsilon-caprolactone) and poly (L-lactic-co-glycolic acid) degradable polymer sponges attenuate astrocyte response and lesion growth in acute traumatic brain injury. *Tissue Eng*. 2007;13:2515-23.
- [147] Rauch MF, Hynes SR, Bertram J, Redmond A, Robinson R, Williams C, et al. Engineering angiogenesis following spinal cord injury: a coculture of neural progenitor and endothelial cells in a degradable polymer implant leads to an increase in vessel density and formation of the blood-spinal cord barrier. *Eur J Neurosci*. 2009;29:132-45.
- [148] Olson HE, Rooney GE, Gross L, Nesbitt JJ, Galvin KE, Knight A, et al. Neural stem cell- and Schwann cell-loaded biodegradable polymer scaffolds support axonal regeneration in the transected spinal cord. *Tissue Eng Part A*. 2009;15:1797-805.
- [149] Chen BK, Knight AM, de Ruitter GC, Spinner RJ, Yaszemski MJ, Currier BL, et al. Axon regeneration through scaffold into distal spinal cord after transection. *J Neurotrauma*. 2009;26:1759-71.
- [150] Rooney GE, Moran C, McMahon SS, Ritter T, Maenz M, Flugel A, et al. Gene-modified mesenchymal stem cells express functionally active nerve growth factor on an engineered poly lactic glycolic acid (PLGA) substrate. *Tissue Eng Part A*. 2008;14:681-90.
- [151] Krych AJ, Rooney GE, Chen B, Schermerhorn TC, Ameenuddin S, Gross L, et al. Relationship between scaffold channel diameter and number of regenerating axons in the transected rat spinal cord. *Acta Biomater*. 2009;5:2551-9.
- [152] Yu D, Neeley WL, Pritchard CD, Slotkin JR, Woodard EJ, Langer R, et al. Blockade of peroxynitrite-induced neural stem cell death in the acutely injured spinal cord by drug-releasing polymer. *Stem Cells*. 2009;27:1212-22.
- [153] Thouas GA, Contreras KG, Bernard CC, Sun GZ, Tsang K, Zhou K, et al. Biomaterials for spinal cord regeneration: outgrowth of presumptive neuronal precursors on electrospun poly(epsilon)-caprolactone scaffolds microlayered with alternating polyelectrolytes. *Conf Proc IEEE Eng Med Biol Soc*. 2008;2008:1825-8.
- [154] Wong DY, Leveque JC, Brumblay H, Krebsbach PH, Hollister SJ, Lamarca F. Macro-architectures in spinal cord scaffold implants influence regeneration. *J Neurotrauma*. 2008;25:1027-37.
- [155] Novikova LN, Pettersson J, Brohlin M, Wiberg M, Novikov LN. Biodegradable poly-beta-hydroxybutyrate scaffold seeded with Schwann cells to promote spinal cord repair. *Biomaterials*. 2008;29:1198-206.

- [156] Sundback CA, Shyu JY, Wang Y, Faquin WC, Langer RS, Vacanti JP, et al. Biocompatibility analysis of poly(glycerol sebacate) as a nerve guide material. *Biomaterials*. 2005;26:5454-64.
- [157] Byrom D. Polymer synthesis by microorganisms: technology and economics. *Trends in Biotechnology*. 1987;5:246-50.
- [158] Wang Y, Kim YM, Langer R. In vivo degradation characteristics of poly(glycerol sebacate). *J Biomed Mater Res A*. 2003;66:192-7.
- [159] Silva GA, Czeisler C, Niece KL, Beniash E, Harrington DA, Kessler JA, et al. Selective differentiation of neural progenitor cells by high-epitope density nanofibers. *Science*. 2004;303:1352-5.
- [160] Kwon BK, Liu J, Lam C, Plunet W, Oschipok LW, Hauswirth W, et al. Brain-derived neurotrophic factor gene transfer with adeno-associated viral and lentiviral vectors prevents rubrospinal neuronal atrophy and stimulates regeneration-associated gene expression after acute cervical spinal cord injury. *Spine*. 2007;32:1164-73.
- [161] Taylor L, Jones L, Tuszynski MH, Blesch A. Neurotrophin-3 gradients established by lentiviral gene delivery promote short-distance axonal bridging beyond cellular grafts in the injured spinal cord. *J Neurosci*. 2006;26:9713-21.
- [162] Novikov LN, Novikova LN, Mosahebi A, Wiberg M, Terenghi G, Kellerth JO. A novel biodegradable implant for neuronal rescue and regeneration after spinal cord injury. *Biomaterials*. 2002;23:3369-76.
- [163] McTigue DM, Horner PJ, Stokes BT, Gage FH. Neurotrophin-3 and brain-derived neurotrophic factor induce oligodendrocyte proliferation and myelination of regenerating axons in the contused adult rat spinal cord. *J Neurosci*. 1998;18:5354-65.
- [164] Bradbury EJ, Moon LD, Popat RJ, King VR, Bennett GS, Patel PN, et al. Chondroitinase ABC promotes functional recovery after spinal cord injury. *Nature*. 2002;416:636-40.
- [165] Putney SD, Burke PA. Improving protein therapeutics with sustained-release formulations. *Nat Biotechnol*. 1998;16:153-7.
- [166] Krewson CE, Dause R, Mak M, Saltzman WM. Stabilization of nerve growth factor in controlled release polymers and in tissue. *J Biomater Sci Polym Ed*. 1996;8:103-17.
- [167] Sayer FT, Oudega M, Hagg T. Neurotrophins reduce degeneration of injured ascending sensory and corticospinal motor axons in adult rat spinal cord. *Exp Neurol*. 2002;175:282-96.
- [168] Piantino J, Burdick JA, Goldberg D, Langer R, Benowitz LI. An injectable, biodegradable hydrogel for trophic factor delivery enhances axonal rewiring and improves performance after spinal cord injury. *Experimental neurology*. 2006;201:359-67.

- [169] Patist CM, Mulder MB, Gautier SE, Maquet V, Jerome R, Oudega M. Freeze-dried poly(D,L-lactic acid) macroporous guidance scaffolds impregnated with brain-derived neurotrophic factor in the transected adult rat thoracic spinal cord. *Biomaterials*. 2004;25:1569-82.
- [170] Willerth SM, Johnson PJ, Maxwell DJ, Parsons SR, Doukas ME, Sakiyama-Elbert SE. Rationally designed peptides for controlled release of nerve growth factor from fibrin matrices. *Journal of Biomedical Materials Research Part A*. 2007;80A:13-23.
- [171] Wood MD, Moore AM, Hunter DA, Tuffaha S, Borschel GH, Mackinnon SE, et al. Affinity-based release of glial-derived neurotrophic factor from fibrin matrices enhances sciatic nerve regeneration. *Acta Biomaterialia*. 2009;5:959-68.
- [172] GrandPre T, Li S, Strittmatter SM. Nogo-66 receptor antagonist peptide promotes axonal regeneration. *Nature*. 2002;417:547-51.
- [173] Tian WM, Zhang CL, Hou SP, Yu X, Cui FZ, Xu QY, et al. Hyaluronic acid hydrogel as Nogo-66 receptor antibody delivery system for the repairing of injured rat brain: in vitro. *J Control Release*. 2005;102:13-22.
- [174] Ma J, Tian WM, Hou SP, Xu QY, Spector M, Cui FZ. An experimental test of stroke recovery by implanting a hyaluronic acid hydrogel carrying a Nogo receptor antibody in a rat model. *Biomed Mater*. 2007;2:233-40.
- [175] Kang CE, Poon PC, Tator CH, Shoichet MS. A new paradigm for local and sustained release of therapeutic molecules to the injured spinal cord for neuroprotection and tissue repair. *Tissue Eng Part A*. 2009;15:595-604.
- [176] Kim H, Tator CH, Shoichet MS. Design of protein-releasing chitosan channels. *Biotechnol Prog*. 2008;24:932-7.
- [177] Tan EY, Law JW, Wang CH, Lee AY. Development of a cell transducible RhoA inhibitor TAT-C3 transferase and its encapsulation in biocompatible microspheres to promote survival and enhance regeneration of severed neurons. *Pharmaceutical research*. 2007;24:2297-308.
- [178] Couch SM, Bakri SJ. Review of Combination Therapies for Neovascular Age-Related Macular Degeneration. *Semin Ophthalmol*.26:114-20.
- [179] El-Mollayess GM, Nouredine BN, Bashshur ZF. Bevacizumab and Neovascular Age Related Macular Degeneration: Pathogenesis and Treatment. *Semin Ophthalmol*.26:69-76.
- [180] Prasad PS, Schwartz SD, Hubschman JP. Age-related macular degeneration: Current and novel therapies. *Maturitas*.66:46-50.
- [181] Anderson OA, Bainbridge JWB, Shima DT. Delivery of anti-angiogenic molecular therapies for retinal disease. *Drug Discov Today*.15:272-82.

[182] Do DV. Antiangiogenic Approaches to Age-Related Macular Degeneration in the Future. *Ophthalmology*. 2009;116:S24-S6.

[183] Adamis AP, Miller JW, Bernal MT, Damico DJ, Folkman J, Yeo TK, et al. INCREASED VASCULAR ENDOTHELIAL GROWTH-FACTOR LEVELS IN THE VITREOUS OF EYES WITH PROLIFERATIVE DIABETIC-RETINOPATHY. *American Journal of Ophthalmology*. 1994;118:445-50.

[184] Aiello LP, Avery RL, Arrigg PG, Keyt BA, Jampel HD, Shah ST, et al. VASCULAR ENDOTHELIAL GROWTH-FACTOR IN OCULAR FLUID OF PATIENTS WITH DIABETIC-RETINOPATHY AND OTHER RETINAL DISORDERS. *N Engl J Med*. 1994;331:1480-7.

[185] Otani A, Takagi H, Oh H, Koyama S, Ogura Y, Matumura M, et al. Vascular endothelial growth factor family and receptor expression in human choroidal neovascular membranes. *Microvasc Res*. 2002;64:162-9.

[186] Campa C, Harding SP. Anti-VEGF Compounds in the Treatment of Neovascular Age Related Macular Degeneration. *Curr Drug Targets*. 12:173-81.

[187] Ciulla TA, Rosenfeld PJ. Anti-vascular endothelial growth factor therapy for neovascular ocular diseases other than age-related macular degeneration. *Current opinion in ophthalmology*. 2009;20:166-74.

[188] Tang Y, Singh J. Biodegradable and biocompatible thermosensitive polymer based injectable implant for controlled release of protein. *International journal of pharmaceutics*. 2009;365:34-43.

[189] Oh HJ, Joo MK, Sohn YS, Jeong B. Secondary Structure Effect of Polypeptide on Reverse Thermal Gelation and Degradation of l/dl-Poly(alanine)-Ploxadmer-l/dl-Poly(alanine) Copolymers. *Macromolecules*. 2008;41:8204-9.

[190] Ogura M, Tokuda H, Imabayashi S, Watanabe M. Preparation and solution behavior of a thermoresponsive diblock copolymer of poly(ethyl glycidyl ether) and poly(ethylene oxide). *Langmuir : the ACS journal of surfaces and colloids*. 2007;23:9429-34.

[191] Minh KN, Lee DS. Injectable Biodegradable Hydrogels. *Macromolecular bioscience*. 10:563-79.

[192] He CL, Kim SW, Lee DS. In situ gelling stimuli-sensitive block copolymer hydrogels for drug delivery. *J Control Release*. 2008;127:189-207.

[193] Park D, Wu W, Wang Y. A functionalizable reverse thermal gel based on a polyurethane/PEG block copolymer. *Biomaterials*. 2011;32:777-86.

[194] Julian K, Terrada C, Fardeau C, Cassoux N, Francais C, LeHoang P, et al. Intravitreal bevacizumab as first local treatment for uveitis-related choroidal neovascularization: long-term results. *Acta Ophthalmol*. 89:179-84.

- [195] Ehlers JP, Decroos FC, Fekrat S. INTRAVITREAL BEVACIZUMAB FOR MACULAR EDEMA SECONDARY TO BRANCH RETINAL VEIN OCCLUSION. *Retin-J Retin Vitro Dis.*31:1856-62.
- [196] Hung KH, Lee SM, Lee SY, Lee FL, Yang CS. Intravitreal Bevacizumab (Avastin) in the Treatment of Macular Edema Associated With Perfused Retinal Vein Occlusion. *J Ocular Pharmacol Ther.*26:85-90.
- [197] Salam A, Mathew R, Sivaprasad S. Treatment of proliferative diabetic retinopathy with antiVEGF agents. *Acta Ophthalmol.*89:405-11.
- [198] Krohne TU, Eter N, Holz FG, Meyer CH. Intraocular Pharmacokinetics of Bevacizumab After a Single Intravitreal Injection in Humans. *American Journal of Ophthalmology.* 2008;146:508-12.
- [199] Swindle-Reilly KE, Shah M, Hamilton PD, Eskin TA, Kaushal S, Ravi N. Rabbit Study of an In Situ Forming Hydrogel Vitreous Substitute. *Investigative Ophthalmology & Visual Science.* 2009;50:4840-6.
- [200] Bakri SJ, Snyder MR, Reid JM, Pulido JS, Ezzat MK, Singh RJ. Pharmacokinetics of Intravitreal Ranibizumab (Lucentis). *Ophthalmology.* 2007;114:2179-82.
- [201] Miyake T, Sawada O, Kakinoki M, Sawada T, Kawamura H, Ogasawara K, et al. Pharmacokinetics of Bevacizumab and Its Effect on Vascular Endothelial Growth Factor after Intravitreal Injection of Bevacizumab in Macaque Eyes. *Investigative Ophthalmology & Visual Science.*51:1606-8.
- [202] Zhu Q, Ziemssen F, Henke-Fahle S, Tatar O, Szurman P, Aisenbrey S, et al. Vitreous levels of bevacizumab and vascular endothelial growth factor-A in patients with choroidal neovascularization. *Ophthalmology.* 2008;115:1750-5.
- [203] Hacker MC, Haesslein A, Ueda H, Foster WJ, Garcia CA, Ammon DM, et al. Biodegradable fumarate-based drug-delivery systems for ophthalmic applications. *J Biomed Mater Res Part A.* 2009;88A:976-89.
- [204] Tolentino M. Systemic and Ocular Safety of Intravitreal Anti-VEGF Therapies for Ocular Neovascular Disease. *Surv Ophthalmol.*56:95-113.
- [205] Kinnunen K, Yla-Herttuala S. Vascular endothelial growth factors in retinal and choroidal neovascular diseases. *Annals of medicine.* 2012;44:1-17.
- [206] Kvanta A, Algever PV, Berglin L, Seregard S. Subfoveal fibrovascular membranes in age-related macular degeneration express vascular endothelial growth factor. *Investigative Ophthalmology & Visual Science.* 1996;37:1929-34.
- [207] Kliffen M, Sharma HS, Mooy CM, Kerkvliet S, deJong P. Increased expression of angiogenic growth factors in age-related maculopathy. *British Journal of Ophthalmology.* 1997;81:154-62.

- [208] Kwak N, Okamoto N, Wood JM, Campochiaro PA. VEGF is major stimulator in model of choroidal neovascularization. *Investigative ophthalmology & visual science*. 2000;41:3158-64.
- [209] Avery RL, Pearlman J, Pieramici DJ, Rabena MD, Castellarin AA, Nasir MA, et al. Intravitreal bevacizumab (Avastin) in the treatment of proliferative diabetic retinopathy. *Ophthalmology*. 2006;113:1695 e1-15.
- [210] Lynch SS, Cheng CM. Bevacizumab for neovascular ocular diseases. *The Annals of pharmacotherapy*. 2007;41:614-25.
- [211] Kleinman ME, Ambati J. Pathophysiology of Retinal Neovascularization. In: Pine JW, editor. *Therapy for Ocular Angiogenesis: Principles and Practice*. Philadelphia, PA: Lippincott Williams & Wilkins; 2012.
- [212] D'Amico DJ. Pegaptanib Sodium for Neovascular Age-Related Macular Degeneration: Two-Year Safety Results of the Two Prospective, Multicenter, Controlled Clinical Trials. *Ophthalmology*. 2006;113:992-1001.e6.
- [213] Fintak DR, Shah GK, Blinder KJ, Regillo CD, Pollack J, Heier JS, et al. Incidence of endophthalmitis related to intravitreal injection of bevacizumab and ranibizumab. *Retina*. 2008;28:1395-9.
- [214] Holz FG, Amoaku W, Donate J, Guymer RH, Kellner U, Schlingemann RO, et al. Safety and efficacy of a flexible dosing regimen of ranibizumab in neovascular age-related macular degeneration: the SUSTAIN study. *Ophthalmology*. 2011;118:663-71.
- [215] Regillo CD, Brown DM, Abraham P, Yue H, Ianchulev T, Schneider S, et al. Randomized, double-masked, sham-controlled trial of ranibizumab for neovascular age-related macular degeneration: PIER Study year 1. *American journal of ophthalmology*. 2008;145:239-48.
- [216] Li F, Hurley B, Liu Y, Leonard B, Griffith M. Controlled release of bevacizumab through nanospheres for extended treatment of age-related macular degeneration. *The open ophthalmology journal*. 2012;6:54-8.
- [217] Pan CK, Durairaj C, Kompella UB, Agwu O, Oliver SC, Quiroz-Mercado H, et al. Comparison of long-acting bevacizumab formulations in the treatment of choroidal neovascularization in a rat model. *Journal of ocular pharmacology and therapeutics : the official journal of the Association for Ocular Pharmacology and Therapeutics*. 2011;27:219-24.
- [218] Park D, Shah V, Rauck BM, Friberg TR, Wang Y. An anti-angiogenic reverse thermal gel as a drug-delivery system for age-related wet macular degeneration. *Macromolecular bioscience*. 2013;13:464-9.
- [219] The R Core Team. *R: A language and environment for statistical computing*. R Foundation for Statistical Computing, Vienna, Austria. . Vienna, Austria2012.
- [220] Pinheiro J, Bates, D., Debroy, S. , Sarkar, D. and the R Development Core Team. *nlme: Linear and Nonlinear Mixed Effects Models*. R Package version 3.1-108. 2013.

- [221] Friberg TR, Siska PE, Somayajula K, Williams J, Eller AW. Interactions of perfluorocarbon liquids and silicone oil as characterized by mass spectrometry. *Graefe's archive for clinical and experimental ophthalmology = Albrecht von Graefes Archiv fur klinische und experimentelle Ophthalmologie*. 2003;241:809-15.
- [222] Friberg TR, Verstraeten TC, Wilcox DK. Effects of emulsification, purity, and fluorination of silicone oil on human retinal pigment epithelial cells. *Investigative ophthalmology & visual science*. 1991;32:2030-4.
- [223] Pruett RC, Schepens CL, Swann DA. Hyaluronic acid vitreous substitute. A six-year clinical evaluation. *Archives of ophthalmology*. 1979;97:2325-30.
- [224] Schramm C, Spitzer MS, Henke-Fahle S, Steinmetz G, Januschowski K, Heiduschka P, et al. The Cross-linked Biopolymer Hyaluronic Acid as an Artificial Vitreous Substitute. *Investigative Ophthalmology & Visual Science*. 2012;53:613-21.
- [225] Sniegowski M, Mandava N, Kahook MY. Sustained intraocular pressure elevation after intravitreal injection of bevacizumab and ranibizumab associated with trabeculitis. *The open ophthalmology journal*. 2010;4:28-9.
- [226] Sampat KM, Garg SJ. Complications of intravitreal injections. *Current opinion in ophthalmology*. 2010;21:178-83.
- [227] Streilein JW, Takeuchi M, Taylor AW. Immune privilege, T-cell tolerance, and tissue-restricted autoimmunity. *Human immunology*. 1997;52:138-43.
- [228] Lu F, Adelman RA. Are intravitreal bevacizumab and ranibizumab effective in a rat model of choroidal neovascularization? *Graefe's archive for clinical and experimental ophthalmology = Albrecht von Graefes Archiv fur klinische und experimentelle Ophthalmologie*. 2009;247:171-7.
- [229] Okano H, Nakamura M, Yoshida K, Okada Y, Tsuji O, Nori S, et al. Steps Toward Safe Cell Therapy Using Induced Pluripotent Stem Cells. *Circulation Research*. 2013;112:523-33.
- [230] Ruff CA, Fehlings MG. Neural stem cells in regenerative medicine: bridging the gap. *Panminerva medica*. 2010;52:125-47.
- [231] Forraz N, Wright KE, Jurga M, McGuckin CP. Experimental therapies for repair of the central nervous system: stem cells and tissue engineering. *Journal of Tissue Engineering and Regenerative Medicine*. 2013;7:523-36.
- [232] Hofstetter CP, Schwarz EJ, Hess D, Widenfalk J, El Manira A, Prockop DJ, et al. Marrow stromal cells form guiding strands in the injured spinal cord and promote recovery. *Proceedings of the National Academy of Sciences*. 2002;99:2199-204.
- [233] Himes BT, Neuhuber B, Coleman C, Kushner R, Swanger SA, Kopen GC, et al. Recovery of Function Following Grafting of Human Bone Marrow-Derived Stromal Cells into the Injured Spinal Cord. *Neurorehabilitation and Neural Repair*. 2006;20:278-96.

- [234] Mahmood A, Lu D, Wang L, Chopp M. Intracerebral transplantation of marrow stromal cells cultured with neurotrophic factors promotes functional recovery in adult rats subjected to traumatic brain injury. *J Neurotrauma*. 2002;19:1609-17.
- [235] Ritfeld GJ, Nandoe Tewarie RDS, Vajn K, Rahiem ST, Hurtado A, Wendell DF, et al. Bone Marrow Stromal Cell-Mediated Tissue Sparing Enhances Functional Repair After Spinal Cord Contusion in Adult Rats. *Cell Transplantation*. 2012;21:1561-75.
- [236] Tschöpe C, Miteva K, Schultheiss HP, Linthout SV. Mesenchymal stromal cells: a promising cell source for the treatment of inflammatory cardiomyopathy. *Current pharmaceutical design*. 2011;17:3295-307.
- [237] Ichim TE, Alexandrescu DT, Solano F, Lara F, Campion RDN, Paris E, et al. Mesenchymal stem cells as anti-inflammatories: Implications for treatment of Duchenne muscular dystrophy. *Cellular Immunology*. 2010;260:75-82.
- [238] Zou J-P, Huang S, Peng Y, Liu H-W, Cheng B, Fu X-B, et al. Mesenchymal Stem Cells/Multipotent Mesenchymal Stromal Cells (MSCs): Potential Role in Healing Cutaneous Chronic Wounds. *The International Journal of Lower Extremity Wounds*. 2012;11:244-53.
- [239] Bernardo ME, Pagliara D, Locatelli F. Mesenchymal stromal cell therapy: a revolution in Regenerative Medicine? *Bone marrow transplantation*. 2012;47:164-71.
- [240] Mahmood A, Lu D, Chopp M. Intravenous administration of marrow stromal cells (MSCs) increases the expression of growth factors in rat brain after traumatic brain injury. *J Neurotrauma*. 2004;21:33-9.
- [241] Caplan AI. Why are MSCs therapeutic? New data: new insight. *The Journal of Pathology*. 2009;217:318-24.
- [242] Hawryluk GW, Mothe A, Wang J, Wang S, Tator C, Fehlings MG. An in vivo characterization of trophic factor production following neural precursor cell or bone marrow stromal cell transplantation for spinal cord injury. *Stem cells and development*. 2012;21:2222-38.
- [243] Nandoe Tewarie RD, Hurtado A, Ritfeld GJ, Rahiem ST, Wendell DF, Barroso MM, et al. Bone marrow stromal cells elicit tissue sparing after acute but not delayed transplantation into the contused adult rat thoracic spinal cord. *J Neurotrauma*. 2009;26:2313-22.
- [244] Ritfeld GJ, Nandoe Tewarie RD, Rahiem ST, Hurtado A, Roos RA, Grotenhuis A, et al. Reducing macrophages to improve bone marrow stromal cell survival in the contused spinal cord. *Neuroreport*. 2010;21:221-6.
- [245] Swanger SA, Neuhuber B, Himes BT, Bakshi A, Fischer I. Analysis of Allogeneic and Syngeneic Bone Marrow Stromal Cell Graft Survival in the Spinal Cord. *Cell Transplantation*. 2005;14:775-86.

- [246] Parr AM, Kulbatski I, Wang X-H, Keating A, Tator CH. Fate of transplanted adult neural stem/progenitor cells and bone marrow–derived mesenchymal stromal cells in the injured adult rat spinal cord and impact on functional recovery. *Surgical neurology*. 2008;70:600-7.
- [247] Kigerl KA, Ankeny DP, Garg SK, Wei P, Guan Z, Lai W, et al. System xc⁻ regulates microglia and macrophage glutamate excitotoxicity in vivo. *Experimental Neurology*. 2012;233:333-41.
- [248] Facchinetti F, Dawson V, Dawson T. Free Radicals as Mediators of Neuronal Injury. *Cell Mol Neurobiol*. 1998;18:667-82.
- [249] Kong Q, Lin C-l. Oxidative damage to RNA: mechanisms, consequences, and diseases. *Cell Mol Life Sci*. 2010;67:1817-29.
- [250] Hamann K, Durkes A, Ouyang H, Uchida K, Pond A, Shi R. Critical role of acrolein in secondary injury following ex vivo spinal cord trauma. *Journal of Neurochemistry*. 2008;107:712-21.
- [251] Siriphorn A, Chompoopong S, Floyd CL. 17 β -Estradiol protects Schwann cells against H₂O₂-induced cytotoxicity and increases transplanted Schwann cell survival in a cervical hemicontusion spinal cord injury model. *Journal of Neurochemistry*. 2010;115:864-72.
- [252] Syntichaki P, Tavernarakis N. The biochemistry of neuronal necrosis: rogue biology? *Nature reviews Neuroscience*. 2003;4:672-84.
- [253] Christenson EM, Anderson JM, Hiltner A. Oxidative mechanisms of poly(carbonate urethane) and poly(ether urethane) biodegradation: In vivo and in vitro correlations. *J Biomed Mater Res Part A*. 2004;70A:245-55.
- [254] McBane JE, Santerre JP, Labow RS. The interaction between hydrolytic and oxidative pathways in macrophage-mediated polyurethane degradation. *J Biomed Mater Res Part A*. 2007;82A:984-94.
- [255] Oudega M. Schwann cell and olfactory ensheathing cell implantation for repair of the contused spinal cord. *Acta Physiologica*. 2007;189:181-9.
- [256] Rauck BM, Friberg TR, Medina Mendez CA, Park D, Shah V, Bilonick RA, et al. Biocompatible reverse thermal gel sustains the release of intravitreal bevacizumab in vivo. *Investigative ophthalmology & visual science*. 2014;55:469-76.
- [257] Azizi SA, Stokes D, Augelli BJ, DiGirolamo C, Prockop DJ. Engraftment and migration of human bone marrow stromal cells implanted in the brains of albino rats—similarities to astrocyte grafts. *Proceedings of the National Academy of Sciences*. 1998;95:3908-13.
- [258] Conget PA, Minguell JJ. Phenotypical and functional properties of human bone marrow mesenchymal progenitor cells. *Journal of Cellular Physiology*. 1999;181:67-73.

- [259] Seshi B, Kumar S, Sellers D. Human Bone Marrow Stromal Cell: Coexpression of Markers Specific for Multiple Mesenchymal Cell Lineages. *Blood Cells, Molecules, and Diseases*. 2000;26:234-46.
- [260] Kakulas BA. A review of the neuropathology of human spinal cord injury with emphasis on special features. *The journal of spinal cord medicine*. 1999;22:119-24.
- [261] Bunge RP, Puckett WR, Becerra JL, Marcillo A, Quencer RM. Observations on the pathology of human spinal cord injury. A review and classification of 22 new cases with details from a case of chronic cord compression with extensive focal demyelination. *Advances in neurology*. 1993;59:75-89.
- [262] Basso DM, Beattie MS, Bresnahan JC. A sensitive and reliable locomotor rating scale for open field testing in rats. *Journal of neurotrauma*. 1995;12:1-21.
- [263] Basso DM, Beattie MS, Bresnahan JC. Graded Histological and Locomotor Outcomes after Spinal Cord Contusion Using the NYU Weight-Drop Device versus Transection. *Experimental Neurology*. 1996;139:244-56.
- [264] Lankhorst AJ, Verzijl MR, Hamers FPT. Experimental spinal cord contusion injury: Comparison of different outcome parameters. *Neuroscience Research Communications*. 1999;24:135-48.
- [265] Joosten EAJ, Veldhuis WB, Hamers FPT. Collagen containing neonatal astrocytes stimulates regrowth of injured fibers and promotes modest locomotor recovery after spinal cord injury. *Journal of Neuroscience Research*. 2004;77:127-42.
- [266] Bolton DAE, Tse ADY, Ballermann M, Misiaszek JE, Fouad K. Task specific adaptations in rat locomotion: Runway versus horizontal ladder. *Behavioural Brain Research*. 2006;168:272-9.
- [267] Kunkel-Bagden E, Dai HN, Bregman BS. Recovery of function after spinal cord hemisection in newborn and adult rats: differential effects on reflex and locomotor function. *Experimental neurology*. 1992;116:40-51.
- [268] Boyce RW, Dorph-Petersen K-A, Lyck L, Gundersen HJG. Design-based Stereology: Introduction to Basic Concepts and Practical Approaches for Estimation of Cell Number. *Toxicologic Pathology*. 2010;38:1011-25.
- [269] Brodbeck WG, Nakayama Y, Matsuda T, Colton E, Ziats NP, Anderson JM. BIOMATERIAL SURFACE CHEMISTRY DICTATES ADHERENT MONOCYTE/MACROPHAGE CYTOKINE EXPRESSION IN VITRO. *Cytokine*. 2002;18:311-9.
- [270] Hill CE, Hurtado A, Blits B, Bahr BA, Wood PM, Bartlett Bunge M, et al. Early necrosis and apoptosis of Schwann cells transplanted into the injured rat spinal cord. *European Journal of Neuroscience*. 2007;26:1433-45.

- [271] Kawabori M, Kuroda S, Ito M, Shichinohe H, Houkin K, Kuge Y, et al. Timing and cell dose determine therapeutic effects of bone marrow stromal cell transplantation in rat model of cerebral infarct. *Neuropathology*. 2013;33:140-8.
- [272] Yasuhara T, Matsukawa N, Hara K, Maki M, Ali MM, Yu SJ, et al. Notch-induced rat and human bone marrow stromal cell grafts reduce ischemic cell loss and ameliorate behavioral deficits in chronic stroke animals. *Stem cells and development*. 2009;18:1501-14.
- [273] Bonilla C, Zurita M, Otero L, Aguayo C, Rico MA, Vaquero J. The severity of brain damage determines bone marrow stromal cell therapy efficacy in a traumatic brain injury model. *The journal of trauma and acute care surgery*. 2012;72:1203-12; discussion 11-2.
- [274] Zhang YJ, Zhang W, Lin CG, Ding Y, Huang SF, Wu JL, et al. Neurotrophin-3 gene modified mesenchymal stem cells promote remyelination and functional recovery in the demyelinated spinal cord of rats. *Journal of the neurological sciences*. 2012;313:64-74.
- [275] Karimi-Abdolrezaee S, Eftekharpour E, Wang J, Morshead CM, Fehlings MG. Delayed transplantation of adult neural precursor cells promotes remyelination and functional neurological recovery after spinal cord injury. *The Journal of neuroscience : the official journal of the Society for Neuroscience*. 2006;26:3377-89.
- [276] Nauta AJ, Fibbe WE. Immunomodulatory properties of mesenchymal stromal cells. *Blood*. 2007;110:3499-506.
- [277] Di Nicola M, Carlo-Stella C, Magni M, Milanese M, Longoni PD, Matteucci P, et al. Human bone marrow stromal cells suppress T-lymphocyte proliferation induced by cellular or nonspecific mitogenic stimuli. *Blood*. 2002;99:3838-43.
- [278] Moon YJ, Lee JY, Oh MS, Pak YK, Park K-S, Oh TH, et al. Inhibition of inflammation and oxidative stress by *Angelica dahuricae* radix extract decreases apoptotic cell death and improves functional recovery after spinal cord injury. *Journal of Neuroscience Research*. 2012;90:243-56.
- [279] Wu L, Shan Y, Liu D. Stability, disposition, and penetration of catalytic antioxidants Mn-porphyrin and Mn-salen and of methylprednisolone in spinal cord injury. *Central nervous system agents in medicinal chemistry*. 2012;12:122-30.
- [280] Chu H, Gao J, Wang Y. Design, synthesis, and biocompatibility of an arginine-based polyester. *Biotechnol Prog*. 2012;28:257-64.
- [281] Chu H, Johnson NR, Mason NS, Wang Y. A [polycation:heparin] complex releases growth factors with enhanced bioactivity. *J Control Release*. 2011;150:157-63.
- [282] Zern BJ, Chu H, Wang Y. Control growth factor release using a self-assembled [polycation:heparin] complex. *PloS one*. 2010;5:e11017.
- [283] Johnson NR, Wang Y. Controlled delivery of heparin-binding EGF-like growth factor yields fast and comprehensive wound healing. *J Control Release*. 2013;166:124-9.

- [284] Johnson NR, Wang Y. Controlled delivery of sonic hedgehog morphogen and its potential for cardiac repair. *PLoS one*. 2013;8:e63075.
- [285] Li H, Johnson NR, Usas A, Lu A, Poddar M, Wang Y, et al. Sustained Release of Bone Morphogenetic Protein 2 via Coacervate Improves the Osteogenic Potential of Muscle-Derived Stem Cells. *Stem Cells Translational Medicine*. 2013;2:667-77.
- [286] Chu H, Gao J, Chen C-W, Huard J, Wang Y. Injectable fibroblast growth factor-2 coacervate for persistent angiogenesis. *Proceedings of the National Academy of Sciences*. 2011;108:13444-9.
- [287] Marti E, Bovolenta P. Sonic hedgehog in CNS development: one signal, multiple outputs. *Trends Neurosci*. 2002;25:89-96.
- [288] Alvarez JI, Dodelet-Devillers A, Kebir H, Ifergan I, Fabre PJ, Terouz S, et al. The Hedgehog pathway promotes blood-brain barrier integrity and CNS immune quiescence. *Science*. 2011;334:1727-31.
- [289] Straface G, Aprahamian T, Flex A, Gaetani E, Biscetti F, Smith RC, et al. Sonic hedgehog regulates angiogenesis and myogenesis during post-natal skeletal muscle regeneration. *Journal of cellular and molecular medicine*. 2009;13:2424-35.
- [290] Lai K, Kaspar BK, Gage FH, Schaffer DV. Sonic hedgehog regulates adult neural progenitor proliferation in vitro and in vivo. *Nature neuroscience*. 2003;6:21-7.
- [291] Hashimoto M, Ishii K, Nakamura Y, Watabe K, Kohsaka S, Akazawa C. Neuroprotective effect of sonic hedgehog up-regulated in Schwann cells following sciatic nerve injury. *J Neurochem*. 2008;107:918-27.
- [292] Reimer MM, Kuscha V, Wyatt C, Sorensen I, Frank RE, Knuwer M, et al. Sonic hedgehog is a polarized signal for motor neuron regeneration in adult zebrafish. *The Journal of neuroscience : the official journal of the Society for Neuroscience*. 2009;29:15073-82.
- [293] Imokawa Y, Yoshizato K. Expression of Sonic hedgehog gene in regenerating newt limb blastemas recapitulates that in developing limb buds. *Proceedings of the National Academy of Sciences*. 1997;94:9159-64.
- [294] Schnapp E, Kragl M, Rubin L, Tanaka EM. Hedgehog signaling controls dorsoventral patterning, blastema cell proliferation and cartilage induction during axolotl tail regeneration. *Development*. 2005;132:3243-53.
- [295] Bambakidis NC, Petrullis M, Kui X, Rothstein B, Karampelas I, Kuang Y, et al. Improvement of neurological recovery and stimulation of neural progenitor cell proliferation by intrathecal administration of Sonic hedgehog. *Journal of neurosurgery*. 2012;116:1114-20.
- [296] Bambakidis NC, Wang RZ, Franic L, Miller RH. Sonic hedgehog-induced neural precursor proliferation after adult rodent spinal cord injury. *Journal of neurosurgery*. 2003;99:70-5.

- [297] Bambakidis NC, Horn EM, Nakaji P, Theodore N, Bless E, Dellovade T, et al. Endogenous stem cell proliferation induced by intravenous hedgehog agonist administration after contusion in the adult rat spinal cord. *J Neurosurg Spine*. 2009;10:171-6.
- [298] Bambakidis NC, Miller RH. Transplantation of oligodendrocyte precursors and sonic hedgehog results in improved function and white matter sparing in the spinal cords of adult rats after contusion. *The spine journal : official journal of the North American Spine Society*. 2004;4:16-26.
- [299] Lowry N, Goderie SK, Lederman P, Charniga C, Gooch MR, Gracey KD, et al. The effect of long-term release of Shh from implanted biodegradable microspheres on recovery from spinal cord injury in mice. *Biomaterials*. 2012;33:2892-901.
- [300] Leskovar A, Moriarty LJ, Turek JJ, Schoenlein IA, Borgens RB. The macrophage in acute neural injury: changes in cell numbers over time and levels of cytokine production in mammalian central and peripheral nervous systems. *J Exp Biol*. 2000;203:1783-95.
- [301] Fawcett JW, Asher RA. The glial scar and central nervous system repair. *Brain Res Bull*. 1999;49:377-91.
- [302] Sirko S, Behrendt G, Johansson PA, Tripathi P, Costa M, Bek S, et al. Reactive glia in the injured brain acquire stem cell properties in response to sonic hedgehog. [corrected]. *Cell stem cell*. 2013;12:426-39.
- [303] Okamoto N, Tobe T, Hackett SF, Ozaki H, Viores MA, LaRochelle W, et al. Transgenic mice with increased expression of vascular endothelial growth factor in the retina: a new model of intraretinal and subretinal neovascularization. *The American journal of pathology*. 1997;151:281-91.
- [304] Krzystolik MG, Afshari MA, Adamis AP, Gaudreault J, Gragoudas ES, Michaud NA, et al. Prevention of experimental choroidal neovascularization with intravitreal anti-vascular endothelial growth factor antibody fragment. *Archives of ophthalmology*. 2002;120:338-46.
- [305] Lyu S, Untereker D. Degradability of polymers for implantable biomedical devices. *International journal of molecular sciences*. 2009;10:4033-65.